Adjoint Sensitivity Analysis Methods for Nonlinear Electric Circuits

Adjungierte Methoden zur Sensitivitätsanalyse für Nichtlineare Elektrische Schaltkreise

Zur Erlangung des akademischen Grades Doktor-Ingenieur (Dr.-Ing.)
Genehmigte Dissertation von Julian Johannes Sarpe, geb. Buschbaum aus Frankfurt am Main
Tag der Einreichung: 01.03.2024, Tag der Prüfung: 25.06.2024

1. Gutachten: Prof. Dr.- Ing. Herbert De Gersem
2. Gutachten: Prof. Dr.- Ing. Idoia Cortes Garcia
3. Gutachten: Prof. Dr.sc.techn. Jan Hansen

Darmstadt, Technische Universität Darmstadt

TECHNISCHE UNIVERSITÄT DARMSTADT

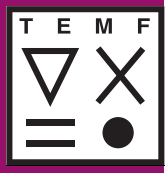

Electrical Engineering and Information Technology Department

Adjoint Sensitivity Analysis Methods for Nonlinear Electric Circuits
Adjungierte Methoden zur Sensitivitätsanalyse für Nichtlineare Elektrische Schaltkreise

Accepted doctoral thesis by Julian Johannes Sarpe, geb. Buschbaum

Date of submission: 01.03.2024
Date of thesis defense: 25.06.2024

Darmstadt, Technische Universität Darmstadt

Bitte zitieren Sie dieses Dokument als:
URN: urn:nbn:de:tuda-tuprints-275947
URL: http://tuprints.ulb.tu-darmstadt.de/27594
Jahr der Veröffentlichung auf TUprints: 2024

Dieses Dokument wird bereitgestellt von tuprints,
E-Publishing-Service der TU Darmstadt
http://tuprints.ulb.tu-darmstadt.de
tuprints@ulb.tu-darmstadt.de

For Teo, Roy & Dexter

Erklärungen laut Promotionsordnung

§ 8 Abs. 1 lit. c PromO

Ich versichere hiermit, dass die elektronische Version meiner Dissertation mit der schriftlichen Version übereinstimmt.

§ 8 Abs. 1 lit. d PromO

Ich versichere hiermit, dass zu einem vorherigen Zeitpunkt noch keine Promotion versucht wurde. In diesem Fall sind nähere Angaben über Zeitpunkt, Hochschule, Dissertationsthema und Ergebnis dieses Versuchs mitzuteilen.

§ 9 Abs. 1 PromO

Ich versichere hiermit, dass die vorliegende Dissertation selbstständig und nur unter Verwendung der angegebenen Quellen verfasst wurde.

§ 9 Abs. 2 PromO

Die Arbeit hat bisher noch nicht zu Prüfungszwecken gedient.

Darmstadt, 01.03.2024

Julian Sarpe

Abstract

This thesis introduces multiple new approaches to efficiently perform adjoint sensitivity analyses for large scale time periodic electric circuits. Firstly, transient forward harmonic adjoint sensitivity analysis combines an efficient transient simulation with a harmonic solution of the adjoint system. Secondly, Parareal adjoint sensitivity analysis sticks to transient simulation for both the forward and the adjoint problem but accelerates those with the Parareal algorithm. Thirdly, the periodic adjoint sensitivity analysis uses a periodic solver, such as periodic Parareal with periodic coarse solver, to efficiently calculate the periodic solution only and uses the solution in a modified adjoint integral. All proposed methods are applied to several application examples, including real world circuit applications with a large number of electrical devices. Most notably, these circuits include a DC-DC converter, a B6 bridge-motor supply circuit and an active filter.

Zusammenfassung

Diese Arbeit befasst sich mit der Entwicklung mehrerer neuer Ansätze zur adjungierten Sensitivitätsanalyse für zeitperiodische elektrische Schaltkreise großen Maßstabs. Diese umfassen die “transient forward harmonic adjoint sensitivity analysis”, welche effiziente transiente Löser mit einem harmonischen Löser für das adjungierte System kombiniert. Außerdem die “Parareal adjoint sensitivity analysis”,welche bei transienter Simulation sowohl für das Vorwärts- als auch für das adjungierte Problem bleibt, diese jedoch mithilfe des Parareal-Algorithmus beschleunigt. Und zuletzt die “periodic adjoint sensitivity analysis”, welche periodische Lösungsverfahren wie den “periodic Parareal with periodic coarse solver” Algorithmus nutzt um eine rein periodische Lösung zu berechnen, welche dann in einem modifizierten adjungierten Integral genutzt werden kann um effizient die Sensitivität für die periodische Lösung zu bestimmen. Alle genannten Methoden werden für verschiedene Anwendungbeispiele genutzt, darunter auch Schaltkreise aus aktiver technischer Entwicklung, welche eine große Anzahl an elektrischen Schaltkreiselementen enthalten. Besonders hervorzuheben sind dabei ein DC-DC-Wandler, eine B6-Brückenmotorversorgungsschaltung und ein aktives Filter.

Contents

1. Introduction

Due to shrinking sizes and for achieving faster development cycle procedures for electronics and power electronics applications, taking care of constraints and optimizations at early stages of the design process has become increasingly important in recent years. This issue rises, since the prototyping becomes more involved and therefore more expensive the more complex the applications become.

The Robert Bosch GmbH in cooperation with the TEMF institute at TU Darmstadt are working on numerical tools and methods that consider relevant aspects within the design process of given products.

Sensitivity analysis is used for root cause analysis but also for the optimization of specific circuit properties such as losses or power consumption. This work is devoted to study reliable and efficient algorithms for sensitivity analysis of time periodic circuits.

1.1. Related Work

In literature, sensitivity analysis is usually classified into two main fields. Statistical Monte Carlo based methods such as polynomial chaos expansion (PCE) are widely used to perform sensitivity analysis. These methods describe the sensitivity by an output variance that is caused by imposing input or design parameter uncertainties. These statistical methods are also referred to as global sensitivity analysis (GSA), as the methods provide the global influence of the uncertainty [70]. One downside of the GSA is the

necessity of many system simulations, which reduces performance if many design parameters are considered. Alternatively, the influence of a design variable or parameter w.r.t. a quantity of interest (QoI) can be described by a derivative of the QoI w.r.t. the design parameter [54]. This class of sensitivities is often referred to as gradient or derivative based sensitivity analysis [70].

1.1.1. Derivative based Sensitivity Analysis using Finite Differences

In many commercial simulation packages, sensitivity analysis is performed using finite differences [1, 83]. Finite differences are a black-box method to numerically approximate the derivative of a function. A finite difference quotient is derived from the Taylor series expansion that approximates the function that is to be derived [31]. The Taylor series expansion for a variable x reads:

$$x(p + \Delta p) = x(p) + \Delta p \frac{\partial x(p)}{\partial p} + \frac{\Delta p^2}{2} \frac{\partial^2 x(p)}{\partial p^2} + \cdots \tag{1.1}$$

The simplest difference quotient is obtained by neglecting all terms higher than order one. After that, the approximation term is solved for $\partial x / \partial p$. The first order finite difference approximation of the derivative reads:

$$\frac{\mathrm{d}x(p)}{\mathrm{d}p} \approx \frac{x(p + \Delta p) - x(p)}{\Delta p}. \tag{1.2}$$

Clearly, the finite difference requires at least two solutions to analyze the sensitivity w.r.t. each design parameter. Consequently, the finite difference approach becomes costly for very large parameter spaces. Even more system simulations are required when the derivative is approximated using higher order differences. The approximation accuracy is decreased for functions with an infinite order, such as cosine, sine, exp or 1/x. The approximation

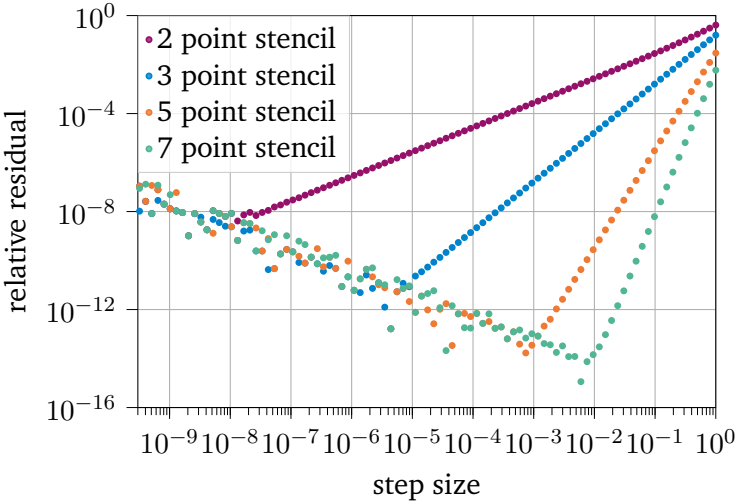

Figure 1.1.: Error of the difference quotient w.r.t. the analytical solution of the derivative $\mathrm{d}\sin(x)/\mathrm{d}x$ depending on the step size for different approximation orders.

accuracy is shown for the numerical derivative of a sine function $\mathrm{d}\sin(x)/\mathrm{d}x$ in Fig. 1.1.

In costly system simulations with large parameter spaces, the finite difference approach is cumbersome. This motivates the use of the adjoint method, which is introduced in detail in chapter 3.

1.1.2. Global Sensitivity Analysis

Global sensitivity analysis (GSA) is a different approach to quantify sensitivities in contrast to the derivative based local sensitivity analysis. As the methods use the variance of the output w.r.t. input uncertainties, GSA is also sometimes refered to as variance based sensitivity analysis in literature.

The sensitivity of a given QoI u w.r.t. the design parameter p is abbreviated by the variable SE_p [70]. For the derivative based sensitivity analysis, this variable reads

$$SE_\mathrm{p} = \frac{\mathrm{d}u}{\mathrm{d}p}. \tag{1.3}$$

For the GSA, the isolated sensitivity w.r.t. a design parameter p is defined by the quotient

$$SE_\mathrm{p} = \frac{(V(E(u|p))}{V(u)}, \tag{1.4}$$

where the variance of the expected value $(V(E(u|p))$ describes the first order influence of p on u and $V(u)$ is the variance of the QoI u [70].

Clearly, both quantities require multiple simulations. Consequently, GSA is often performed using Monte Carlo methods [37]. However, these methods require a very large number of simulations.

Since large numbers of simulations are not endorsed for most applications, more advanced methods for GSA were developed over time. One of the most notable methods for GSA are Sobol indices, named after the Russian mathematician Ilya M. Sobol [79]. In a similar setting, GSA based on a PCE to determine the Sobol indices was previously applied to sensitivity analysis for electric circuits, for example in [93].

While PCE outperforms classical Monte Carlo methods, it is still not feasible for large scale circuits. In newer developments, PCE was used for large scale problems, but even in later publications, the number of uncertain design parameters does not exceed 100 [91]. Considering this current state of science, GSA was consequently not further considered in this thesis.

Sensitivities are often plotted in a stackplot. This type of plot gives the relative normalized sensitivity at each time instance or frequency. That way, the sum of the sensitivities adds up to one in each timestep. Here, Sensitivities for a half-wave rectifier example, similar to the one depicted in section 6.2, are calculated. Fig. 1.2 shows the stackplot of sensitivities for the half-wave rectifier.

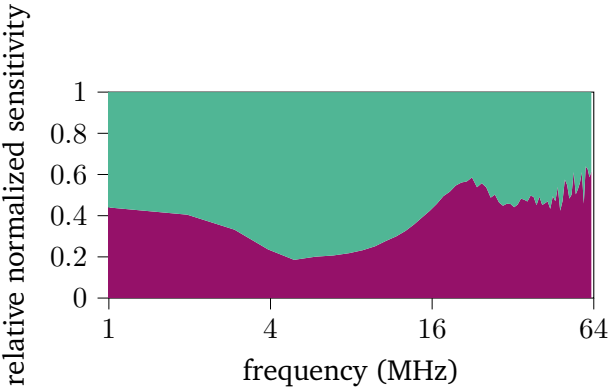

Figure 1.2.: Example of a stackplot depicting the sensitivities of a half-wave rectifier model with two uncertainties.

1.1.3. Parallel-in-Time Adjoint Sensitivity Approaches

Several approaches combining parallel-in-time (PinT) algorithms with adjoint sensitivity analysis (ASA) have been published previously. Firstly, several publications exist that combine the Paraexp algorithm with ASA, such as [78, 19]. Paraexp splits the time integration problem into a homogeneous and an inhomogeneous term. This approach works well for linear systems, ideally ones with an analytical representation for the homogeneous problem [33]. Since a main goal of this thesis aims at methods that are as universally applicable as possible, this approach was not further considered, as it highly limits the pool of numerical problems that can be tackled.

Another more recent publication utilizes the parallel full approximation scheme in space and time (PFASST) in combination with ASA. The PFASST method is closely related to Parareal, but it also uses a coarsening in space additional to coarsening in time [23]. Götschel et al. [33] use the PFASST method to efficiently perform ASA for partial differential equation (PDE)

problems such as heat transport. The implementation is similar to the Parareal ASA introducted in section 5.1, but PFASST is not applicable for circuit simulations.

1.2. Motivation and Research Goals

The goal of this thesis is the development of efficient methods for sensitivity analysis for large scale nonlinear circuits. Moreover, the methods must be as universally applicable as possible, as the ultimate goal is the usability in an industrial setting. Simulating large scale circuits is very challenging due to their extensive parameter spaces. Moreover, when conducting transient simulations, especially for nonlinear circuits, the simulation can require a large number of timesteps in order to simulate the circuit with a required accuracy. Existing methods for sensitivity analysis are either good for sensitivity analysis with long transients and multiple quantities of interest (QoIs) or large parameter spaces [54, 13, 4, 93]. If the circuit employs both long transients and large parameter spaces, conventional methods are often not applicable or exhibit a very slow performance.

Commercial simulation packages usually rely on finite difference based sensitivity analysis, which is very costly [83, 1]. This necessitates further developments in this field for practical industrial applications.

Adjoint sensitivity in particular is a method that performs strongly in a many parameter setting. But, to analyze nonlinear time dependent circuits, a transient circuit simulation is usually required. In the transient case, adjoint sensitivity analysis requires one individual simulation of the transient adjoint problem for every time instance that is considered. This is particularly problematic if time dependent sensitivities are considered, as these analyses require the solution for many adjoint problems.

The downsides of the existing methods for sensitivity analysis in nonlinear circuits motivate the work on more efficient approaches. To avoid rising

simulation wall-clock times, transient sensitivity analysis can be either avoided by approximating the nonlinear circuit problem in a different way, or the transient simulation itself can be accelerated. Both of these general approaches find application within the developed methods in the course of this thesis.

During this thesis, several new methods were developed to tackle the downsides of existing methods for sensitivity analysis. This enables sensitivity analysis to also be useful for more complex circuit examples, which are presented in chapter 6.

1.3. Structure of the Thesis

This thesis is structured in eight chapters. After this introduction, the second chapter explains the most important fundamentals which are used for the methods proposed in this thesis. These fundamentals include basic calculations and solutions for DAEs. Furthermore, the chapter contains modeling approaches for circuits and also explains how circuit problems are solved using the modified nodal analysis (MNA). In the last two sections, harmonic balance (HB) and parallel-in-time (PinT) methods are introduced, which are utilized to optimize the ASA in the later chapters. The basic understanding of these fundamentals is required to fully understand the methods.

The third chapter gives an overview of existing sensitivity analysis methods, particularly the direct sensitivity analysis (DSA) and the ASA in different computational domains.

The fourth chapter introduces the transient forward harmonic ASA (TFHA). The TFHA is a newly developed method for sensitivity analysis which uses a forward transient solution in combination with a harmonic adjoint solution similar to the one that is obtained from HB analysis.

The fifth chapter introduces two PinT methods for sensitivity analysis,

namely the Parareal and the PP-PC. Furthermore, the periodic ASA extends transient ASA to be suitable for the analysis of only the steady state solution.

The sixth chapter demonstrates the practicability of the three new sensitivity analysis methods. This is done by applying each of the methods to different circuit examples to show the advantages and also potential downsides of the respective methods. Additionally, the chapter contains two sections that present possible fields of application in research and development, where the proposed methods can be used.

Finally, the seventh chapter concludes this thesis and gives an outlook for future work in this field.

After the main part of this thesis, the appendix presents supplemental information and derivations that were used in this thesis but would decrease the reading comprehensibility in the main part.

2. Modeling and System Analysis

This chapter reviews the most important methods and concepts from circuit theory and mathematics which are used throughout this thesis. The presented methods help the comprehensive understanding of the concepts and results that are discussed in the later chapters. For further information, the reader is encouraged to also consult the cited literature.

The description of electric systems in time domain is commonly based on differential algebraic equations (DAEs). To understand how to solve the mathematical system introduced in the later part of this chapter, the theory for DAEs is introduced to begin with.

2.1. Differential-Algebraic Equations

DAEs are an important subclass of differential equations that appear in different fields of applications. These fields of applications include different electrical applications, structural dynamics, thermodynamics, fluid mechanics and many more [17, 92, 55, 80], making DAEs an inabundant tool for the modeling in engineering applications.

DAEs are defined as a system of ordinary differential equations (ODE) that require a simultaneous solution of a set of algebraic equations [30]. To understand the specific properties of DAEs, a standard ODE is considered first:

$$\boldsymbol{f}(t, \boldsymbol{y}(t)) = \boldsymbol{y}'(t). \tag{2.1}$$

Depending on the stiffness of the ODE, different types of solvers can be used for the problem solution [90]. While forward differential formulas (FDF) often perform faster, these methods can encounter stability issues depending on the system [64]. The simplest FDF is a forward Euler scheme as a first order FDF:

$$\boldsymbol{y}_{n+1} = \boldsymbol{y}_n + h\boldsymbol{f}(t_n, \boldsymbol{y}_n). \tag{2.2}$$

Since forward differential formulas such as (2.2) approximate the solution for the next timestep based on the solutions at previous timesteps, these methods are also referred to as explicit methods. In contrast, stiff ODEs are typically solved by using backward differential formulas (BDF). BDFs have the advantage of a larger stability region [64]. Additionally, BDFs can often be applied to problems in which forward methods are not applicable at all [61]. The simplest BDF is the backward Euler scheme, which is a first order BDF [61]. The backward Euler scheme for the solution of a general ODE $\boldsymbol{f}(t, \boldsymbol{y}(t))$ reads

$$\boldsymbol{y}_{n+1} = \boldsymbol{y}_n + h\boldsymbol{f}(t_{n+1}, \boldsymbol{y}_{n+1}). \tag{2.3}$$

Since the solution for the next timestep is dependent on itself in all backward schemes, these schemes are also referred to as implicit schemes [10].

To understand the issues along the solution of a DAE problem and the necessity for the backward scheme, a general form of the DAE problem is considered

$$\boldsymbol{F}(t, \boldsymbol{y}(t), \boldsymbol{y}'(t)) = 0. \tag{2.4}$$

In contrast to ODEs, the DAE problem has special requirements regarding the equation and solver properties [77]. Firstly, in order to find a continuous solution for $\boldsymbol{F}$, the variable $\boldsymbol{y}(t)$ needs to be continuously differentiable. Secondly, the system can be split into an algebraic part, which only depends on the solution and the derivatives at the current timestep and a differential part, which contains only dependencies on time derivatives [77]. The second property is particularly important to keep in mind, as it can be

related to the physical properties of the problem setting. If a physical system simultaneously relates changes both in space and time, the resulting mathematical problem will often be a DAE. This is the case for example in circuit problems or quasistatic field simulations.

The general DAE equation (2.4) cannot be solved with a forward scheme, since the solution itself also depends on the derivative $\boldsymbol{y}'(t)$, which is usually not initially available [61]. It is however possible to approximate the derivative $\boldsymbol{y}'(t)$ by a linear combination of the solution $\boldsymbol{y}(t)$ and the respective solutions at previous timesteps $\boldsymbol{y}(t - T_\mathrm{i})$ [61]. Using a BDF, the derivative $\boldsymbol{y}'(t)$ is approximated by the backward difference of $\boldsymbol{y}(t)$. Applying first order backward differences for the derivative $\boldsymbol{y}'(t)$, the approximation reads

$$\boldsymbol{F}(t_{n+1}, \boldsymbol{y}_{n+1}, (\boldsymbol{y}_{n+1} - \boldsymbol{y}_n)/(t_{n+1} - t_n)) = 0 \tag{2.5}$$

for the general DAE problem (2.4). The approximation (2.5) corresponds to the backward Euler scheme.

As mentioned before, circuits are one example for a physical problem where DAEs are necessary for the mathematical description. Circuits contain both spatial charge and current distributions as well as time dependencies, resulting in a DAE system. A DAE system which is for example used for circuit simulation reads [89]:

$$\boldsymbol{A}\dot{\boldsymbol{x}}(t) + \boldsymbol{B}\boldsymbol{x}(t) = \boldsymbol{s}. \tag{2.6}$$

Here, $\boldsymbol{A}$ and $\boldsymbol{B}$ are system matrices, $\boldsymbol{x}$ is the solution vector and $\boldsymbol{s}$ is the right hand side (rhs) source term. In many circuit applications, the matrix $\boldsymbol{A}$ is singular and therefore not invertible [89]. Resultingly, it is impossible to solve Eq.(2.6) directly for $\dot{\boldsymbol{x}}(t)$. Following that, solving problem (2.6) involves a necessary approximation of the derivative $\dot{\boldsymbol{x}}$ along the solution run. Analogously to the general DAE example, the occurring derivative is approximated using backward differences:

$$\boldsymbol{A}(\boldsymbol{x}_{n+1} - \boldsymbol{x}_n)/(t_{n+1} - t_n) + \boldsymbol{B}\boldsymbol{x}_{n+1} = \boldsymbol{s}_{n+1}. \tag{2.7}$$

Moving the terms that correspond with the solution at timestep n to the rhs and substitution of $\Delta t = t_{n+1} - t_n$ gives a solvable equation system:

$$\left(\frac{\boldsymbol{A}}{\Delta t} + \boldsymbol{B}\right) \boldsymbol{x}_{n+1} = \frac{\boldsymbol{A}}{\Delta t}\boldsymbol{x}_n + \boldsymbol{s}_{n+1}. \tag{2.8}$$

In contrast to explicit methods, where $\boldsymbol{A}$ would be required to be nonsingular, for the implicit solver it is sufficient that $(\boldsymbol{A}/\Delta t + \boldsymbol{B})$ is nonsingular [11]. This solution is analogously found when using different BDFs or a trapezoidal method [11].

Several considerations arising from DAEs must be remembered in the following chapters. Firstly, matrix $\boldsymbol{B}$ is possibly singular and therefore not generally invertible. This is particularly important in transient adjoint sensitivity analysis (ASA), because the structure of the equation system is required to be mimetic in order to remain solvable. Secondly, all solvers are constrained to implicit methods. In Parareal approaches, which are introduced in Sec. 2.5, where efficient explicit methods can normally be chosen for the coarse solver, this imposes limitations on the possibilities of optimizations.

2.2. Circuit Fundamentals

The developed methods throughout this thesis are applied to the numerical analysis and optimization of electric circuits. In general, electrical circuit models are used as a simplified representation of a real world physical problem in terms of lumped circuit elements. Lumped circuit elements include resistors R, capacitors C, self inductors L, mutual inductors M as well as dependent and independent sources and many special linear and nonlinear device models.

This section gives an introduction to the most relevant circuit fundamentals. Additionally, important special cases of circuits are explained in order to better understand the numerical application examples.

2.2.1. Kirchhoff's Laws and Incidence Matrices

Kirchhoff's laws are among the most well known and important theorems in the field of electrical engineering. Kirchhoff's laws are based on Maxwell's equations and can be seen as a circuit theoretic special version of the conservation laws. There are two Kirchhoff laws.

The first law is Kirchhoff's current law (KCL), that states that the sum of all currents I_k flowing into a node must be equal to all currents that flow out of the same node. If the currents I_k are defined with a directivity, e.g. positive if flowing into the node and negative if flowing out of the node, the law is given by the sum:

$$\sum_{k=1}^{n} I_k = 0. \tag{2.9}$$

The second law is Kirchhoff's voltage law (KVL), that states that the sum of all voltages V_k in any closed loop in the circuit must be zero. Analogously, if the voltages in the loop are defined with a directivity, the law can be expressed as a sum:

$$\sum_{k=1}^{n} V_k = 0. \tag{2.10}$$

Kirchhoff's laws can be expressed in the form of a matrix equation using the definition of an incidence matrix corresponding to the given circuit topology. The incidence matrix is a construct from graph theory. If the circuit is modeled as a directed graph, the incidence matrix can be used to describe the circuit topology. For a directed graph, the incidence matrix describes the relation between nodes and edges in the given graph. The incidence matrix entries are given by:

$$\mathbf{B}_{ij} = \begin{cases} -1 & \text{if edge } e_j \text{ comes out of node } n_i, \\ 1 & \text{if edge } e_j \text{ goes into node } n_i, \\ 0 & \text{otherwise.} \end{cases} \tag{2.11}$$

In the context of electric circuits, the incidence matrix of a directed graph that corresponds to the circuit topology gives the relation between nodal quantities (imposed currents, node potentials) and edge quantities (current flowing along an edge, voltage drops). Using the incidence matrix, Kirchhoff's laws can be rewritten as a single matrix equation. Assuming no imposed external currents, KCL follows as:

$$\mathbf{B}\boldsymbol{I}_{\text{edges}} = 0, \tag{2.12}$$

where I_{edge} is the vector of all currents in the circuit. KVL follows accordingly using the transpose of the incidence matrix. Assuming no external potentials are imposed on nodes in the circuit, KVL is written as:

$$\mathbf{B}^{\mathsf{T}}\boldsymbol{V}_{\text{nodes}} = 0, \tag{2.13}$$

in terms of the incidence matrix. Here, V_{nodes} denotes the vector of node potentials in the graph that corresponds to the circuit topology. Using a sub graph, that describes only specific parts of the circuit, incidence matrices can also be utilized to implement devices in nodal analysis (see for example [46]) that have no definition in terms of electric admittance Y. This is used for modified nodal analysis (MNA), which is further described in section 2.3.

2.2.2. Nonlinear Circuit Theory

Many practical circuit applications are not limited to linear components. Particularly in electronics, nonlinear devices are necessary for the basic functionality of the circuits [42]. These devices include functional elements such as diodes and switches. But also non-functional components can lead to nonlinear behavior. These nonlinearities can result from material imperfections or physical effects on the circuit boards such as eddy currents or stray effects [22, 7]. Consequently, dealing with nonlinear effects is indispensable for circuit analysis.

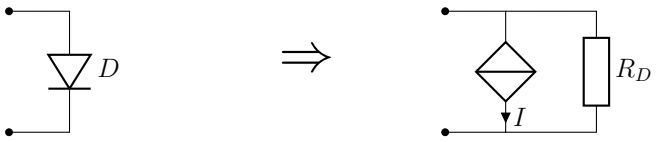

(a) A simple Diode

(b) Diode incremental model

Figure 2.1.: Circuit symbol of a simple diode (left) and its corresponding incremental model with a controlled current source and a resistance (right).

One approach for the analysis of nonlinear devices is the incremental model [89, 62]. Incremental models linearize the devices for a specific region of operation. The incremental model for a simple diode is shown in Fig. 2.1. This incremental model is particularly simple to implement. For the linearization, an equation based model for the nonlinear device is required. The given nonlinear device is then linearized using a first order Taylor approximation of the system [89]. For a basic diode model, the device can be characterized by Shockley's diode equation:

$$I = I_0(e^{k_B V} - 1), \tag{2.14}$$

where I_0 is the reverse threshold current, k_B is Boltzmann's constant and V is the voltage drop across the diode. The solution of Shockley's equation (2.14) is used as the current of the current source in the incremental model (Fig. 2.1). The admittance of the resistor in the incremental model (Fig. 2.1) is obtained by solving the derivative of (2.14) w.r.t. the voltage drop V. The resulting admittance is given as:

$$Y_D = \frac{\partial I}{\partial V} = k_B I_0 e^{k_B V}. \tag{2.15}$$

The incremental model is advantageous if only few different types of nonlinear devices are needed, since it requires a specific model implementation

for each device. This necessity is also a downside of the incremental model as this means it cannot be used as a blackbox approach [62]. Another downside arises from the limitation to weakly nonlinear devices, since the linearization approach does not work for very narrow linear regions [89].

Alternatively, the solution to the nonlinear equation system can be approximated by Newton's method or other related methods. Newton's method is a numerical black box technique that is used to approximate the root of a function. This iterative method is widely employed for numerical problems, where the solutions are not analytically available such as nonlinear differential equations [61]. The basic idea behind Newton's method is to start with an initial guess for the root of the function and iteratively updating the solution with the update formula

$$x_{n+1} = x_n - \frac{f(x_n)}{f'(x_n)}, \tag{2.16}$$

until a root is approximated with a desired accuracy. The steps along Newton's method can be described as:

1. Start with an initial guess x_0 for the root of the function $f(x_n)$.
2. Compute the function value, $f(x_n)$, and its derivative, $f'(x_n)$, for the current iterate x_n.
3. Calculate a new estimate, x_{n+1}, using Eq. (2.16).
4. Repeat steps 2 and 3 until the root is approximated with the desired accuracy.

Note here that it is required that the function $f(x)$ is differentiable in order to execute step 2 of the Newton iteration. Newton's method is a very effective method to find the roots for a wide range of functions. Newton's method is particularly efficient when the initial guess is close to the solution for the root. However, Newton's method may not converge for all functions.

Careful consideration of the problem setting and the initial guess is required to be able to avoid these issues.

Both Newton's method and the incremental model use a first order linearization method in order to obtain a linearized version of the given problem. Newton's method is advantageous if many nonlinear devices are present in the circuit, as it is not necessary to linearize each element separately using this approach. Additionally, Newton's method is a black box method, which means that it can be applied to other mathematical problems without any knowledge of the underlying physical model. Resultingly, many freely available libraries which implement Newton's method, can readily be used to obtain the solution of the nonlinear problem.

Regardless of the linearization method, equation based models for nonlinear devices are required in order to perform the simulation. This can be a limiting factor, as it implies that any modifications and additional methods that utilize the equation system of the given circuit problem necessitate access to these models.

2.2.3. PWM-Switched Circuits

Switched circuits with a pulse width modulation (PWM) pose a very special case for circuit simulation. Firstly, PWMs require extensive modeling [88]. Secondly, PWMs leads to a simulation result that contains fast transitions at switching points, whereas the PWM period length can be several magnitudes larger. This makes PWM switched circuits a very challenging numerical problem, as the methods to simulate such circuits must be able to resolve very fast transitions while the dimensions and runtime of the possibly long simulation periods are limited [39, 50]. In practice, PWM inputs are commonly found in power converters. Ideally, the time-average of a PWM signal converges to a reference signal that is to be generated [50]. This property is utilized in power converters for example to generate a sinusoidal output within a DC-AC converter. A PWM can be defined by four parameters

that describe the signal properties:

1. The switching frequency f_s, which is the inverse of the switching cycle T_s for a single pulse window. This pulse window includes both on- and off-time. There exist constant switching frequency PWM and varying switching frequency PWM.

2. The duty cycle D quantifies the relative proportion of the on-time t_on w.r.t. the duration of the switching cycle T_s.

3. The amplitude modulation ratio, that gives the ratio of the amplitude of the modulated signal $m(t)$ w.r.t. the carrier signal $s(t)$.

4. The frequency modulation ratio, that gives the maximum deviation between the frequency of the modulated signal f_m and the switching frequency f_s.

One way to generate a modulated PWM signal $m(t)$ is the mathematical comparison between the reference signal $d(t)$, which is usually the desired output signal of the circuit and the carrier signal $s(t)$ through a signum (sgn) function:

$$m(t) = \mathrm{sgn}(d(t) - s(t)). \tag{2.17}$$

This modulation is illustrated using a sawtooth carrier and a sinusoidal reference signal as shown in Fig. 2.2 (a) and (b). The modulated signal is obtained using Eq. (2.17). The resulting modulated signal is shown in Fig. 2.2 (c). As expected, the duty cycle D is larger in the parts where the amplitude of the sinusoidal reference signal is larger, while the duty cycle is smaller elsewhere. That way, a PWM signal can easily be generated and controlled. Note here that for the generation, it is important that the amplitude of the reference signal is smaller than that of the carrier signal. If this is not ensured, the two signals might not have an intersection in some switching cycles. Resultingly, the PWM signal will not switch in the switching cycles without an intersection, which in turn will lead to information loss.

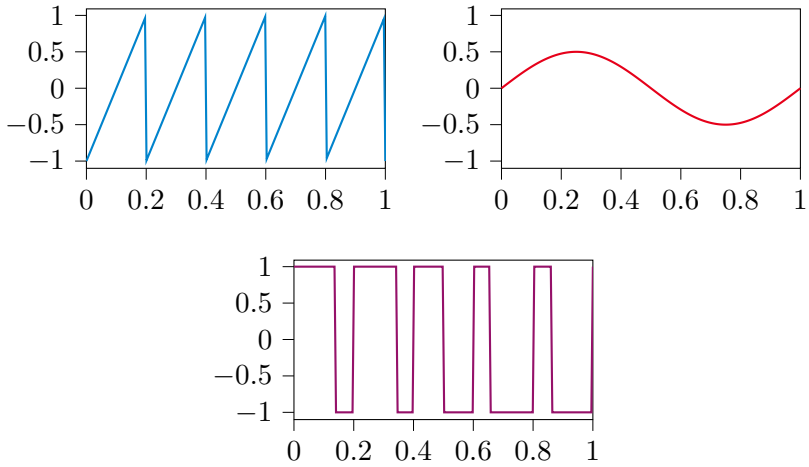

Figure 2.2.: A sawtooth carrier signal (upper left) and a sinusoidal reference signal (upper right) used to generate the PWM modulated signal (bottom) using Eq. (2.17).

2.2.4. Equivalent Electrical Circuit Methods

Complex devices can pose a difficult task when it comes to their implementation in terms of lumped circuit elements. In particular, when additional electromagnetic field effects must be taken into account, the behavior of a real world device can significantly diverge from its purely functional lumped element model. Equivalent electrical circuit (EEC) methods can provide a powerful tool for the implementation of field effects within a circuit simulation. This tool is particularly valuable when analyzing disturbance prone electrical systems, such as printed circuit boards (PCBs), integrated circuits (ICs), and other high-frequency structures. EECs try to model the electromagnetic behavior within the low-frequency end of the spectrum as

an electrical circuit. This allows for the analysis of the circuit's electrical characteristics, also including electromagnetic compatibility (EMC) effects.

One of the earliest methods to automatically generate EECs from 3D CAD models was the partial element equivalent circuit (PEEC) method. This method was introduced by Ruehli in 1974 [68]. For the PEEC method, integral equations are used to model surface charges and current densities in a multiconductor system [68]. Integral equation formulations are particularly advantageous for physical problems where the free space are is large. This advantage results from the fact that integral equation formulations only require a discretization of the surface. In contrast, free space differential equation methods such as 3D finite element method (FEM) require a discretization of the entire free space area. However, the PEEC method can also exhibit disadvantages. For more complex physical problems, such as an near-field control (NFC) antenna, the PEEC formulation will result in an equation system with a very large number of DoFs [85]. Resultingly, it becomes very hard for engineers to interpret the analogies of the lumped elements of the EEC model that is derived from PEEC.

Particularly in EMC applications, an intuitive representation of the physical processes is a vital task [86]. This requirement arises from the development process, where the goal is to model the actual behavior of a circuit, including parasitic field effects. To identify possible issues with the physical layout, it is also advantageous to construct the coupled simulation with EEC elements in a way where lumped elements directly correspond to physical layout dimensions.

If this formulation is modeled accordingly, the physical processes in the given problem are given in a very intuitive way [86]. However, the method proposed by Traub et al. [86] requires a 3D FEM simulation to obtain the EEC model which also poses the before mentioned issue, that the simulation performance lacks for large free spaces which contain many connected nodes to discretize.

Based on the direct correspondence, further analyses such as sensitivity

analysis can be used to identify and optimize the physical layout automatically [73]. Even though the proposed method of [86] results in much smaller circuit models than the PEEC method, the resulting circuit models can still significantly exceed the number of lumped elements of the functional circuit itself.

Throughout this thesis, several methods to efficiently calculate sensitivities with respect to many lumped elements as design parameters were developed. All of these methods were also applied to problems that included EEC models derived through the method of [86], in order to optimize the sensitivity analysis w.r.t. geometric variations as described in [73].

2.3. Modified Nodal Analysis

Modified Nodal Analysis (MNA) is a well known method for the numerical analysis of electric circuits. The MNA was introduced in 1975 by Ho et al. [16] and has since been implemented in many commercial and noncommercial circuit analysis tools.

2.3.1. Modified Nodal Analysis for DC Circuit Analysis

MNA modifies the classic nodal analysis to include impedance stamps for specific electric and electronic devices. These devices include inductances and voltage sources as well as a large variety of controlled sources and nonlinear devices such as switches [89]. In the simple static case, the MNA equation system reads:

$$\boldsymbol{F}(\boldsymbol{x}) = \boldsymbol{A}\boldsymbol{x} - \boldsymbol{i}_\mathrm{s} = 0. \tag{2.18}$$

The solution vector $\boldsymbol{x}$ gathers the node potentials $\boldsymbol{u}_\mathrm{nodes}$ for all nodes and the edge currents $\boldsymbol{i}_\mathrm{edges}$ for the impedance devices. The right hand side source vector $\boldsymbol{i}_\mathrm{s}$ contains all independent source excitations. The MNA matrix $\boldsymbol{A}$

contains the nodal admittance matrix $\boldsymbol{Y}$ as well as the edge impedance matrix $\boldsymbol{Z}$ that gathers the behavior of impedance devices. The incidence matrices $\boldsymbol{B}$ and $\boldsymbol{B}^\mathsf{T}$ serve as coupling terms between the admittance and impedance parts of the equation system. The assembled matrix is structured as:

$$\boldsymbol{A} = \left(\begin{array}{c|c} \boldsymbol{Y} & \boldsymbol{B}^\mathsf{T} \\ \hline \boldsymbol{B} & \boldsymbol{Z} \end{array}\right). \tag{2.19}$$

The right hand side $\boldsymbol{i}_\mathrm{s}$ of the nodal analysis is modified accordingly, such that it contains all input nodal currents $\boldsymbol{i}_\mathrm{nodes}$ and edge voltages $\boldsymbol{u}_\mathrm{edges}$ for the respective impedance devices:

$$\boldsymbol{i}_\mathrm{s} = \left(\begin{array}{c|c} \boldsymbol{i}_\mathrm{nodes} & \boldsymbol{u}_\mathrm{edges} \end{array}\right)^\mathsf{T}. \tag{2.20}$$

2.3.2. Modified Nodal Analysis for Transient Circuit Analysis

In the original publication by Ho et al [16], the MNA was derived for transient analysis. The transient MNA is a very common example for a modeling approach that results in a DAE system. This DAE system reads:

$$\boldsymbol{F}(\boldsymbol{x}, \dot{\boldsymbol{x}}, t) = \boldsymbol{A}_\mathrm{C}\dot{\boldsymbol{x}}(t) + \boldsymbol{A}_\mathrm{G}\boldsymbol{x}(t) - \boldsymbol{i}_\mathrm{s}(t) = 0, \qquad \boldsymbol{x}(t=0) = 0. \tag{2.21}$$

The system matrix $\boldsymbol{A}_\mathrm{C}$ gathers the reactive element contributions which are used to model devices such as capacitors and inductors. The system matrix $\boldsymbol{A}_\mathrm{G}$ gathers contributions from resistors and other resistive elements as well as specific impedance stamps to voltage sources or dependent sources. Analogously to the static case, the solution vector $\boldsymbol{x}$ gathers the nodal voltages as well as the edge currents and the right hand side source vector $\boldsymbol{i}_\mathrm{s}$ contains all independent source excitations. If the circuit contains nonlinear devices, a linearization of the system is required. This is usually implemented with the Newton method or similar related methods for

nonlinear equations [89]. The linearization along the Newton iteration can be implemented with the definition of the resistive Jacobian matrix $\boldsymbol{J}_{\mathrm{G}}$:

$$\boldsymbol{J}_{\mathrm{G}}(\boldsymbol{x}(t), t) = \boldsymbol{A}_{\mathrm{G}} - \frac{\partial \boldsymbol{i}_{\mathrm{nl}}(\boldsymbol{x}(t), t)}{\partial \boldsymbol{x}(t)}. \tag{2.22}$$

Here, $\boldsymbol{i}_{\mathrm{nl}}$ is the vector that models the node behavior of nonlinear resistive devices. Resultingly, the vector is zero at all nodes where no nonlinear devices are attached [89, 48]. Analogously, nonlinear reactive devices, such as nonlinear capacitors, are linearized with the definition of the reactive Jacobian matrix $\boldsymbol{J}_{\mathrm{C}}$:

$$\boldsymbol{J}_{\mathrm{C}}(\dot{\boldsymbol{x}}(t), t) = \boldsymbol{A}_{\mathrm{C}} - \frac{\partial \boldsymbol{i}_{\mathrm{nl}}(\dot{\boldsymbol{x}}(t), t)}{\partial \dot{\boldsymbol{x}}(t)}. \tag{2.23}$$

The resulting differential equation containing nonlinear elements is of a mimetic structure to the linear case:

$$\begin{aligned} \boldsymbol{F}(\boldsymbol{x}, \dot{\boldsymbol{x}}, t) &= \boldsymbol{J}_{\mathrm{C}}(\dot{\boldsymbol{x}}(t), t)\dot{\boldsymbol{x}}(t) + \boldsymbol{J}_{\mathrm{G}}(\boldsymbol{x}(t), t)\boldsymbol{x}(t) - \boldsymbol{i}_{\mathrm{s}}(t) = 0, \\ \boldsymbol{x}(t = 0) &= 0. \end{aligned} \tag{2.24}$$

The linearization based on Eq. (2.22) and (2.23) is performed in every timestep for transient analyses.

In many applications, the simulation is not started from a zero state $\boldsymbol{x}(t = 0) = 0$ but rather for a specified operation state. A simple example for this is an amplifier tuned with a DC voltage [42]. To improve convergence for these situations, a DC operation point (DCOP) analysis is performed prior to the solution for the first timestep [49]. For a DCOP analysis, the circuit is reduced to only conductive DC elements. All reactive elements are replaced with their DC equivalent, i.e. capacitors are replaced with an open circuit, and inductors are replaced with a short [42]. Based on the reduced circuit, the DCOP analysis is performed using the static MNA described in section 2.3.1.

2.3.3. Modified Nodal Analysis for AC Circuit Analysis

For the harmonic solution of a linear system, the transient MNA DAE system (2.21) can easily be collapsed to a DAE system with only one system matrix in alternating current (AC) domain. For the description in AC domain, the system quantities, i.e. the solution vector and the excitation are written in terms of a complex phasor representation:

$$\tilde{\underline{\boldsymbol{x}}}(\omega, t) = \underline{\boldsymbol{x}} e^{\mathrm{j}\omega t} \tag{2.25}$$

and

$$\tilde{\underline{\boldsymbol{i}}}_{\mathbf{s}}(\omega, t) = \underline{\boldsymbol{i}}_{\mathbf{s}} e^{\mathrm{j}\omega t} \tag{2.26}$$

with the angular frequency $\omega = 2\pi f$, the complex number $\mathrm{j} = \sqrt{-1}$ and the amplitudes $\underline{\boldsymbol{x}}$ and $\underline{\boldsymbol{i}}_{\mathbf{s}}$, respectively.

The AC MNA directly follows by plugging the complex amplitudes from (2.25) and (2.26) into the transient MNA formulation (2.21):

$$\underline{\boldsymbol{F}}(\underline{\boldsymbol{x}}, \omega) = \boldsymbol{A}_{\mathrm{C}} \mathrm{j}\omega \underline{\boldsymbol{x}} + \boldsymbol{A}_{\mathrm{G}} \underline{\boldsymbol{x}} - \underline{\boldsymbol{i}}_{\mathbf{s}} = 0. \tag{2.27}$$

The time derivative is simplified to a multiplication with $\mathrm{j}\omega$ for the complex phasor representation. Since the multiplication is associative and commutative, the system matrices $\boldsymbol{A}_{\mathrm{C}}$ and $\boldsymbol{A}_{\mathrm{G}}$ can be added to a single system matrix $\underline{\boldsymbol{A}}$:

$$\underline{\boldsymbol{A}} = \boldsymbol{A}_{\mathrm{G}} + \mathrm{j}\omega \boldsymbol{A}_{\mathrm{C}}. \tag{2.28}$$

The final MNA equation system for the AC case is followingly mimetic to the static case such that:

$$\underline{\boldsymbol{F}}(\underline{\boldsymbol{x}}, \omega) = \underline{\boldsymbol{A}} \underline{\boldsymbol{x}} - \underline{\boldsymbol{i}}_{\mathbf{s}} = 0. \tag{2.29}$$

In general, the AC MNA is only applicable in the linear case. In many applications, this is not the case since most electronic circuits contain nonlinear devices as well. However, with some considerations it is also possible to calculate nonlinear circuit problems in frequency domain. One such method is presented in the following section.

2.4. Harmonic Balance Analysis

Harmonic balance (HB) analysis is a numerical method to approximate the steady state of a nonlinear problem in frequency domain. The term harmonic was originally used in music theory. A harmonic is the member of a harmonic series. A harmonic series consists of an oscillation with a fundamental frequency and several oscillations whose frequencies are multiples of the fundamental frequency [34]. A superposition of harmonics can also be used to approximate the time waveform in other dynamic systems. Throughout the HB analysis, the solution of a nonlinear system is approximated in frequency domain. Nakla and Vlach [51] introduced the concept of HB in 1976. In some applications, HB analysis is advantageous compared to transient analysis. A suitable application for HB is the analysis of nonlinear systems that also contain models which are only available in frequency domain. These models include transmission lines or S-parameter multipoles [48]. Another application case is the analysis of systems that exhibit long transient processes, since the convergence rate of the HB iterations is quicker than computing the transient processes for these systems [48].

The HB iteration process is outlined in the flowchart in Fig. 2.3. The HB method requires an initial estimate for the spectral solution to start the iteration process. Without prior knowledge of the solution, the initial guess can be set to zero for every frequency. However, the convergence of the HB method can be significantly increased if a better initial estimate is provided [48]. In very simple applications, the initial estimate can be provided by an educated guess. A popular example for such an application is the voltage across a diode which is excited by a sinusoidal input, because a capped sine wave is an obvious choice for the approximation of the solution [48]. An examplary solution for the voltage across the diode is shown in Fig. 2.4. For more complex circuits, the initial estimate is often provided by a DC operating point analysis. This approach is analogous to

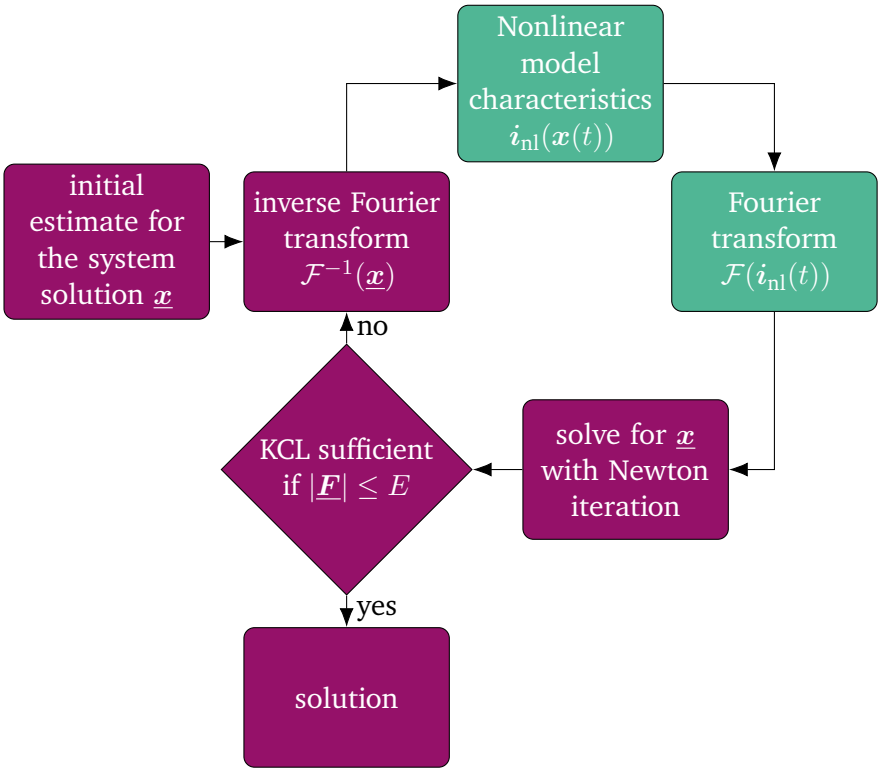

Figure 2.3.: Flowchart to describe the iteration steps along the HB analysis. Frequency domain operations in purple, time domain operations in green.

the DC operating point analysis prior to a nonlinear transient simulation as previously described in section 2.3.2. Alternatively, a linear approximation of the circuit can be used to perform an AC simulation prior to the HB. This is particularly suitable for circuits with very weak nonlinearities.

The initial estimate is transformed to time domain using inverse Fourier transform. This transformation must be performed individually for every

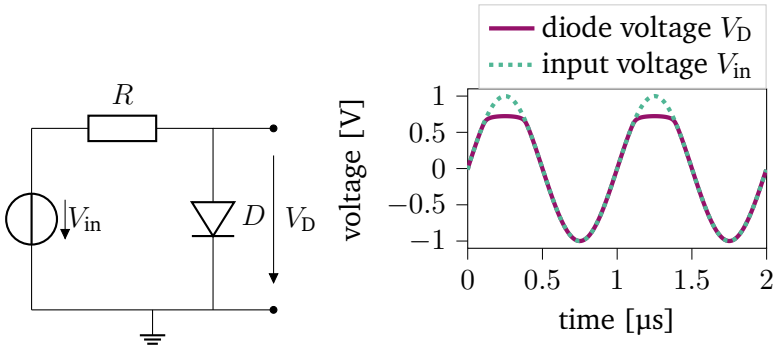

Figure 2.4.: Voltage across a diode with a series resistor and a sinusoidal excitation.

node potential oder edge current. The time domain solution is then used to approximate the behavior of nonlinear devices based on given equation models to describe their nonlinear behavior. For a diode model, this equation model would be based upon a Shockley diode equation [76]. As nonlinear devices are dependent on the circuit solution $\underline{\boldsymbol{x}}$ itself, the linearized contributions for the devices are added to the Jacobian. AC analysis requires the solution to be contained in a single system matrix rather than a time stepping as in transient simulation. Resultingly, the nonlinear models must be linearized for all frequencies simultaneously [48, 51]. The Jacobian for the HB analysis is found analogously to the Jacobian for nonlinear transient analysis:

$$\underline{\boldsymbol{J}} = \underline{\boldsymbol{A}} - \frac{\partial \underline{\boldsymbol{i}}_{\text{nl}}(\underline{\boldsymbol{x}})}{\partial \underline{\boldsymbol{x}}}. \tag{2.30}$$

The linearization is performed for each nonlinear device using equation

$$\underline{\boldsymbol{J}}_{\text{device}} = \frac{\partial \underline{i}_{\text{nl,device}}(\underline{\boldsymbol{x}})}{\partial \underline{\boldsymbol{x}}} = \Gamma \frac{\partial i_{\text{nl,device}}(\boldsymbol{x}(t))}{\partial \boldsymbol{x}(t)} \Gamma^{-1}. \tag{2.31}$$

Here, Γ is the matrix form of the discrete Fourier transform (DFT) operator

$$\Gamma = \mathcal{F}\{I_n\} = \sum_{k=0}^{N-1} I_{n,k} e^{-\frac{\mathrm{j}\pi}{N} nk}, \tag{2.32}$$

where I_n is the identity matrix of dimension $n \times n$ and $I_{n,k}$ is its k-th row. Conversely, Γ^{-1} is the matrix form of the inverse discrete Fourier transform (IDFT) operator [48]

$$\Gamma^{-1} = \mathcal{F}^{-1}\{I_n\} = \frac{1}{N} \sum_{k=0}^{N-1} I_{n,k} e^{\frac{\mathrm{j}\pi}{N} nk}. \tag{2.33}$$

The DFT and IDFT matrices are densely occupied. As a result, the nodes where nonlinear devices are attached, lead to densely occupied submatrices in the HB equation system. This is logical, as nonlinear device contributions interconnect the solution across a spectrum of frequencies. Particularly in the case of strongly nonlinear devices, this can pose a numerical bottleneck, as these interactions connect the solution across a very wide spectrum of frequencies. The result of this is a very large Jacobian, since all frequency components have to be simulated in a single system matrix, as explained before. To enable linear devices to be simulated simultaneously for several frequencies, a linear conversion submatrix

$$\underline{\boldsymbol{Y}}_{\text{conv}} = \begin{pmatrix} \underline{y}(0) & 0 & 0 & \cdots & 0 \\ 0 & \underline{y}(\omega_\text{p}) & 0 & \cdots & 0 \\ 0 & 0 & \underline{y}(2\omega_\text{p}) & \cdots & 0 \\ \vdots & \vdots & \vdots & \ddots & \vdots \\ 0 & 0 & 0 & \cdots & \underline{y}(k\omega_\text{p}). \end{pmatrix} \tag{2.34}$$

is defined, that matches the dimension of the nonlinear submatrices [48]. Here, k is the maximum number of harmonic frequencies taken into consideration. The name conversion submatrix derives from the conversion of

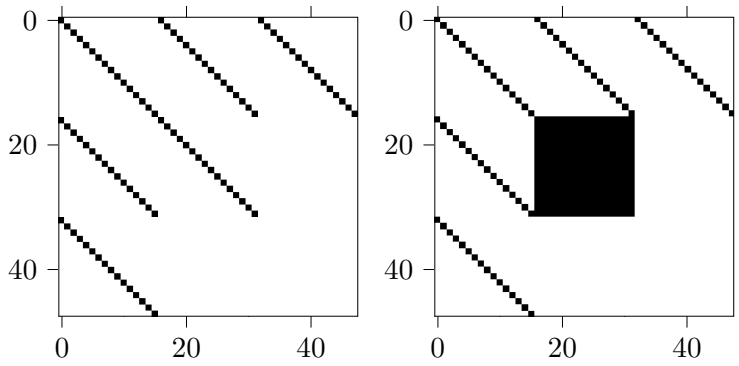

Figure 2.5.: Matrix structure of the modified nodal analysis matrix for a circuit with three nodes approximated with 16 harmonics. Left: linear circuit, right: circuit with one nonlinear device attached to the second node.

a scalar quantity to a matrix form for several harmonics. This conversion matrix is clearly sparse. As a result, many linear contributions will lead to a sparse HB Jacobian, while many nonlinear contributions lead to a denser HB Jacobian. For illustration purposes, this is shown for two virtual circuit problems with 4 DoFs and 16 harmonics where one circuit contains only linear elements and the other additionally contains one nonlinear device attached between one node and ground. Fig. 2.5 shows the comparison of the two system matrices. The more nonlinear devices are present and the stronger the nonlinearities, the denser the matrix will be. This is a major issue that has to be taken into account when working with the HB

method [48, 65]. The final equation system which is used throughout the Newton iteration within the HB analysis is given analogously to the linear AC MNA problem:

$$\underline{\boldsymbol{F}}(\underline{\boldsymbol{x}}, \omega) = \underline{\boldsymbol{J}}\underline{\boldsymbol{x}} - \underline{\boldsymbol{i}_\mathbf{s}} = 0. \tag{2.35}$$

Throughout the HB analysis iteration, the Newton steps and the error estimation by KCL are executed in frequency domain. After each HB analysis iteration, the residual is calculated as the norm of vector $\underline{\boldsymbol{F}}$:

$$\varepsilon_{\text{HB}} = \|\underline{\boldsymbol{F}}\|. \tag{2.36}$$

As per definition in Eq. (2.35), ε_{HB} is 0 if the final solution is found. Accordingly, the HB analysis iteration is repeated until ε_{HB} is smaller than a predefined threshold.

2.5. Parallel-in-Time Methods

The parallelization of ODE or DAE solvers is challenging, as the problem itself is inherently sequential. Traditional time integration methods, such as described in section 2.3.2, compute the solution sequentially for each timestep. This is particularly computationally expensive for very complex problems or problems with a fine time resolution.

Parallel-in-time (PinT) methods, are computational algorithms that are used to cut down the wall-clock time of the simulation for time-dependent problems. A broad overview over a large number of publications related to PinT methods is gathered in [59]. The shorter simulation times are achieved by parallel processing. The parallelization happens by simulating different time subintervals in parallel on different processing cores of a computer or simulation cluster.

PinT methods can be utilized for these problems and offer a potentially significant speedup of the wall-clock time for problems that require a large

number of timesteps. There are different approaches that aim to implement a PinT method.

This section presents the outline for two specific PinT methods. Both of the presented methods are based on a multiple shooting approach [53]. At first, the Parareal is outlined and explained. Secondly, the periodic Parareal with initial-value coarse problem (pp-ic) and the periodic Parareal with periodic coarse problem (pp-pc) are explained. These two methods are periodic extensions to the Parareal algorithm.

2.5.1. Parareal

Parareal is a popular PinT method that aims to cut-down on wall clock time for time integration. Parareal was first published in 2000 by Maday and Turinici [47] and is based on multiple shooting methods [53, 28]. One major advantage of the Parareal is its non-intrusiveness, which enables the Parareal to be applied to a large variety of time-dependent PDE problems in principle.

Two different time domain solvers are used throughout the Parareal iteration. A fast coarse solver $\mathcal{G}$ delivers a rough approximation of the solution X, which is used to perform updates in each Newton iteration. The fine solvers $\mathcal{F}$, executed for N temporal subintervals in parallel, to provide an accurate solution inside the subintervals. Since the Parareal is non-intrusive, the fine and coarse solvers can be chosen freely [47, 28].

The coarse solver is usually a fast but less accurate solver, such as a transient solver with large time steps. Since the coarse solver is executed within the serial part of the iteration, it needs to be as efficient as possible (Amdahl's law [35]). The fine solver must be more accurate than the coarse solver for the Parareal to deliver satisfying results. However, the fine solver can be less efficient, since it is executed in parallel. A more expensive solver such as a transient solver of higher order with small time steps is suitable as the fine solver. Non-intrusiveness is also often advantageous when specific

solver details are not available or modifiable by the user as is often the case in industrial applications with proprietary solvers.

The individual steps of the Parareal iteration are briefly outlined as a flowchart in Fig. 2.6. To understand the entire process of the Parareal algorithm, the steps will be described for a general ODE problem similar to the one introduced in Eq. (2.1). Consider the general ODE with defined initial condition:

$$\boldsymbol{x}'(t) = \boldsymbol{f}(t, \boldsymbol{x}(t)) \tag{2.37}$$

$$\boldsymbol{x}(0) = \boldsymbol{x}_0, \tag{2.38}$$

in the time interval

$$t \in (0, T]. \tag{2.39}$$

To introduce a time parallelization, the time interval is split into N subintervals

$$t_n \in (T_{n-1}, T_n], \tag{2.40}$$

where n is the index of the respective subinterval. The number of subintervals N is determined by considerations about the numerical problem and the number of simulation cores that are available for the simulation. For each of the subintervals, a different ODE initial value problem (IVP) is defined:

$$\boldsymbol{x}_n'(t) = \boldsymbol{f}(t_n, \boldsymbol{x}_n(t)) \tag{2.41}$$

$$\boldsymbol{x}_n(t_{n-1}) = \boldsymbol{x}_{n-1}. \tag{2.42}$$

Each of the N IVPs is solved by the defined fine solver in parallel. Since Parareal is based on the multiple shooting method, the update equation to find the final solution can be defined analogously. For that, the fine solver operator $\mathcal{F}$ is used as a so called propagator [28]. The subsequent iteration for the solution of a numerical problem along the multiple shooting method is based on Newton's method. The iteration for the multiple shooting

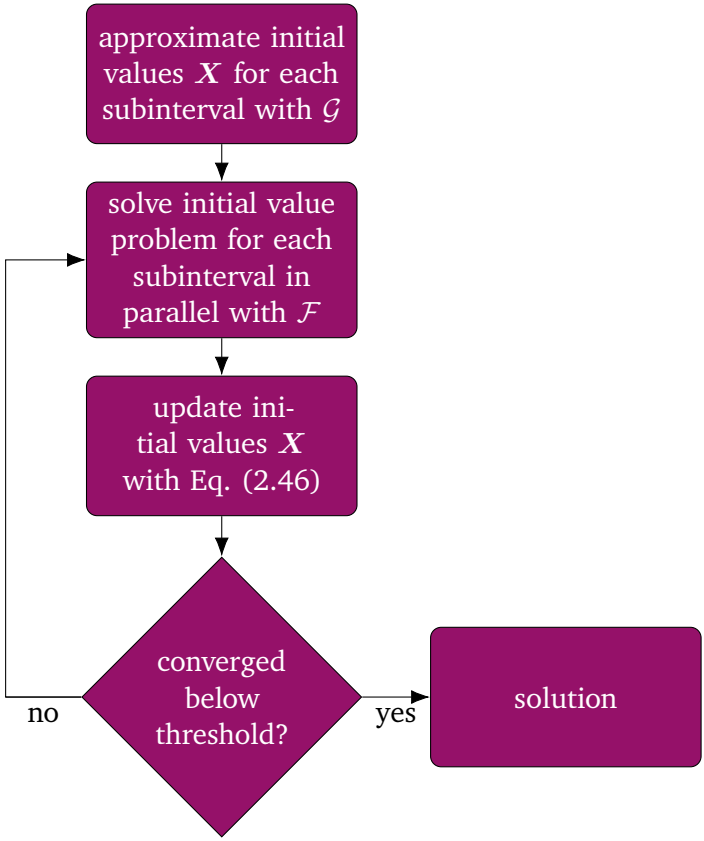

Figure 2.6.: Flowchart outlining the iteration steps along the Parareal approach.

method that solves for the approximate solution $\boldsymbol{X}$ to the IVP is then given as

$$\boldsymbol{X}_n^{k+1} = \mathcal{F}(\boldsymbol{X}_{n-1}^k) + \boldsymbol{J}_{\mathcal{F}} \left[\boldsymbol{X}_{n-1}^{k+1} - \boldsymbol{X}_{n-1}^k \right], \tag{2.43}$$

with the iteration index k. The Jacobian $\boldsymbol{J}_{\mathrm{F}}$ is defined as

$$\boldsymbol{J}_{\mathcal{F}} = \frac{\partial \mathcal{F}(\boldsymbol{X}_{n-1}^k)}{\partial \boldsymbol{X}_{n-1}^k}. \tag{2.44}$$

Since the explicit calculation of the Jacobian is numerically expensive, especially if several iteration steps are necessary, the derivative is alternatively obtained by an approximation. Using the coarse solver $\mathcal{G}$ as a second propagator, the derivative can be roughly approximated by a finite difference. This approximation reads:

$$\boldsymbol{J}_{\mathcal{F}} \left[\boldsymbol{X}_{n-1}^{k+1} - \boldsymbol{X}_{n-1}^k \right] \approx \mathcal{G}(\boldsymbol{X}_{n-1}^{k+1}) - \mathcal{G}(\boldsymbol{X}_{n-1}^k). \tag{2.45}$$

Plugging Eq. (2.45) into the multiple shooting iteration (2.43) leads to the update equation for the Parareal:

$$\boldsymbol{X}_n^{k+1} = \mathcal{F}(\boldsymbol{X}_{n-1}^k) + \mathcal{G}(\boldsymbol{X}_{n-1}^{k+1}) - \mathcal{G}(\boldsymbol{X}_{n-1}^k). \tag{2.46}$$

While the fine solver runs are all executed in parallel, the update equation, and thus, the coarse solver is running sequentially. As a result, it is a major concern that the coarse solver is as numerically cheap as possible. Since the iteration of the Parareal is started with inexact initial values $\boldsymbol{X}_{n-1}$ at the subinterval boundaries, the updates have to be performed along multiple iteration steps. The error is controlled by the maximum discontinuity at the subinterval boundaries normalized over the vector space of $\boldsymbol{X}$.

$$\varepsilon_{\text{parareal}} = \max_{1 \leq n \leq N-1} \| \boldsymbol{X}_n^k - \mathcal{F}(\boldsymbol{X}_{n-1}^k) \| \tag{2.47}$$

The iterative process ends when the error falls below a defined threshold.

2.5.2. Periodic Parareal Extensions: PP-IC and PP-PC

The PP-IC and the PP-PC pose two approaches that modify the Parareal in order to tackle time-periodic simulation problems [29]. The necessary iteration steps along the PP-IC and PP-PC are almost identical to the ones described above for the Parareal. To illustrate the steps, a periodic IVP is considered. The general case for an ODE with periodic boundary condition reads:

$$\boldsymbol{x}'(t) = \boldsymbol{f}(t, \boldsymbol{x}(t)) \tag{2.48}$$

$$\boldsymbol{x}(0) = \boldsymbol{x}(T), \tag{2.49}$$

in the time interval

$$t \in (0, T]. \tag{2.50}$$

The necessary iteration steps for the PP-IC are derived by introducing an additional time-periodic condition in each iteration step. The update equation for the PP-IC reads:

$$\boldsymbol{X}_n^{k+1} = \mathcal{F}(\boldsymbol{X}_{n-1}^k) + \mathcal{G}(\boldsymbol{X}_{n-1}^{k+1}) - \mathcal{G}(\boldsymbol{X}_{n-1}^k) \tag{2.51}$$

$$\boldsymbol{X}_0^{k+1} = \boldsymbol{X}_N^{k+1}. \tag{2.52}$$

The PP-IC only differs from the standard Parareal in the additional update of the IC with the end value of the previous iteration. The PP-IC is also sometimes referred to as a forward-in-time Parareal, since the update of the initial condition is always propagated over the length of one period.

Resultingly, the PP-IC might result in a slow convergence rate if the transient process throughout the solution of the analyzed system is very long. The possible gain lies in the subsequent parallelization of each period of the solution. Following this, the possible performance gain of the PP-IC compared to the sequential solution is particularly large if the period length is long compared to the constants of the problem.

Another advantage of the PP-IC is its non-intrusiveness. The PP-IC does not require a further insight in the numerical problem and therefore can be applied as a black box method in the same manner as the standard Parareal.

Similarly to the termination criterion of the Parareal (2.47), the error of the PP-IC iteration is quantified by a jump condition. In addition to the quantification of the maximum jump out of all the subintervals, the jump between the final solution of the iteration with its initial value is used as a further termination criterion. When the jump converges to zero, a steady state is reached. The error quantification for the PP-IC reads:

$$\varepsilon_{\text{PP-IC}} = \max\left\{\varepsilon^k_{\text{parareal}}, \|\boldsymbol{X}^k_n - \mathcal{F}(\boldsymbol{X}^k_{n-1})\|\right\}. \tag{2.53}$$

The second approach to implement a periodic extension of the Parareal is the PP-PC. The PP-PC introduces a coupling between the terminal value of the iteration for one period and its initial value. As opposed to the PP-IC, this coupling is not based on a loose coupling through a forward iteration, but rather by introducing an additional implicit update equation for the initial value. The modified update for the PP-PC reads:

$$\boldsymbol{X}^{k+1}_n = \mathcal{F}(\boldsymbol{X}^k_{n-1}) + \mathcal{G}(\boldsymbol{X}^{k+1}_{n-1}) - \mathcal{G}(\boldsymbol{X}^k_{n-1}) \tag{2.54}$$

$$\boldsymbol{X}^{k+1}_0 = \mathcal{F}(\boldsymbol{X}^k_{N-1}) + \mathcal{G}(\boldsymbol{X}^{k+1}_{N-1}) - \mathcal{G}(\boldsymbol{X}^k_{N-1}). \tag{2.55}$$

This update is implicit, as the initial value at $\boldsymbol{X}^{k+1}_0$ in each iteration is obtained by the terminal value of the same iteration $\mathcal{G}(\boldsymbol{X}^{k+1}_{N-1})$. This implicity can be relaxed by an additional fixed point iteration [29]. Application of the fixed point iteration, i.e. to the PP-PC iteration at iteration step $k+1$, reads:

$$\boldsymbol{X}^{k+1,s+1}_0 = \mathcal{G}(\boldsymbol{X}^{k+1,s}_{N-1}) + \mathcal{F}(\boldsymbol{X}^k_{N-1}) - \mathcal{G}(\boldsymbol{X}^k_{N-1}), \tag{2.56}$$

where s is the index of the inner fixed point iteration.

Usually, the Jacobi method is used for the fixed point iteration in the PP-PC [29, 69]. The Jacobi method is a general iterative algorithm that is

used to determine the solutions of diagonally dominant systems of linear equations [69]. Resultingly, Eq. (2.56) must be written in a matrix form for the Jacobi method to be applicable [27]. Using the abbreviation:

$$\boldsymbol{b}_n^k = \mathcal{F}(\boldsymbol{X}_{n-1}^k) - \mathcal{G}(\boldsymbol{X}_{n-1}^k), \tag{2.57}$$

the matrix form reads:

$$\begin{bmatrix} \boldsymbol{X}_0^{k+1,s+1} \\ \boldsymbol{X}_1^{k+1,s+1} \\ \vdots \\ \boldsymbol{X}_{N-1}^{k+1,s+1} \end{bmatrix} = \begin{bmatrix} 0 & & & \mathcal{G}(\cdot) \\ \mathcal{G}(\cdot) & 0 & & \\ & \ddots & \ddots & \\ & & \mathcal{G}(\cdot) & 0 \end{bmatrix} \begin{bmatrix} \boldsymbol{X}_N^{k+1,s} \\ \boldsymbol{X}_1^{k+1,s} \\ \vdots \\ \boldsymbol{X}_{N-1}^{k+1,s} \end{bmatrix} + \begin{bmatrix} \boldsymbol{b}_N^k \\ \boldsymbol{b}_1^k \\ \vdots \\ \boldsymbol{b}_{N-1}^k \end{bmatrix}. \tag{2.58}$$

Evidently, in Eq. (2.58), the calculation processed for the discrete solution values $\boldsymbol{X}_n^{k+1,s+1}$ for $n = 0$ to $N-1$ are independent. This independence resolves the previously mentioned implicity and makes the PP-PC problem solvable as a black box approach. However, it must be noted that this iteration relaxes the periodicity constraint. As a result, the iteration might not provide a converged solution instantly but rather requires several Jacobi iterations to approach a solution, decreasing performance [45].

3. Sensitivity Analysis for Electric Circuits

In general, sensitivity analysis calculates the influence of a design parameter p in the numerical circuit problem on a defined quantity of interest (QoI) $u(\boldsymbol{x}(p))$. In circuits, design parameters are the values of the circuit devices such as resistors R, capacitors C or inductors L. The QoI $u(\boldsymbol{x}(p))$ is often a voltage or current in the circuit, but it can also be defined as a derived quantity such as a power loss. The methods developed in this thesis are limited to gradient based sensitivity analysis methods. This is firstly a result of the previously implemented sensitivity analysis chain developed in previous works throughout the project [12, 81, 74]. Secondly, particularly adjoint based sensitivity analysis methods are more suited for very large parameter spaces compared to global sensitivity analysis [82]. The parameter space in the used applications often exceeds several thousand elements, especially if the circuit problem is extended with EEC elements modeling parasitic effects.

Obtaining the numerical value of the sensitivity for a QoI w.r.t. a design parameter $\mathrm{d}u(\boldsymbol{x}(p))/\mathrm{d}p$ from sensitivity of a solution vector $\mathrm{d}\boldsymbol{x}(p)/\mathrm{d}p$ is performed through the chain rule:

$$\frac{\mathrm{d}u(\boldsymbol{x}(p))}{\mathrm{d}p} = \frac{\partial u(\boldsymbol{x}(p))}{\partial \boldsymbol{x}(p)} \frac{\mathrm{d}\boldsymbol{x}(p)}{\mathrm{d}p}. \tag{3.1}$$

If $\boldsymbol{x}$ consists of the node potentials of a circuit solution, and the QoI u is an edge voltage within the circuit, this mapping operator is an incidence

vector where the value at the corresponding node indices is either 1 or -1, depending on the defined direction of the edge voltage.

This chapter presents fundamentals of sensitivity analysis methods used throughout this thesis. These fundamentals are limited to gradient based sensitivity analysis methods, since variance based sensitivities were not used in this thesis. The chapter is destinguished between static, transient and harmonic systems. In each of these three subdomains, different direct sensitivity analysis (DSA) [54] and adjoint sensitivity analysis (ASA) approaches are presented.

3.1. Sensitivity Analysis for DC Systems

First, the sensitivity analysis for DC systems is introduced. DC systems are simplest for sensitivity analysis, as the equation system contains no complex phasors as in AC systems, and as the equation system has a simpler structure than for transient problems. Static circuits are usually limited to resistor circuits, since no devices can be present that would involve a time derivative to relate voltages and currents [20]. This follows from the property of capacitors and inductors which exhibit transients due to their energy storage capability. Originally, ASA was published for circuits and derived using Tellegen's theorem [8, 84]. Tellegen's theorem is briefly introduced and utilized for the adjoint sensitivity analysis in appendix A.2. Beginning this chapter, the DSA and the ASA are derived based on the previously introduced equation system for circuits. DSA solves for the sensitivity by one additional DC solver run for the sensitivity analysis w.r.t. all design parameters p and calculates the sensitivities for all QoIs in a post-processing step. In contrast, ASA solves one additional adjoint system for each QoI that can be utilized to analyze the sensitivities w.r.t. all design parameters p in a post processing step.

3.1.1. Direct Sensitivity Analysis

DSA is an approach that uses symbolic differentiation of the equation system w.r.t. the model parameters p [54]. The DSA is a better choice compared to conventional numerical differentiation methods, as it does not suffer from issues with highly dynamic systems and small design parameter values as explained in sec. 1.1. The QoI does not directly depend on the model parameters p. But, the QoI u indirectly depends on p through the system solution $u = u(\boldsymbol{x}(p))$. Consequently, calculation of the sensitivity $\mathrm{d}u/\mathrm{d}p$ also involves a previous calculation of the gradient $\mathrm{d}\boldsymbol{x}/\mathrm{d}p$ [13]. To solve for the sensitivity information $\mathrm{d}\boldsymbol{x}/\mathrm{d}p$ through DSA, the entire equation (2.18) is derived w.r.t. p. The independent source terms $\boldsymbol{i}_\mathrm{s}$ are assumed to be independent of p. The derived equation then follows as:

$$\boldsymbol{A}\frac{\mathrm{d}\boldsymbol{x}}{\mathrm{d}p} + \frac{\mathrm{d}\boldsymbol{A}}{\mathrm{d}p}\boldsymbol{x} = 0. \tag{3.2}$$

Note here that the derivative $\mathrm{d}\boldsymbol{A}/\mathrm{d}p$ is very sparse, since the design parameters p are variables in the entries of matrix $\boldsymbol{A}$. Resultingly, the derivative matrix $\mathrm{d}\boldsymbol{A}/\mathrm{d}p$ is only nonzero on indices corresponding to nodes or edges where the device for the respective parameter p is attached. Equation (3.2) can easily be solved for the sensitivity $\mathrm{d}\boldsymbol{x}/\mathrm{d}p$. But, especially for the sensitivity analysis w.r.t. many design parameters p, the solution is costly as it involves one linear system solution for each design parameter p.

3.1.2. Adjoint Sensitivity Analysis

ASA eliminates the necessity for many necessary solutions of Eq. (3.2). Resultingly, ASA is very efficient for sensitivity analysis in large parameter spaces. The ASA can be derived from the DSA equation (3.2). First, Eq. (3.2) is solved for $\mathrm{d}\boldsymbol{x}/\mathrm{d}p$

$$\frac{\mathrm{d}\boldsymbol{x}}{\mathrm{d}p} = -\boldsymbol{A}^{-1}\frac{\mathrm{d}\boldsymbol{A}}{\mathrm{d}p}\boldsymbol{x}. \tag{3.3}$$

In a second step, the equation is modified with the previously defined mapping operator (3.1) to obtain the sensitivity for the QoI u

$$\frac{\mathrm{d}u}{\mathrm{d}p} = -\left(\frac{\partial u}{\partial \boldsymbol{x}}\right)^{\mathsf{T}} \boldsymbol{A}^{-1} \frac{\mathrm{d}\boldsymbol{A}}{\mathrm{d}p}\boldsymbol{x}. \tag{3.4}$$

Since this analysis still involves a matrix product with the dense inverse of the system matrix $\boldsymbol{A}^{-1}$ for every design parameter p to be analyzed, additional considerations are necessary. Here, the definition of the adjoint system which requires one additional solver run with the system matrix is used

$$\boldsymbol{A}^{\mathsf{T}}\boldsymbol{\lambda} = \frac{\partial u}{\partial \boldsymbol{x}}. \tag{3.5}$$

The resulting adjoint solution vector $\boldsymbol{\lambda}$ can be substituted into (3.4), reformulating the matrix-matrix multiplication to a vector-matrix multiplication. Conveniently, the vector-matrix multiplication with $\boldsymbol{\lambda}$ involves much fewer operations than a matrix-matrix multiplication. Namely, using a naive matrix multiplication approach, the complexity is reduced from $\mathcal{O}\left(n^3\right)$ to $\mathcal{O}\left(n^2\right)$ with $n \times n$ being the dimension of matrix $\boldsymbol{A}$ [18]. This vector-matrix multiplication delivers the result for the ASA as:

$$\frac{\mathrm{d}u}{\mathrm{d}p} = -\boldsymbol{\lambda}^{\mathsf{T}} \frac{\mathrm{d}\boldsymbol{A}}{\mathrm{d}p}\boldsymbol{x}. \tag{3.6}$$

Note here that the adjoint solution can be repurposed for the sensitivity analysis w.r.t. all design parameters p in Eq. (3.6). However, the adjoint solution has to be calculated separately for each QoI. This makes the ASA particularly performant for sensitivity analysis in large parameter spaces for one or a few QoIs.

3.2. Sensitivity Analysis for Transient Systems

In transient systems, the sensitivity analysis is not as simple, as the equation system cannot be represented by only one system matrix. As introduced in section 2.3.2, transient circuit analysis involves solving a system of DAEs which describe the time dependent system behavior. Because transient simulations require the sequential, stepwise solution at every timestep, the sensitivity analysis must be performed sequentially for each timestep as well. In contrast to static systems, two different types of QoIs are considered in transient systems. Firstly, QoIs can be defined as the solution such as a voltage, current or power loss corresponding to a specific time instance:

$$u(\boldsymbol{x}(t)), \tag{3.7}$$

where $\boldsymbol{x}(t)$ is the solution vector at the observed time instance. Secondly, integrated QoIs are considered, which are obtained as the integral over the entire observed operation time:

$$U = \int_{t_0}^{t_\text{end}} u(\boldsymbol{x}(t)) \, \mathrm{d}t. \tag{3.8}$$

In this section, the DSA is analogously introduced as for static systems. Based on the DSA, ASA is derived for the transient case.

3.2.1. Transient Direct Sensitivity Analysis

Analogously to the static derivation, DSA for the transient case is obtained by symbolic derivation of the equation system used for the system solution (2.24) w.r.t. the respective design parameter p:

$$\frac{\mathrm{d}\boldsymbol{F}(t)}{\mathrm{d}p} = \boldsymbol{J}_\mathrm{C}(t)\frac{\mathrm{d}\dot{\boldsymbol{x}}(t)}{\mathrm{d}p} + \boldsymbol{J}_\mathrm{G}(t)\frac{\mathrm{d}\boldsymbol{x}(t)}{\mathrm{d}p} + \frac{\mathrm{d}\boldsymbol{J}_\mathrm{C}(t)}{\mathrm{d}p}\dot{\boldsymbol{x}}(t) + \frac{\mathrm{d}\boldsymbol{J}_\mathrm{G}(t)}{\mathrm{d}p}\boldsymbol{x}(t) = 0. \tag{3.9}$$

Eq. (3.9) is the formulation for the DSA of a nonlinear transient circuit problem. Because the sensitivities for different QoIs can be obtained from the solution of (3.9) in post processing, the numerical complexity of the DSA is nearly independent of the number of QoIs. DSA requires the solution of the transient circuit problem w.r.t. the solution vector $\boldsymbol{x}(t)$ as a first step. Based on that, the relation:

$$\boldsymbol{i}_{\mathrm{s,DSA}} = \frac{\mathrm{d}\boldsymbol{J}_{\mathrm{C}}(t)}{\mathrm{d}p}\dot{\boldsymbol{x}}(t) + \frac{\mathrm{d}\boldsymbol{J}_{\mathrm{G}}(t)}{\mathrm{d}p}\boldsymbol{x}(t) \tag{3.10}$$

can be considered as a source term, because both the transient solution $\boldsymbol{x}(t)$ is known from the forward transient circuit solution and the derivatives of the Jacobians $\mathrm{d}\boldsymbol{J}_{\mathrm{G}}/\mathrm{d}p$ and $\mathrm{d}\boldsymbol{J}_{\mathrm{C}}/\mathrm{d}p$ may be assembled analytically. Following this, Eq. (3.9) can be analogously solved for $\mathrm{d}\boldsymbol{x}/\mathrm{d}p$ equivalently to a general DAE system. As the analysis already involves solving the derivative $\mathrm{d}\dot{\boldsymbol{x}}/\mathrm{d}p$ for every time instance, the complexity for the DSA is not larger than for the circuit problem itself for large numbers of time instances. Throughout the DSA, individual solutions of Eq. (3.9) are required for each design parameter. As a result, DSA is numerically expensive if the sensitivity w.r.t. many design parameters p must be analyzed.

3.2.2. Transient Adjoint Sensitivity Analysis

ASA was originally published for transient circuit analysis by Rohrer and Director in 1969 [21]. Similarly to the DC case presented in sec. 3.1, the ASA is derived based on DSA. In transient circuit problems, ASA is not as advantageous as in the DC case for every application. In particular, if time dependent sensitivities must be analyzed, the ASA can fall behind DSA since each time instance has to be handled as a separate QoI. Resultingly, the trade off involves choosing the appropriate method by weighing the number of parameters p against the number of QoIs u.

To obtain the ASA from the DSA in the transient case, the differential equation (3.9) is integrated over time and $\boldsymbol{\lambda}$ is introduced as a Lagrange

multiplier:

$$\int_{t_0}^{t_{\text{end}}} \boldsymbol{\lambda}^{\mathsf{T}}(t, t_{\text{end}}) \Bigg(\boldsymbol{J}_{\text{C}}(t) \frac{\mathrm{d}\dot{\boldsymbol{x}}(t)}{\mathrm{d}p} + \boldsymbol{J}_{\text{G}}(t) \frac{\mathrm{d}\boldsymbol{x}(t)}{\mathrm{d}p} + \frac{\mathrm{d}\boldsymbol{J}_{\text{C}}(t)}{\mathrm{d}p} \dot{\boldsymbol{x}}(t) + \frac{\mathrm{d}\boldsymbol{J}_{\text{G}}(t)}{\mathrm{d}p} \boldsymbol{x}(t) \Bigg) \, \mathrm{d}t = 0. \quad (3.11)$$

With integration by parts, the time derivative $\mathrm{d}\dot{\boldsymbol{x}}(t)/\mathrm{d}p$ vanishes. The start and end values of $\mathrm{d}\boldsymbol{x}(t)/\mathrm{d}p$ have to be given explicitly in the general case:

$$\begin{aligned} \int_{t_0}^{t_{\text{end}}} \left(-\dot{\boldsymbol{\lambda}}^{\mathsf{T}}(t, t_{\text{end}}) \boldsymbol{J}_{\text{C}}(t) + \boldsymbol{\lambda}^{\mathsf{T}}(t, t_{\text{end}}) \boldsymbol{J}_{\text{G}}(t) \right) \frac{\mathrm{d}\boldsymbol{x}(t)}{\mathrm{d}p} \, \mathrm{d}t \\ = - \int_{t_0}^{t_{\text{end}}} \boldsymbol{\lambda}^{\mathsf{T}}(t, t_{\text{end}}) \left(\frac{\mathrm{d}\boldsymbol{J}_{\text{C}}(t)}{\mathrm{d}p} \dot{\boldsymbol{x}}(t) + \frac{\mathrm{d}\boldsymbol{J}_{\text{G}}(t)}{\mathrm{d}p} \boldsymbol{x}(t) \right) \mathrm{d}t \\ - \left[\boldsymbol{\lambda}^{\mathsf{T}}(t, t_{\text{end}}) \boldsymbol{J}_{\text{C}}(t) \frac{\mathrm{d}\boldsymbol{x}(t)}{\mathrm{d}p} \right]_{t_0}^{t_{\text{end}}}, \quad (3.12) \end{aligned}$$

with boundary conditions

$$\frac{\mathrm{d}\boldsymbol{x}}{\mathrm{d}p}(t = t_0) = 0 \quad (3.13)$$

and

$$\boldsymbol{\lambda}(t = t_{\text{end}}, t_{\text{end}}) = 0. \quad (3.14)$$

Without loss of generality, the Lagrange multiplier $\boldsymbol{\lambda}$ is chosen as the solution of the adjoint equation system:

$$\boldsymbol{J}_{\text{C}}^{\mathsf{T}}(t) \dot{\boldsymbol{\lambda}}(t, t_{\text{end}}) - \boldsymbol{J}_{\text{G}}^{\mathsf{T}}(t) \boldsymbol{\lambda}(t, t_{\text{end}}) = \frac{\partial u(\boldsymbol{x}(t))}{\partial \boldsymbol{x}(t)}. \quad (3.15)$$

The adjoint solution is found by solving Eq. (3.15) backward in time in order to enforce the necessary terminal condition (3.14) for t_{end}.

When substituting (3.15) into (3.12), we get:

$$-\int_{t_0}^{t_{\text{end}}} \left(\frac{\partial u(\boldsymbol{x}(t))}{\partial \boldsymbol{x}(t)}\right)^{\mathsf{T}} \frac{\mathrm{d}\boldsymbol{x}(t)}{\mathrm{d}p}\,\mathrm{d}t = -\int_{t_0}^{t_{\text{end}}} \boldsymbol{\lambda}^{\mathsf{T}}(t, t_{\text{end}}) \left(\frac{\mathrm{d}\boldsymbol{J}_{\mathrm{C}}(t)}{\mathrm{d}p}\dot{\boldsymbol{x}}(t) + \frac{\mathrm{d}\boldsymbol{J}_{\mathrm{G}}(t)}{\mathrm{d}p}\boldsymbol{x}(t)\right)\,\mathrm{d}t. \quad (3.16)$$

Resubstitution of $\boldsymbol{s}$ and multiplication with -1 yields the integration for the sensitivity of the QoI u:

$$\frac{\mathrm{d}U}{\mathrm{d}p} = \int_{t_0}^{t_{\text{end}}} \frac{\mathrm{d}u}{\mathrm{d}p}(t)\,\mathrm{d}t = \int_{t_0}^{t_{\text{end}}} \boldsymbol{\lambda}^{\mathsf{T}}(t, t_{\text{end}}) \left(\frac{\mathrm{d}\boldsymbol{J}_{\mathrm{C}}(t)}{\mathrm{d}p}\dot{\boldsymbol{x}}(t) + \frac{\mathrm{d}\boldsymbol{J}_{\mathrm{G}}(t)}{\mathrm{d}p}\boldsymbol{x}(t)\right)\,\mathrm{d}t. \quad (3.17)$$

To obtain the sensitivity for the voltage at a certain time step, the generalized version of Leibniz integral rule can be applied to the term on the right hand side [25]. It states that

$$\begin{aligned}
&\frac{\mathrm{d}}{\mathrm{d}t_{\text{end}}} \int_{t_0}^{t_{\text{end}}} G(\boldsymbol{x}, \dot{\boldsymbol{x}}, t, t_{\text{end}})\,\mathrm{d}t \\
&= G(\boldsymbol{x}, \dot{\boldsymbol{x}}, t_{\text{end}}) \frac{\mathrm{d}t_{\text{end}}}{\mathrm{d}t_{\text{end}}} - G(\boldsymbol{x}, \dot{\boldsymbol{x}}, t_0) \frac{\mathrm{d}t_0}{\mathrm{d}t_{\text{end}}} + \int_{t_0}^{t_{\text{end}}} \frac{\partial G(\boldsymbol{x}, \dot{\boldsymbol{x}}, t, t_{\text{end}})}{\partial t_{\text{end}}}\,\mathrm{d}t \\
&= G(\boldsymbol{x}, \dot{\boldsymbol{x}}, t_{\text{end}}) - G(\boldsymbol{x}, \dot{\boldsymbol{x}}, t_0) \frac{\mathrm{d}t_0}{\mathrm{d}t_{\text{end}}} + \int_{t_0}^{t_{\text{end}}} \frac{\partial G(\boldsymbol{x}, \dot{\boldsymbol{x}}, t, t_{\text{end}})}{\partial t_{\text{end}}}\,\mathrm{d}t. \quad (3.18)
\end{aligned}$$

$\mathrm{d}u/\mathrm{d}p$ does not depend on t_{end} in equation (3.17). Resultingly, the integral is eliminated by the derivation without application of Leibniz integral rule

to the left hand side of Eq. (3.17). Applied to equation (3.17), this yields

$$\begin{aligned}\frac{\mathrm{d}u}{\mathrm{d}p}(t=t_{\text{end}}) = \boldsymbol{\lambda}^{\mathsf{T}}(t_{\text{end}},t_{\text{end}})\left(\frac{\mathrm{d}\boldsymbol{J}_{\mathrm{C}}(t_{\text{end}})}{\mathrm{d}p}\dot{\boldsymbol{x}}(t_{\text{end}}) + \frac{\mathrm{d}\boldsymbol{J}_{\mathrm{G}}(t_{\text{end}})}{\mathrm{d}p}\boldsymbol{x}(t_{\text{end}})\right)\\ + \boldsymbol{\lambda}^{\mathsf{T}}(t_0,t_{\text{end}})\left(\frac{\mathrm{d}\boldsymbol{J}_{\mathrm{C}}(t_0)}{\mathrm{d}p}\dot{\boldsymbol{x}}(t_0) + \frac{\mathrm{d}\boldsymbol{J}_{\mathrm{G}}(t_0)}{\mathrm{d}p}\boldsymbol{x}(t_0)\right)\frac{\mathrm{d}t_0}{\mathrm{d}t_{\text{end}}}\\ + \int_{t_0}^{t_{\text{end}}}\frac{\partial\boldsymbol{\lambda}^{\mathsf{T}}(t,t_{\text{end}})}{\partial t_{\text{end}}}\left(\frac{\mathrm{d}\boldsymbol{J}_{\mathrm{C}}(t)}{\mathrm{d}p}\dot{\boldsymbol{x}}(t) + \frac{\mathrm{d}\boldsymbol{J}_{\mathrm{G}}(t)}{\mathrm{d}p}\boldsymbol{x}(t)\right)\mathrm{d}t.\end{aligned} \tag{3.19}$$

The first term on the right hand side is 0 as the adjoint solution $\boldsymbol{\lambda}$ is 0 at time t_{end} per definition. The second term on the right hand side vanishes, as Eq. (3.13) implies that $t_0 = 0$. The sensitivity for the QoI at time instance t_{end} is therefore given by

$$\begin{aligned}&\frac{\mathrm{d}u}{\mathrm{d}p}(t=t_{\text{end}})\\ &\qquad= \int_{t_0}^{t_{\text{end}}}\frac{\partial\boldsymbol{\lambda}^{\mathsf{T}}(t,t_{\text{end}})}{\partial t_{\text{end}}}\left(\frac{\mathrm{d}\boldsymbol{J}_{\mathrm{C}}(t)}{\mathrm{d}p}\dot{\boldsymbol{x}}(t) + \frac{\mathrm{d}\boldsymbol{J}_{\mathrm{G}}(t)}{\mathrm{d}p}\boldsymbol{x}(t)\right)\mathrm{d}t.\end{aligned} \tag{3.20}$$

Alternatively, the sensitivity at specific time instances can be analyzed through modification of the QoI. Defining the modified QoI $q(t)$ operator as:

$$q(u(\boldsymbol{x}(t)),t_{\text{end}}) = \delta(t-t_{\text{end}})u(\boldsymbol{x}(t)), \tag{3.21}$$

where $\delta(t-t_{\text{end}})$ is the discrete delta operator. The modified mapping operator is found analogously to Eq. (3.1) as:

$$\frac{\mathrm{d}q}{\mathrm{d}p}(t) = \frac{\partial q(u(\boldsymbol{x}(t)),t_{\text{end}})}{\partial\boldsymbol{x}(t)}\frac{\mathrm{d}\boldsymbol{x}(t)}{\mathrm{d}p} = \delta(t-t_{\text{end}})\frac{\partial u(\boldsymbol{x}(t))}{\partial\boldsymbol{x}(t)}\frac{\mathrm{d}\boldsymbol{x}(t)}{\mathrm{d}p}. \tag{3.22}$$

using the mapping operator $\mathrm{d}q/\mathrm{d}\boldsymbol{x}$ as the rhs for the modified adjoint problem:

$$\boldsymbol{J}_{\mathrm{C}}^{\mathsf{T}}(t)\dot{\boldsymbol{\lambda}}_{\delta}(t,t_{\text{end}}) - \boldsymbol{J}_{\mathrm{G}}^{\mathsf{T}}(t)\boldsymbol{\lambda}_{\delta}(t,t_{\text{end}}) = \frac{\partial q(u(\boldsymbol{x}(t)),t_{\text{end}})}{\partial\boldsymbol{x}(t)}, \tag{3.23}$$

using the modified mapping operator as well as the adjoint solution $\boldsymbol{\lambda}_\delta$ for the integral evaluation as shown in Eq. (3.17), the sensitivity at the time instance t_{end} is obtained as:

$$\begin{aligned}\frac{\mathrm{d}u}{\mathrm{d}p}(t = t_{\text{end}}) &= \int_{t_0}^{t_{\text{end}}} \frac{\mathrm{d}q}{\mathrm{d}p}(t)\ \mathrm{d}t \\ &= \int_{t_0}^{t_{\text{end}}} \boldsymbol{\lambda}_\delta^{\mathsf{T}}(t, t_{\text{end}}) \left(\frac{\mathrm{d}\boldsymbol{J}_{\mathrm{C}}(t)}{\mathrm{d}p} \dot{\boldsymbol{x}}(t) + \frac{\mathrm{d}\boldsymbol{J}_{\mathrm{G}}(t)}{\mathrm{d}p} \boldsymbol{x}(t) \right) \mathrm{d}t. \end{aligned} \tag{3.24}$$

The integral on the left hand side in Eq. (3.24) results in the sensitivity of the unmodified QoI at a single time instance due to the sifting property of the delta operator [58]. This approach is advantageous if only few time instances that are scattered over time must be analyzed, since only one single adjoint solution is required for the sensitivity at one specific time instance. A possible downside of this approach is the increased stiffness of the adjoint DAE that results from the delta excitation [32].

3.3. Sensitivity Analysis for Harmonic Systems

Harmonic systems can generally be simulated in frequency domain if only linear devices are contained. One advantage of using frequency domain methods is the avoidance of a long transient simulation in which the solution for each time instance depends on the previous timestep. Analogously to the AC case, the complex phasor representation is used to indicate the frequency dependence of the variables. As in section 2.3.3, underscores are used for the phasor representation.

3.3.1. Direct Sensitivity Analysis in Frequency Domain

Analogously to the static and transient cases, DSA is derived by symbolic differentiation of the equation system from Eq.(2.27) for the sensitivity

analysis in AC domain:

$$\frac{\mathrm{d}\underline{\boldsymbol{F}}(\boldsymbol{x})}{\mathrm{d}p} = \frac{\mathrm{d}\underline{\boldsymbol{A}}}{\mathrm{d}p}\underline{\boldsymbol{x}} + \underline{\boldsymbol{A}}\frac{\mathrm{d}\underline{\boldsymbol{x}}}{\mathrm{d}p} = 0. \tag{3.25}$$

Solving Eq.(3.25) for $\mathrm{d}\underline{\boldsymbol{x}}/\mathrm{d}p$ gives the sensitivity in frequency in the same way as derived for static systems.

Die AC DSA shows identical disadvantages as for the other formulations, namely, the decreasing performance for the sensitivity analysis w.r.t. many design parameters p. A way to improve on this is the ASA in frequency domain.

3.3.2. Adjoint Sensitivity Analysis in Frequency Domain

In order to avoid the solution of a different equation system for each design parameter p using Eq. (3.25), the sensitivity for QoI u can be obtained defining the adjoint system for the AC analysis:

$$\underline{\boldsymbol{A}}^{\mathsf{H}}\underline{\boldsymbol{\lambda}} = \frac{\partial \underline{u}}{\partial \underline{\boldsymbol{x}}} \tag{3.26}$$

The system is mimetic to the static case as in Eq. (3.5). The major difference lies in the complex nature of the equation system, and, resultingly, the usage of the Hermitian adjoint of the system matrix in the adjoint system as opposed to the transpose in the static case. The sensitivity of the QoI $\underline{u}$ w.r.t. the design parameter p followingly also involves the Hermitian adjoint of the adjoint solution $\underline{\boldsymbol{\lambda}}$ and is given as:

$$\frac{\mathrm{d}\underline{u}}{\mathrm{d}p} = -\underline{\boldsymbol{\lambda}}^{\mathsf{H}}\frac{\mathrm{d}\underline{\boldsymbol{A}}}{\mathrm{d}p}\underline{\boldsymbol{x}}. \tag{3.27}$$

The adjoint solution $\underline{\boldsymbol{\lambda}}$ can be reused for each design parameter p but is required to be calculated for every frequency separately. Since both operations are numerically cheap, especially compared to transient simulations,

this method is to be preferred for time-periodic linear circuits. But, for nonlinear systems, the analysis cannot be performed independently for each frequency and therefore the AC ASA is not naturally applicable. However, with some considerations the HB method introduced in section 2.4 can be utilized for sensitivity analysis.

3.3.3. Harmonic Direct Sensitivity Analysis

For nonlinear harmonic systems, the HB method can be utilized for sensitivity analysis. Analogously to the previously introduced cases, DSA is derived by symbolic differentiation of the reverse initial condition from Eq.(2.27) for the HB method. Based on the harmonic balance equation system (2.35), the symbolic differentiation w.r.t. the design parameters p yields:

$$\frac{\mathrm{d}\underline{\boldsymbol{F}}(\underline{\boldsymbol{x}})}{\mathrm{d}p} = \frac{\mathrm{d}\underline{\boldsymbol{J}}}{\mathrm{d}p}\underline{\boldsymbol{x}} + \underline{\boldsymbol{J}}\frac{\mathrm{d}\underline{\boldsymbol{x}}}{\mathrm{d}p} = 0. \tag{3.28}$$

The Jacobian in (3.28) is borrowed from the converged solution of the nominal problem [4]. Here, the DSA requires solving a linear system.

If many design parameters p are analyzed, the numerical efficiency of HB based DSA decreases, because solution of Eq.(3.28) involves a matrix multiplication with the dense matrix $\underline{\boldsymbol{J}}^{-1}$. This dense matrix multiplication can be avoided by introducing an HB based ASA.

3.3.4. Harmonic Adjoint Sensitivity Analysis

Adjoint sensititvity analysis in combination with HB was originally proposed by Bandler et al. [4] in 1988. The approach uses an HB analysis to simulate the circuit problem. The Hermitian adjoint of the Jacobian that was linearized for the circuit solution is then used as the system matrix for the adjoint system. The adjoint system for the HB case (3.28) therefore

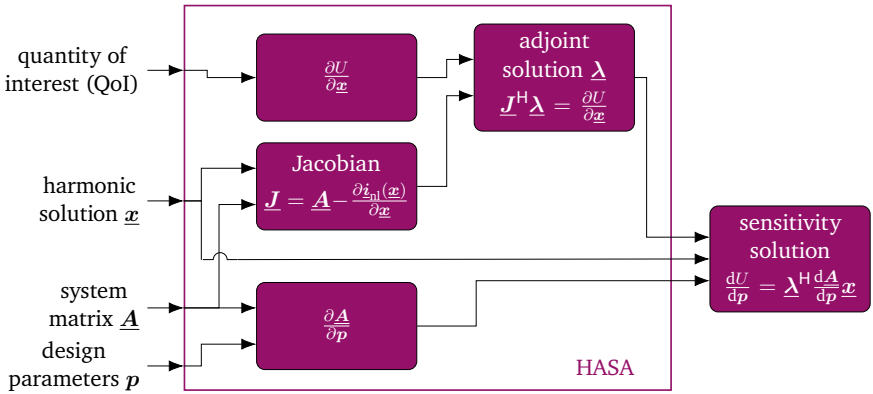

Figure 3.1.: Flowchart for the HB based ASA (HASA)

reads:

$$\underline{\boldsymbol{J}}^{\mathsf{H}} \underline{\boldsymbol{\lambda}} = \frac{\partial \underline{u}}{\partial \underline{\boldsymbol{x}}}. \tag{3.29}$$

As the Jacobian does not depend on the adjoint solution $\boldsymbol{\lambda}$, the adjoint problem is linear. The sensitivity of the QoI $\underline{u}$ w.r.t. the design parameter p follows as:

$$\frac{\mathrm{d}\underline{u}}{\mathrm{d}p} = -\left(\frac{\partial \underline{u}}{\partial \underline{\boldsymbol{x}}}\right)^{\mathsf{H}} \underline{\boldsymbol{J}}^{-1} \frac{\mathrm{d}\underline{\boldsymbol{J}}}{\mathrm{d}p} \underline{\boldsymbol{x}} = -\underline{\boldsymbol{\lambda}}^{\mathsf{H}} \frac{\mathrm{d}\underline{\boldsymbol{J}}}{\mathrm{d}p} \underline{\boldsymbol{x}}. \tag{3.30}$$

In frequency domain, the adjoint solution can be reused for all considered frequencies, which eliminates the issues encountered in the transient analysis but increases the number of DoFs for large frequency spaces. Compared to the harmonic direct sensitivity analysis, HB based ASA (HASA) does not contain any dense matrix multiplications, which improves performance. The procedure is outlined in Fig. 3.1.

The issue that remains is the bad performance for strongly nonlinear systems. This is particularly problematic when the Jacobian has to be approximated along many convergence steps of the HB iteration (Eq.(2.27)).

A hybrid time-frequency domain method, that eliminates the issue of many Newton iteration steps, is proposed in the following section.

4. Transient Forward Harmonic Adjoint Sensitivity Analysis

In this chapter, the TFHA is proposed as a new method to calculate sensitivities for the steady state in a nonlinear system. Bandler et al [4] proposes a procedure which uses a forward HB solver in combination with a harmonic adjoint sensitivity anaylsis. This approach was recapitulated in section 3.3.4. It is however not compulsory to obtain the forward solution of the given system by HB for the sole purpose of sensitivity analysis. This option motivates the development of the TFHA method [72]. In a first step, the forward circuit solution $\boldsymbol{x}(t)$ is obtained using a transient solver of choice. The transient solution has to be performed until a periodic steady state is reached. Based on the linearization of the transient solver, the adjoint solution is obtained by a harmonic analysis. This procedure modifies the HB based ASA by taking the forward solution out of the solver loop and thus making it variable. The steps along the TFHA are outlined in the flowchart 4.1.

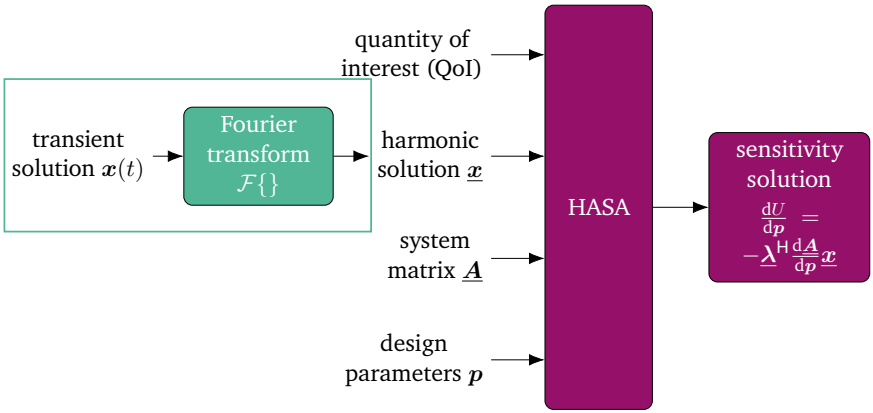

Figure 4.1.: Flowchart for the transient forward harmonic ASA (TFHA). Time domain operations in green, frequency domain operations in purple.

4.1. Harmonic Jacobian Approximation from Transient Solution

Alternatively to the entire HB iteration described in section 2.4, the Jacobian can be calculated based on a given steady state solution, improving efficiency. This approach is advantageous in several cases. Firstly, there are some cases where the HB might show convergence issues, which may occur for oscillating systems or systems with strong nonlinearities [48, 65]. Secondly, in practical applications, the engineers often have available steady state solutions from previous analyses, which can directly be used in further analyses.

Once the solution for the steady state is found, the Jacobian $\underline{\boldsymbol{J}}$ is calculated through Eq. (2.31) using the Fourier transform $\underline{\boldsymbol{x}}$ of the periodic solution $\boldsymbol{x}$. The Jacobian is then used as the system matrix for the adjoint problem. The adjoint solution is obtained by solving Eq. (3.30) in the same way described

in section 2.4. Subsequently, the adjoint solution is combined with the symbolic derivative of system matrix $\mathrm{d}\underline{\boldsymbol{J}}/\mathrm{d}p$ to calculate the sensitivities.

4.2. Error Estimation

Due to the approximation with a finite number of harmonics, the calculation is exposed to information loss which results in a residual error. Since the Newton iteration from the HB analysis is not performed in the same way for the TFHA, it is initially not known if the number of harmonics is sufficient for a desired accuracy. However, one approach involves the principle that a Fourier approximation converges if the number of harmonics approaches infinity [38]. The residual error can be approximated. It is quantified by the Euclidean distance of the residual [3]

$$\mathcal{E}_{\text{abs}} = \left\| \left(\frac{\mathrm{d}u}{\mathrm{d}p} \right)_{\text{exact}} - \left(\frac{\mathrm{d}u}{\mathrm{d}p} \right)_{\text{approx}} \right\|_2 . \tag{4.1}$$

Without prior considerations of the spectral circuit behavior, the sensitivity is determined by iteratively increasing the number of harmonics. The Euclidean distance of the solution with fewer harmonics against the solution with more harmonics quantifies the residual. This is analogous to the Zienkiewicz-Zhu error estimator [95]. The quantification of the relative error (Eq.(4.2)) is finally used as a termination criterion to assess convergence

$$\mathcal{E}_{\text{rel}} \approx \frac{\left\| \left(\frac{\mathrm{d}u}{\mathrm{d}p} \right)_{\text{fine}} - \left(\frac{\mathrm{d}u}{\mathrm{d}p} \right)_{\text{coarse}} \right\|_2}{\left\| \left(\frac{\mathrm{d}u}{\mathrm{d}p} \right)_{\text{fine}} \right\|_2} . \tag{4.2}$$

4.3. Conclusion

The TFHA can perform ASA for time periodic circuit problems with very few numerical simulations. If the simulation must employ an error estimation, multiple solutions of the adjoint problem with increasing numbers of harmonics are required. The dimension of the Jacobian increases with the number of harmonics.

Particularly strongly nonlinear circuits require a large number of harmonics for accurate simulation results [66]. Resultingly, the TFHA is not applicable for these types of circuits. However, the TFHA can be very advantageous for weakly nonlinear circuits with a long transient. Additionally, in comparison to transient ASA, the TFHA scales very good for large parameters spaces. Thus, the TFHA is particularly fast for the ASA in weakly nonlinear large scale circuits.

5. Parallel-in-Time Adjoint Sensitivity Analysis

Parallel-in-time (PinT) methods in combination with adjoint sensitivity analysis (ASA) were introduced in a couple of publications. These approaches include the combination of the paraexp method [26] combined with ASA as introduced in [78]. Apart from that, split time domain methods were previously used to avoid storage issues in ASA. These methods, where the adjoint problem is split into subintervals which are then solved sequentially, are referred to as checkpointing schemes in literature [14]. Particularly focusing on the Parareal method, adjoint systems have previously been utilized to improve the Parareal convergence as shown in [63]. Opposed to that, it is however also advantageous to utilize the Parareal method to speed up the wall-clock time of the ASA [71], which is presented in the following section.

5.1. Parareal Adjoint Sensitivity Analysis

As introduced in section 3.2.2, the calculation of time-dependent sensitivities involves solving multiple adjoint problems, which causes a computational bottleneck. Parallel algorithms can be utilized to cut down wall-clock time. The Parareal algorithm was introduced in section 2.5.1. The adjoint sensitivity analysis finds application only in post-processing after the initial system simulation. The non-intrusiveness of the Parareal allows it to be

utilized for solving both the forward system and the adjoint system.

Some considerations are required for the Parareal to be efficient and stable during the adjoint sensitivity analysis. In particular, the adjoint system is always linear, but can show sharp jumps, particularly for example in switched systems. In these cases, a careful consideration of the subintervals must be taken, because having a subinterval boundary on a sharp jump may prevent Parareal convergence.

The transient ASA benefits from short observed time intervals with a minimal number of analyzed time instances. The complexity of the simulation increases with a larger number of time instances to analyze, as the adjoint solution (3.15) requires an individual backwards integration for each time instance. Nontheless, the use of Parareal accelerates the simulation of each adjoint solution.

The efficiency of the Parareal method is quantified by the total wall-clock time for the simulation of one adjoint solution. The solver used for the fine solution is the same as the sequential solver. The coarse solver is analogous to the fine solver, but it solves only every 100th timestep, leading to a faster but less accurate simulation. In this setup, the Parareal algorithm convergences within two iterations, regardless of the number of subintervals. The adjoint solution for $19.1\,\mathrm{s}$ serves as a reference in the benchmark, as it lies in the middle of the observed time period. The efficiency of the Parareal ASA is assessed using two metrics. The first metric, the speedup

$$S_\mathrm{p} = T_\mathrm{s}/T_\mathrm{p}, \tag{5.1}$$

compares the total parallel wall-clock time (T_p) to the sequential wall-clock time (T_s). The second metric, the parallel efficiency

$$E_\mathrm{p} = S_\mathrm{p}/N, \tag{5.2}$$

puts the speedup in relation to the number of processors N.

Especially when large parallelization is available, i.e. many simulation cores can be used, the speedup of the wall clock time can be significant

in many examples. The examples are presented in chapter 6. But, the Parareal itself does not employ any modifications to the ASA by default. In the following section, a consideration for periodic ASA will be made and derived.

5.2. Periodic Adjoint Sensitivity Analysis

With existing methods, the ASA for periodic problems is performed by calculating the difference of the transient ASA for the begin and the end of the steady state period [56]. This still involves lengthy integrals and requires the circuit solution to be calculated for the entire transient.

Utilizing the PP-PC, the forward simulation can be reduced to a much shorter timespan, especially for problems where the transient is much longer than the steady state period. To utilize that system solution, the transient ASA first needs to be modified to accommodate periodic systems. Originally, the transient ASA requires the initial values of the forward solution $\boldsymbol{x}(t)$ and the adjoint solution $\lambda(t, t_\mathrm{end})$ to be zero at $t = 0$ or $t = t_\mathrm{end}$, respectively. Therefore, some considerations are required first in order to be able to employ the PP-PC in combination with the ASA. For the periodic modification of the transient ASA, the integral for the sensitivity is modified to cover the duration of one period with the period time T_p:

$$\frac{\mathrm{d}U}{\mathrm{d}p} = \int_{(t_\mathrm{m}-T_\mathrm{p})}^{t_\mathrm{m}} \frac{\mathrm{d}u}{\mathrm{d}p}(t)\,\mathrm{d}t = \int_{(t_\mathrm{m}-T_\mathrm{p})}^{t_\mathrm{m}} \boldsymbol{\lambda}^\mathsf{T}(t, t_\mathrm{end}) \left(\frac{\mathrm{d}\boldsymbol{J}_\mathrm{C}}{\mathrm{d}p}\dot{\boldsymbol{x}}(t) + \frac{\mathrm{d}\boldsymbol{J}_\mathrm{G}}{\mathrm{d}p}\boldsymbol{x}(t) \right) \mathrm{d}t - \left[\boldsymbol{\lambda}^\mathsf{T}(t, t_\mathrm{end}) \boldsymbol{J}_\mathrm{C}(\boldsymbol{x}(t)) \frac{\mathrm{d}\boldsymbol{x}}{\mathrm{d}p}(t) \right]_{(t_\mathrm{m}-T_\mathrm{p})}^{t_\mathrm{m}} . \quad (5.3)$$

Consequently, the boundary term on the right hand side can be eliminated

if

$$\boldsymbol{\lambda}^{\mathsf{T}}(t_{\mathrm{m}}, t_{\mathrm{end}})\boldsymbol{J}_{\mathrm{C}}(\dot{\boldsymbol{x}}(t_{\mathrm{m}}))\frac{\mathrm{d}\boldsymbol{x}}{\mathrm{d}p}(t_{\mathrm{m}}) = \boldsymbol{\lambda}^{\mathsf{T}}(t_{\mathrm{m}} - T_{\mathrm{p}}, t_{\mathrm{end}})\boldsymbol{J}_{\mathrm{C}}(\dot{\boldsymbol{x}}(t_{\mathrm{m}} - T_{\mathrm{p}}))\frac{\mathrm{d}\boldsymbol{x}}{\mathrm{d}p}(t_{\mathrm{m}} - T_{\mathrm{p}}). \quad (5.4)$$

This condition is fulfilled if the adjoint solution as well as the forward system solution and the system matrices are periodic. Choosing t_{m} to be a time instance where both the forward and the adjoint solution are in a periodic state, Eq. (5.3) reduces to the integral only without any boundary conditions to consider

$$\frac{\mathrm{d}U}{\mathrm{d}p} = \int_{(t_{\mathrm{m}}-T_{\mathrm{p}})}^{t_{\mathrm{m}}} \frac{\mathrm{d}u}{\mathrm{d}p}(t)\,\mathrm{d}t = \int_{(t_{\mathrm{m}}-T_{\mathrm{p}})}^{t_{\mathrm{m}}} \boldsymbol{\lambda}^{\mathsf{T}}(t, t_{\mathrm{end}}) \left(\frac{\mathrm{d}\boldsymbol{J}_{\mathrm{C}}}{\mathrm{d}p}\dot{\boldsymbol{x}}(t) + \frac{\mathrm{d}\boldsymbol{J}_{\mathrm{G}}}{\mathrm{d}p}\boldsymbol{x}(t) \right) \mathrm{d}t. \quad (5.5)$$

A downside of this approach is the limitation to integrated QoIs, whereas time dependent QoIs can be analyzed using the transient ASA as well. To explain this limitation, the same steps as for the derivation of the time dependent sensitivity analysis using transient ASA are applied here. Using Leibniz integral rule (3.18) for the periodic sensitivity integral (5.3) results in an equation that is similar to the previously derived formulation in (3.19):

$$\begin{aligned}\frac{\mathrm{d}u}{\mathrm{d}p}(t_{\mathrm{m}}) = {} & \boldsymbol{\lambda}^{\mathsf{T}}(t_{\mathrm{m}}, t_{\mathrm{end}}) \left(\frac{\mathrm{d}\boldsymbol{J}_{\mathrm{C}}}{\mathrm{d}p}\dot{\boldsymbol{x}}(t_{\mathrm{m}}) + \frac{\mathrm{d}\boldsymbol{J}_{\mathrm{G}}}{\mathrm{d}p}\boldsymbol{x}(t_{\mathrm{m}}) \right) \\ & - \boldsymbol{\lambda}^{\mathsf{T}}(t_{\mathrm{m}} - T_{\mathrm{p}}, t_{\mathrm{end}}) \left(\frac{\mathrm{d}\boldsymbol{J}_{\mathrm{C}}}{\mathrm{d}p}\dot{\boldsymbol{x}}(t_{\mathrm{m}} - T_{\mathrm{p}}) + \frac{\mathrm{d}\boldsymbol{J}_{\mathrm{G}}}{\mathrm{d}p}\boldsymbol{x}(t_{\mathrm{m}} - T_{\mathrm{p}}) \right) \\ & + \int_{(t_{\mathrm{m}}-T_{\mathrm{p}})}^{t_{\mathrm{m}}} \frac{\partial}{\partial t_{\mathrm{m}}}\boldsymbol{\lambda}^{\mathsf{T}}(t, t_{\mathrm{end}}) \left(\frac{\mathrm{d}\boldsymbol{J}_{\mathrm{C}}}{\mathrm{d}p}\dot{\boldsymbol{x}}(t) + \frac{\mathrm{d}\boldsymbol{J}_{\mathrm{G}}}{\mathrm{d}p}\boldsymbol{x}(t) \right) \mathrm{d}t. \end{aligned} \quad (5.6)$$

In contrast to the transient simulation, the first term on the right hand side in (5.6) is not zero, as the periodic adjoint solution is not set to zero at time t_{end}. But, due to the assumption of periodicity in both the adjoint and the forward system solution, the first terms cancel each other. However, the derivative $\partial/\partial t_{\text{m}} \boldsymbol{\lambda}^{\mathsf{T}}(t, t_{\text{end}})$ is also zero, as $\boldsymbol{\lambda}^{\mathsf{T}}(t, t_{\text{end}})$ does not depend on the period end time t_{m}. Illustratively, this is explained by the property that the integral over one period of a periodic solution is independent of the choice of the start and end times as long as these times are one period apart. As a consequence, the ASA cannot be performed for time dependent QoIs using the periodic ASA.

5.3. Conclusion

Parareal methods are very suitable to speed up the adjoint sensitivity analysis in many cases. The simulation can be sped up with increasing numbers of subintervals as long as the parallel efficiency does not decrease for a given numerical problem. Consequently, the Parareal approach can be used to greatly speed up simulation times, particularly when significant parallelization is available, such as with simulation clusters. Due to the non-intrusiveness of Parareal, the approach can be applied both to the forward circuit simulation as well as the adjoint simulation.

Periodic methods can be additionally utilized to reduce the transient simulation time and additionally shorten the required time interval for the adjoint simulation. With that approach, it is however not possible to analyze the sensitivity w.r.t. every time instance.

Parareal ASA is particularly suitable for sensitivity analysis of circuit problems that require a very large number of time steps which also have very large parameter spaces. Periodic ASA is suitable for the sensitivity analysis of circuits with a long transient where the QoI is one period of steady state operation, which is often the case in power converters. Both

Parareal and PP-PC are applied to different practical examples in chapter 6 to show their advantages.

6. Applications

This chapter presents applications for the developed sensitivity analysis methods. In the first five sections of this chapter, different circuit examples are presented. These circuit examples include an RC-filter and a half-wave rectifier which are very simple circuits to show the feasibility of the sensitivity analysis methods. Furthermore, the proposed methods are used to conduct a sensitivity analysis for a buck converter. This circuit exhibits a very long transient but is comparably small scale. Additionally, an active filter is analyzed using the proposed sensitivity analysis methods. This example has a small bandwidth but a considerable number of design parameters. Moreover, the proposed methods are applied for the sensitivity analysis of a B6 bridge-motor control circuit. This circuit exhibits both broadband behavior and large number of design parameters. In the last two sections of this chapter, the application of these sensitivity analysis methods for active research and development problems is shown. A linear RC-filter circuit will demonstrate the advantages and disadvantages of the algorithms. This example is particularly suitable to show this, since an analytical reference solution can be derived.

6.1. RC-Filter

An RC-filter is an academic example that demonstrates the most basic features of the sensitivity analysis methods. The circuit contains linear elements only and is not oscillatory. The circuit schematic is shown in

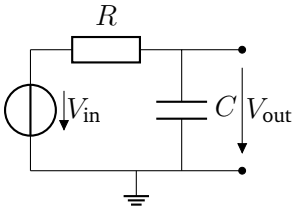

Figure 6.1.: Schematic of the RC-filter.

Fig. 6.1. This form of an RC-filter shows lowpass characteristics. The nominal model parameters are:

- $V_{\text{in}} = \hat{V}_{\text{in}} \sin(\omega t) = (1\,\text{V}) \sin(\omega t)$
- $R = 20\,\Omega$
- $C = 10\,\text{nF}$

The filtering behavior is given by the QoI of the transfer function $V_{\text{out}}/V_{\text{in}}$. As the input amplitude $\hat{V}_{\text{in}}$ is constant, the QoI can be reduced to only V_{out} which will still demonstrate the filtering behavior. This section showcases the most basic functions of the proposed methods in comparison to an analytically available reference. It is possible to find an analytical solution for the transfer function $V_{\text{out}}/V_{\text{in}}$ in time and frequency domain, which serves as the ground truth. Following the analytical solution, the proposed methods, namely TFHA, Parareal adjoint and PP-PC adjoint sensitivity analysis will be applied as a validation.

Analytical Solution for the RC-Filter in Frequency Domain

The frequency domain solution for the output voltage of the RC-Filter can easily be derived using a voltage divider:

$$\underline{V}_{\text{out}} = \frac{1}{1 + \text{j}\omega RC} \underline{V}_{\text{in}}. \tag{6.1}$$

The sensitivity can analytically be calculated as the derivative of Eq. (6.1) w.r.t. a design parameter, here, for example the resistance value R:

$$\frac{\mathrm{d}\underline{V_{\text{out}}}}{\mathrm{d}R} = -\frac{\mathrm{j}\omega C}{(1+\mathrm{j}\omega RC)^2}\underline{V_{\text{in}}}. \tag{6.2}$$

Since the input source is sinusoidal, its signal is represented by the complex number of $\mathrm{j1\,V}$ in frequency domain. Assuming the excitation frequency of $f = 1\,\mathrm{MHz}$, the sensitivity results in:

$$\begin{aligned}\frac{\mathrm{d}\underline{V_{\text{out}}}}{\mathrm{d}R} &= -\frac{\mathrm{j}2\pi(1\,\mathrm{MHz})(10\,\mathrm{nF})}{(1+\mathrm{j}2\pi(1\,\mathrm{MHz})(20\,\Omega)(10\,\mathrm{nF}))^2}(\mathrm{j1\,V}) \\ &\approx (-5.4703 - \mathrm{j}23.7395)\mathrm{mV}\,\Omega^{-1}. \end{aligned} \tag{6.3}$$

Analytical Solution for the RC-Filter in Time Domain

The output voltage V_{out} is characterized in time domain by the mesh ODE

$$\frac{\mathrm{d}V_{\text{out}}}{\mathrm{d}t} + \frac{1}{RC}V_{\text{out}} - \frac{1}{RC}V_{\text{in}} = 0. \tag{6.4}$$

The initial value of V_{out} is zero as no previous charges in the circuit are assumed. The analytical solution for the output voltage V_{out} is (see Appendix A.3):

$$V_{\text{out}} = \frac{\hat{V}_{\text{in}}}{1+(\omega RC)^2}\left(\omega RC e^{-\frac{1}{RC}t} - \sin(\omega t) - \omega RC\cos(\omega t)\right). \tag{6.5}$$

For the mentioned device values, the transient of the output voltage V_{out} is plotted as a function over time in Fig. 6.2. To illustrate the circuit behavior, two different input frequencies are considered. As expected for an RC-filter with lowpass characteristics, the amplitude of the output voltage V_{out} is reduced for higher frequency for the same V_{out}.

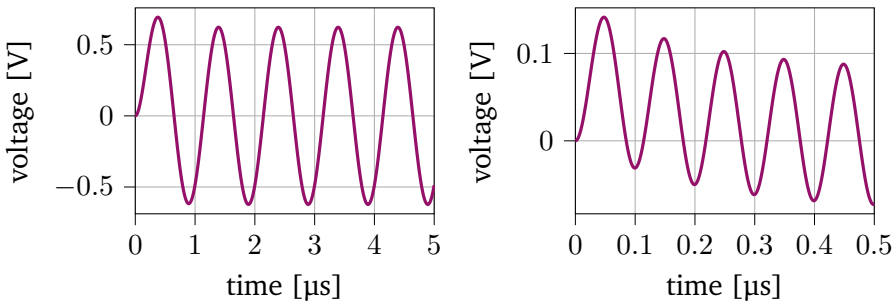

Figure 6.2.: Output voltage for the RC-filter with two different input frequencies ($1\,\mathrm{MHz}$ left and $10\,\mathrm{MHz}$ right).

To obtain the transient reference solution for the sensitivities, Eq. (6.5) must be derived w.r.t. the design parameters. As an example we will perform this for the sensitivity w.r.t. the resistance value of R. Symbolic derivation w.r.t. the capacitance value C is analogous. The sensitivity for the output voltage V_{out} w.r.t. the resistance R is analytically given as the symbolic derivative:

$$\frac{\mathrm{d}V_{\text{out}}}{\mathrm{d}R} = \frac{\omega C e^{-\frac{1}{RC}t}\left(\left(\frac{t}{RC}+1\right)\left(1+(\omega RC)^2\right)-2\left(\omega RC\right)^2\right)}{\left(1+(\omega RC)^2\right)^2} \tag{6.6}$$

$$-\frac{2(\omega C)^2 R\sin(\omega t)}{\left(1+(\omega RC)^2\right)^2}-\frac{\omega C\cos(\omega t)\left(1-(\omega RC)^2\right)}{\left(1+(\omega RC)^2\right)^2}. \tag{6.7}$$

A step-by-step derivation is given in appendix A.3. Analogously to the solution for the output voltage V_{out}, the analytical solution for the sensitivity is calculated and plotted for both the $1\,\mathrm{MHz}$ and the $10\,\mathrm{MHz}$ case in Fig. 6.3.

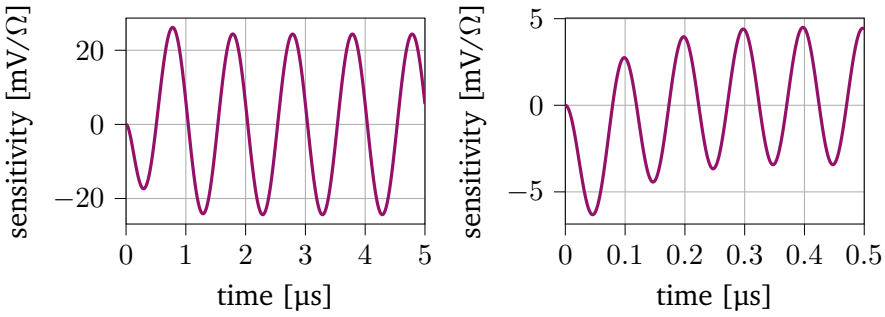

Figure 6.3.: Sensitivity of the output voltage w.r.t. to the parameter R for the RC-filter with two different input frequencies ($1\,\mathrm{MHz}$ left and $10\,\mathrm{MHz}$ right).

Transient Forward Harmonic Adjoint Sensitivity Analysis (TFHA)

Using the TFHA, the sensitivity is calculated using a transient circuit simulation in combination with a harmonic adjoint simulation (see section 3.3.4). Performing the ASA for the linear RC-filter example with the TFHA is not involved. Since no nonlinear devices are present in the circuit, the Jacobian matrix in frequency domain is identical to the MNA system matrix, such that:

$$\underline{\boldsymbol{J}} = \begin{pmatrix} 1/R & -1/R & 1 \\ -1/R & \mathrm{j}\omega C + 1/R & 0 \\ 1 & 0 & 0 \end{pmatrix} = \begin{pmatrix} 0.05\,\Omega^{-1} & -0.05\,\Omega^{-1} & 1 \\ -0.05\,\Omega^{-1} & (0.05 + \mathrm{j}0.02\pi)\Omega^{-1} & 0 \\ 1 & 0 & 0 \end{pmatrix}, \tag{6.8}$$

for $f = 1\,\mathrm{MHz}$. Due to harmonic excitation and the absence of nonlinear devices, the solution for one period is fully described by the base frequency component in frequency domain. The base frequency component is obtained by a Fourier transform of the final period from the transient MNA simulation.

The circuit solution for the base frequency component reads:

$$\underline{\boldsymbol{x}} = \begin{pmatrix} \underline{V}_{\text{in}} \\ \underline{V}_{\text{out}} \\ \underline{I}_{\text{V}_{\text{in}}} \end{pmatrix} = \begin{pmatrix} (0.0258 - \text{j}0.9951)\text{V} \\ (-0.4789 - \text{j}0.3984)\text{V} \\ (-0.0252 + \text{j}0.0298)\text{A} \end{pmatrix}. \tag{6.9}$$

For comparison, the analytical solution obtained with a voltage divider and Ohm's law results to:

$$\underline{\boldsymbol{x}} = \begin{pmatrix} \underline{V}_{\text{in}} \\ \underline{V}_{\text{out}} \\ \underline{I}_{\text{V}_{\text{in}}} \end{pmatrix} = \begin{pmatrix} -\text{j}1\,\text{V} \\ (-0.4872 - \text{j}0.3877)\text{V} \\ (-0.0244 + \text{j}0.0306)\text{A} \end{pmatrix}. \tag{6.10}$$

The deviation between the numerical (6.10) and the analytical solution (6.9) mainly originates from three sources.

1. The circuit solution using MNA introduces a time-stepping error that propagates in the transient solver.
2. The solution is not ideally periodic due to the modeling of the capacitors which will only converge to an ideally periodic solution after an infinite transient.
3. Following the non-ideal periodicity, the approximation with one base frequency leads to a truncation error, since more frequencies would be required to describe the residual transient.

All these error sources have to be taken into account when utilizing the TFHA for ASA.

The TFHA sensitivity is calculated using the steps described in section 3.3.4. Defining $\underline{V}_{\text{out}}$ as QoI the adjoint solution $\underline{\boldsymbol{\lambda}}$ is calculated using Eq. (3.29) yielding:

$$\underline{\boldsymbol{\lambda}} = \begin{pmatrix} 0 \\ (7.7545 + \text{j}9.7446)\text{V} \\ (0.3877 + \text{j}0.4872)\text{A} \end{pmatrix}. \tag{6.11}$$

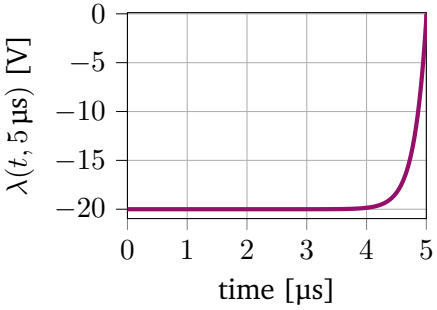

Figure 6.4.: Adjoint solution $\lambda(t, 5\,\mu s)$ corresponding to the last time instance plotted as a time dependent variable.

The sensitivity value is then calculated through Eq. (3.30), leading to:

$$\frac{\mathrm{d}\underline{V}_{\mathrm{out}}}{\mathrm{d}R} = -\underline{\boldsymbol{\lambda}}^{\mathsf{H}} \frac{\mathrm{d}\boldsymbol{J}}{\mathrm{d}R} \underline{\boldsymbol{x}} = (-4.7527 - \mathrm{j}23.8638)\mathrm{mV}\,\Omega^{-1}. \tag{6.12}$$

This equals the analytical solution with an error margin of 3 % which arises from the before mentioned error sources.

Parareal ASA

The second proposed method is the Parareal ASA. Performing this type of sensitivity analysis is a bit more involved, since an individual adjoint solution for each time instance is required. The adjoint solution in each time instance is calculated using Eq. (3.15). For illustration of the general shape, the adjoint solution $\lambda(t, 5\,\mu s)$ corresponding to the last time instance is plotted in Fig. 6.4. Since the adjoint rhs is a constant value, the adjoint variable asymptotically converges to a specific constant value in linear circuits with stationary inputs. The sensitivity is subsequently obtained along the integral evaluation of Eq. (3.19) to evaluate the sensitivity value

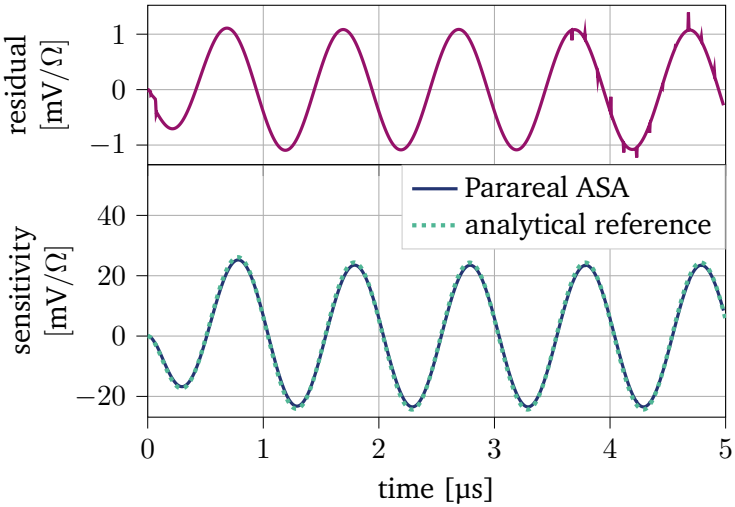

Figure 6.5.: Sensitivity of the output voltage w.r.t. to the parameter R for the RC-filter. Comparison of the Parareal ASA solution with the analytical reference (bottom) and the residual (top).

in each timestep. As a numerical method, the Parareal ASA is exposed to different error sources in the same way as the TFHA.

1. As before, the circuit solution using MNA introduces a time-stepping error that propagates in the transient solver.
2. The solution of the adjoint problem (3.15) introduces an additional time-stepping error that propagates in the transient solver.
3. The errors of the solutions for each time instance are accumulated within the integral evaluation in Eq. (3.19).

To quantify the accuracy of the Parareal ASA, the resulting sensitivity is compared to the analytical solution. The comparison is shown in Fig. 6.5. The

residual deviation is largest for the maximum amplitude of the oscillation. The relative error is bounded below $5\,\%$ for each relative value.

PP-PC ASA

The PP-PC ASA can only be utilized to analyze the sensitivity for the integral over one period of steady state operation, as described in section 5.2. For the given circuit example, which is linear and has a stationary input, this sensitivity must be zero. This is also illustrated in Fig. 6.4 and Fig. 6.2. Using both shown variables in the sensitivity analysis, the sensitivity is found by the integral over one period of a scaled sinusoidal oscillation with no offset, which is zero. Consequently, the error of the PP-PC ASA is trivially quantified by the nonzero result for the sensitivity in this example. In the first step, the adjoint solution of one period of steady state operation is found using the PP-PC method described in section 2.5.2. The adjoint solution is calculated using a threshold of 1 µV for the PP-PC convergence. The periodic adjoint solution is shown in Fig. 6.6.

The adjoint solution results in an exponential curve in each of the subinter-

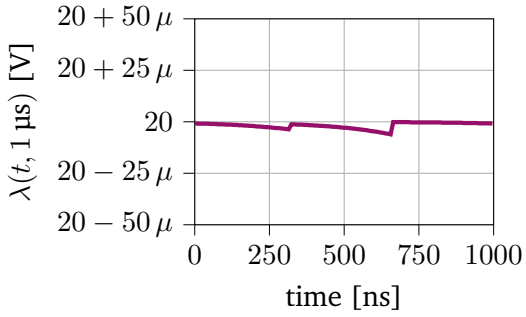

Figure 6.6.: Periodic adjoint solution $\lambda(t)$ obtained through PP-PC simulation.

vals which converges to $20\,\mathrm{V}$ as the size of the discontinuities is minimized. Using the periodic circuit solution, the sensitivity for the integral over one period is calculated using Eq. (5.3):

$$\int_{4\,\mu\mathrm{s}}^{5\,\mu\mathrm{s}} \frac{\mathrm{d}V_{\mathrm{out}}}{\mathrm{d}R}\,\mathrm{d}t = -0.3163\,\mathrm{nV\,s\,\Omega^{-1}}. \tag{6.13}$$

This result is around eight magnitudes smaller than the amplitude of the stepwise sensitivity for each time instance, which can be explained by the mentioned error sources, particularly the discontinuities of the adjoint solution.

6.2. Half-Wave Rectifier Circuit

A half-wave rectifier is one of the simplest nonlinear circuits, as it consists of only one nonlinear component and two linear components. In contrast to the RC-filter, no analytical reference is available due to the nonlinearity. However, it is possible to analyze the sensitivities for this circuit with all the proposed methods nonetheless. The DSA solution performed with the Xyce simulation software serves as a reference for the sensitivities [43].

This most basic nonlinear circuit serves as an example to validate the applicability of the proposed sensitivity analysis methods for nonlinear systems. The circuit structure of the half-wave rectifier is shown in Fig. 6.7.

The nominal device values of the half-wave rectifier are:

- $V_{\mathrm{in}} = 5\,\mathrm{V}\sin(\omega t)$
- $R = 20\,\Omega$
- $C = 200\,\mathrm{nF}$

To begin the analysis, the QoI is selected as the output voltage of the half-wave rectifier. The QoI is shown in Fig. 6.8 in comparison with the input voltage V_{in}. The sensitivity is analyzed with the different methods.

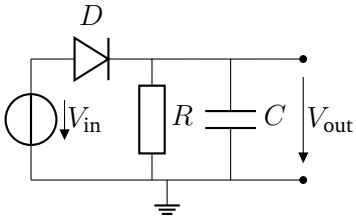

Figure 6.7.: Schematic of the half-wave rectifying circuit.

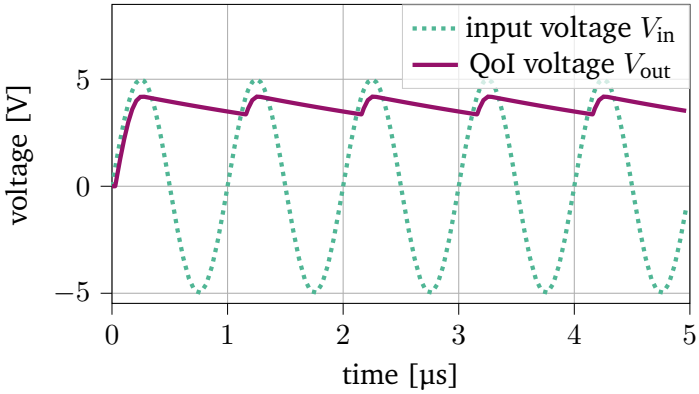

Figure 6.8.: Input and output voltage of the half-wave rectifier.

TFHA and Parareal ASA

In the first part, the sensitivity analysis is performed using the TFHA and the Parareal ASA. To compare both methods to the reference, the frequency domain solution calculated with the TFHA is transformed back to time domain. This way, the comparison can be plotted over time in a single graph. The TFHA is executed with the following simulation parameters:

- number of harmonics k: 64

- base frequency w_p: 1 MHz

The base frequency is the lowest frequency of the input source. In contrast, the number of harmonics is a trade-off between accuracy and dimension of the harmonic Jacobian matrix. While more harmonics would be possible for this example in theory, the simulation time would significantly fall behind.

The Parareal adjoint uses the simulation parameters and convergence constraints:

- number of subintervals N: 6
- discontinuity threshold: 10^{-4}

More subintervals would reduce convergence because the number of timesteps in the coarse solver would get too small otherwise. The discontinuity threshold was chosen arbitrarily.

Even thought the circuit itself is small scale with only one weakly nonlinear device, the numerical properties of the adjoint problem are challenging for both the Parareal ASA as well as the TFHA. The reason lies in the adjoint solution itself. To explain this, the adjoint solution is shown in figure 6.9.

In contrast to the circuit solution, the adjoint solution has steep changes. Therefore, the waveform of the adjoint solution is much more broadband. As a result, a larger number of harmonics are required to analyze this circuit example with the desired accuracy using the THFA. Analogously, the Parareal ASA requires five iterations for the adjoint problem simulated with the Parareal to converge whereas the circuit solution converges in only one iteration. Similarly, five Parareal iterations are required for the convergence of the adjoint problem. In contrast, the circuit solution achieves convergence in just one Parareal iteration.

After the adjoint solution is found by a method of choice, the sensitivity is analyzed as described in sec. 3.3.4 and 3.2.2. The results of the sensitivity analysis w.r.t. the design parameter R are shown in Fig. 6.10. Note here, that the TFHA only calculates the sensitivity for one period of steady state

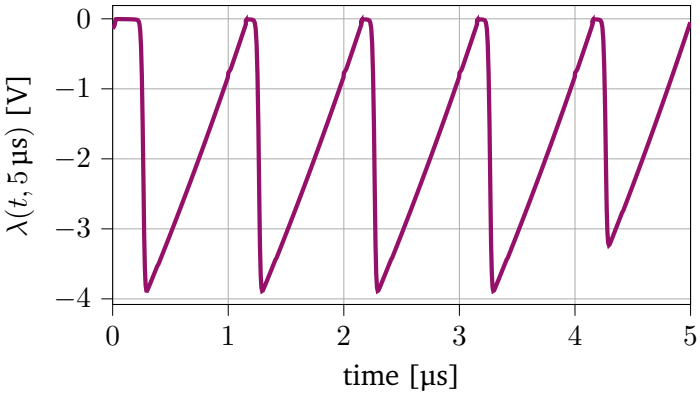

Figure 6.9.: Adjoint solution $\lambda(t, 5\,\mu s)$ at the QoI node for the final time instance at $5\,\mu s$.

operation. For the comparison, this periodic solution is repeated for five periods of operation.

The solutions are in accordance. Particularly the Parareal ASA is extremely accurate within $2\,\%$ of error margin when compared to the reference solution. The TFHA shows spurious oscillations close to steep changes of the resulting function. These oscillations are a result of Gibbs' phenomenon, and convergence occurs only when the number of harmonics approaches infinity. This indicates that the TFHA is less suitable for this circuit example.

Periodic ASA

Lastly, the periodic ASA is applied to this example. For the periodic solution, a PP-PC solver as introduced in sec. 2.5.2 is used. The PP-PC converges in two outer iterations, which can be expected as the transients in this circuit are weak. The result is the integral over one period of operation for the

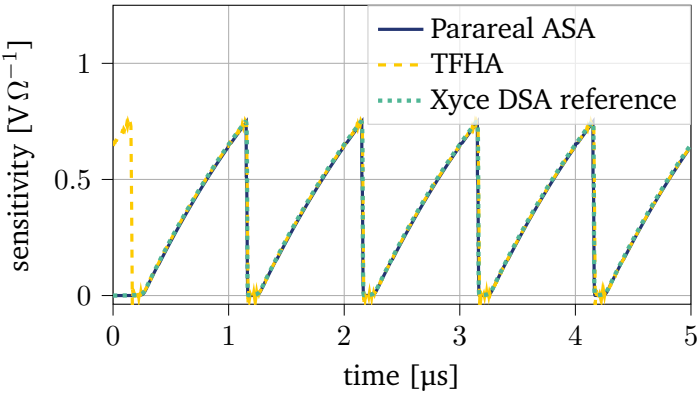

Figure 6.10.: Sensitivity of the output voltage V_{out} of the half-wave rectifier w.r.t. the resistor R.

sensitivity of the QoI. Consider the integral QoI:

$$U = \int V_{\text{out}}(t)\, \mathrm{d}t. \tag{6.14}$$

For reference, the Xyce DSA reference from the previous subsection is integrated over time for one period:

$$\left.\frac{\mathrm{d}U}{\mathrm{d}R}\right|_{\text{reference}} = \int_{4\,\mu\text{s}}^{5\,\mu\text{s}} \frac{\mathrm{d}V_{\text{out}}(t)}{\mathrm{d}R}\, \mathrm{d}t = -0.3712\,\mu\text{V s}\,\Omega^{-1}. \tag{6.15}$$

The periodic solution along the ASA is calculated using the integral Eq. (5.5) resulting in the integral sensitivity value of:

$$\left.\frac{\mathrm{d}U}{\mathrm{d}R}\right|_{\text{periodic}} = -0.3643\,\mu\text{V s}\,\Omega^{-1}, \tag{6.16}$$

which is in accordance with the reference value. The error compared to the reference is around $1.86\,\%$ error for the periodic ASA solution. The PP-PC

simulation requires two iterations for convergence. As the transient simulation is only five periods in duration, the speedup is marginal in comparison to the transient ASA for this example. However, it has been shown, that the periodic ASA is a suitable approach to accurately analyze sensitivities based only on the periodic solution. This is extremely advantageous for applications with long transients.

6.3. Buck Converter

Buck converters, also known as step-down converters, are among the most frequently used circuits in power electronics [24]. Buck converters are a DC-DC converter that converts a higher DC input voltage to a lower DC output voltage. The applications include power supplies, chargers, and controlled power systems such as DC supplied train motors.

The functionality of a buck converter involves the use of a switch, such as a transistor [36]. This switch connects and disconnects the input voltage to an inductor in a defined duty cycle. The output voltage is adjusted by modification of this duty cycle.

Here, an academic example of a buck converter (Fig. 6.11) is analyzed using the proposed methods for ASA. This buck converter was used and simulated in literature before, such as in [36].

The numerical simulations are executed for the model parameters shown in table 6.1. The considered QoI is the buck converters' output voltage. The time dependent QoI is a charging curve topped with oscillations that

Table 6.1.: Model parameters used for the circuit simulation and analysis of the buck converter.

V_{in}	f_{s}	L	R_L	C	R
$100\,\text{V}$	$500\,\text{Hz}$	$1\,\text{mH}$	$10\,\text{m}\Omega$	$100\,\mu\text{F}$	$0.8\,\Omega$

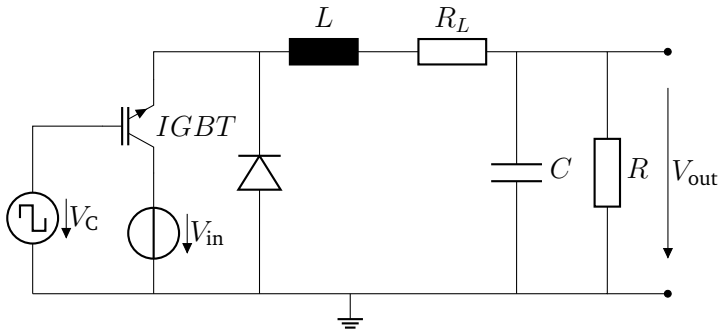

Figure 6.11.: Schematic of the DC-DC buck-converter circuit.

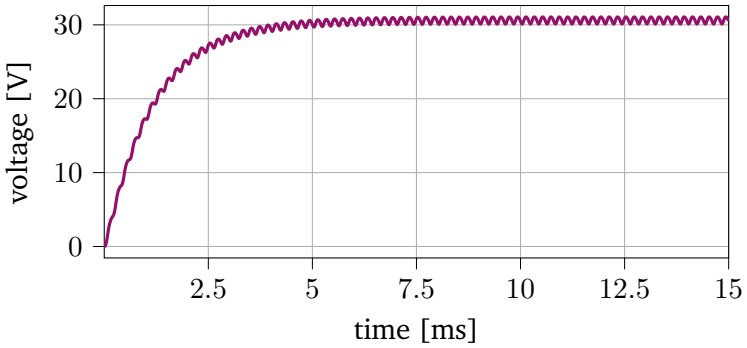

Figure 6.12.: Output voltage V_{out} of the DC-DC converter plotted as a function over time.

originate from the charging and discharging of the capacitor. The QoI is plotted for the transient process in Fig. 6.12. The charging curve converges to the desired DC value. Since this example has a comparably long transient, the periodic methods, namely TFHA and PPPC ASA, are well suited for its sensitivity analysis. This is particularly advantageous when the goal is to analyze sensitivities associated with steady state operation.

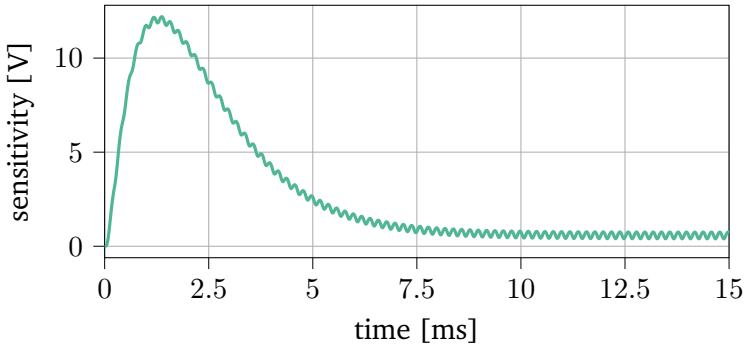

Figure 6.13.: Sensitivity of the output voltage V_{out} w.r.t. the parameter R of the DC-DC-Converter calculated with Xyce DSA for reference plotted as a function over time.

TFHA

The sensitivity analysis is performed using the TFHA and the PPPC ASA for the steady state. The TFHA is performed with the simulation parameters:

- number of harmonics k: 50
- base frequency w_{p}: $5\,\text{kHz}$

The base frequency is given by the lowest frequency of the input source. In contrast, the number of harmonics is a trade-off between accuracy and dimension of the harmonic Jacobian matrix.

The Xyce DSA solution serves as a ground truth for sensitivity analysis. The reference sensitivity is plotted over time for the sensitivity analysis w.r.t. the design parameter R in Fig. 6.13. Resistor R is at the output of the buck converter. Thus, it is not surprising that its influence is largest within the transient, i.e. when the capacitor is charging. In the steady state, the influence of the resistance R is smaller. Nonetheless, it is the

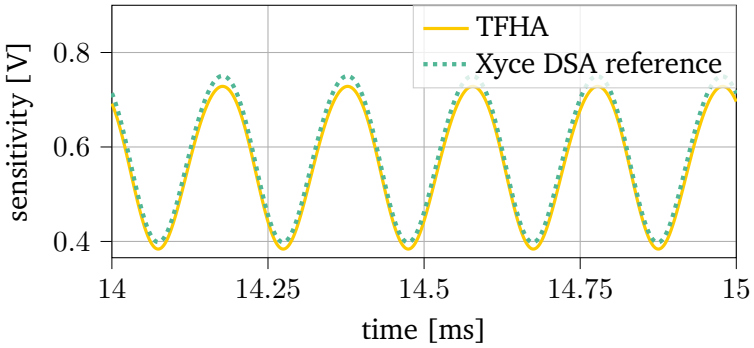

Figure 6.14.: Output voltage V_{out} sensitivity w.r.t. the resistance R of the DC-DC-Converter calculated with the THFA compared to the Xyce DSA reference solution plotted as a function over time for the last five periods.

most influential design parameter in the steady state, because the cyclic charging and discharging of the capacitance C is regulated by it.

To compare the TFHA sensitivity with the reference solution, the last five periods are considered. As in the previous example, the TFHA solution is copied for five periods to better visualize the comparison. For the first analysis, the influence of design parameter R is visualized in Fig. 6.14. Clearly, the amplitude of the TFHA solution is slightly smaller, and lies within a $3\,\%$ error margin. This is explained by the truncation of frequencies, which results in the loss of the higher frequency components and thus, a slight damping. Nonetheless, the TFHA does not show any spurious oscillations and is therefore generally well suited to analyze the sensitivities for this example.

The influence of the resistor R leads to weak oscillations but a rather high midpoint value. In contrast, the sensitivity w.r.t. the capacitor C is plotted in Fig. 6.15. Clearly, the capacitor influences the oscillation strongly but has a very small midpoint value. This will also be discussed with the periodic

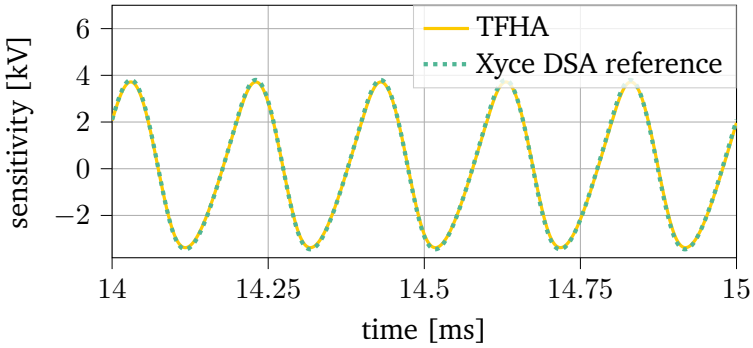

Figure 6.15.: Sensitivity of the output voltage V_{out} w.r.t. the capacitance C of the DC-DC converter calculated with the THFA compared to the Xyce DSA reference solution plotted as a function over time for the last five periods.

ASA in the next subsection. The error in this example is slightly lower, at around $2.1\,\%$. This smaller error originates from the larger oscillation component in the base frequency range, which can be accurately described by the TFHA.

Periodic ASA

In the first step of the periodic ASA, the adjoint solution is simulated using a PP-PC solver. The solver uses the simulation parameters:

- number of subintervals N: 2
- discontinuity threshold: 10^{-4}

The number of subintervals had to be limited because the period is extremely small compared to the entire simulation time span. This leads to convergence issues if the number of timesteps of the coarse solver is too

Table 6.2.: Sorted list of parameter sensitivities integrated over one period using equation. Periodic ASA compared with reference Xyce DSA integrated over one period. Since Xyce does not allow for sensitivity analysis w.r.t. inductances, the reference is not available for L

device label	sensitivity value	Xyce DSA reference	error
R	$116.6009\,\mu\mathrm{V\,s}$	$116.8457\,\mu\mathrm{V\,s}$	$0.2095\,\%$
R_L	$-74.2263\,\mu\mathrm{V\,s}$	$-74.2264\,\mu\mathrm{V\,s}$	$0.0002\,\%$
L	$397.5767\,\mathrm{nV\,s}$	-	-
C	$6.358\,981\,\mathrm{nV\,s}$	$22.762\,97\,\mathrm{nV\,s}$	$257.96\,\%$

small. Alternatively, the number of subintervals could only be increased if more timesteps where used for the coarse solver, which would contradict the speedup goal. With the given parameters, the PP-PC adjoint simulation converges in nine iterations, leading to a significant speedup even for two subintervals, since the timespan of the steady state is only $1.3\,\%$ of the entire simulation duration.

The results in table 6.2 illustrate one downside of the pure integral observation. The capacitor strongly influences the oscillation but is deemed negligible when looking only at the integral. Due to the high amplitude and the small mean value of the oscillation, the integral of the oscillating Xyce DSA solution and the PPPC ASA solution are very far apart. This means that depending on the design parameter, the integral of the steady state might not be sufficient to analyze the circuit behavior. If oscillations must be minimized, this method is not well suited.

6.4. Active Filter Circuit

This section presents the application of the proposed methods for sensitivity analysis to an active filter circuit (see 6.16). This circuit is a good example

for a medium sized circuit with a limited bandwidth.

The presented circuit contains an additional filtering stage between a power converter appliance that is connected to a line impedance stabilization network (LISN) with a common mode (CM) choke [2, 44]. Particularly, a voltage sensing current injection (VSCI) filter is used in the given example. This type of active filter is widely employed in different fields of electrical engineering, most prominently for active noise cancellation [57]. At this point, it is not necessary for the analysis to specifically define which type of power converter produces the noise injection modeled by the current source signal. Therefore, the noise source characteristic of the power converter is represented by a random noise current source.

The injected noise I_{noise} from the current source is discontinuous and therefore broadband. It is connected to the LISN with a filtering stage. Ahead of the OPAMP connection, the capacitor C_1 provides galvanic decoupling for the filter input node OP_{in}. Furthermore, the voltage divider formed by R_1 and R_2 reduces the input voltage at node OP_{in} to prevent damage on the logical devices within the OPAMP. The circuit does not exhibit long transients. Resultingly, the proposed methods TFHA and Parareal ASA are well suited candidates to perform a sensitivity analysis.

As the noise disturbance originates in a switched power converter, it is safe to assume that the noise has a specific shape and is also periodic.

For the sensitivity analysis of this example, two different QoIs are considered. As a first analysis, the voltage at the filter output stage OP_{out} serves as the QoI. The sensitivities for this QoI indicate which design parameters can influence the filtered signal, that is ultimately interfering with the LISN. The time dependent QoI is plotted in figure 6.17.

The second analysis employs the negating filter input voltage at node OP_{in} as QoI. The sensitivities for this QoI indicate which design parameters influence the interference before the active filter stage. The QoI at the input node OP_{in} is expected to be more highly oscillating because of the low-pass characteristics of the OPAMP. The time dependent QoI for the negating

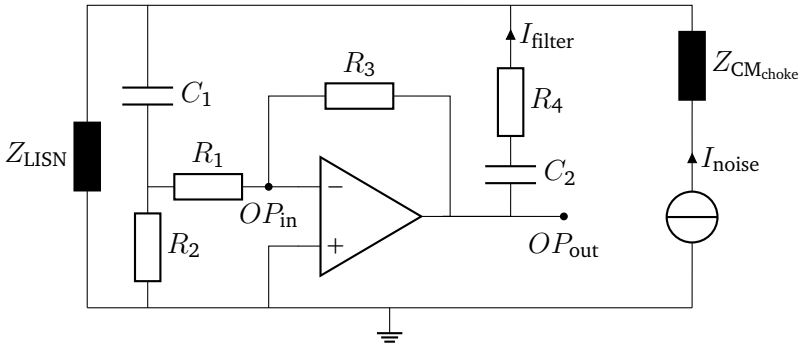

Figure 6.16.: Functional schematic for the nonlinear active filter circuit.

filter input voltage is plotted in figure 6.18.

TFHA and Parareal ASA

The sensitivity analysis is performed using the TFHA and the Parareal ASA. The TFHA is executed with simulation parameters:

- number of harmonics k: 50
- base frequency w_{p}: $10\,\text{kHz}$

The base frequency is the lowest frequency of the noise injection source. In contrast, the number of harmonics is a trade-off between accuracy and dimension of the harmonic Jacobian matrix.

The Parareal ASA uses the simulation parameters:

- number of subintervals N: 24
- discontinuity threshold: 10^{-4}

Here, the number of subintervals is chosen as the number of physical processing cores. The discontinuity threshold is chosen arbitrarily as before.

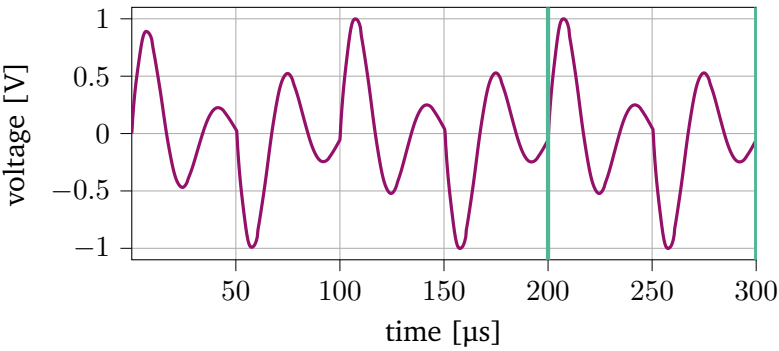

Figure 6.17.: The QoI at the output node of the filter stage OP_{out} in circuit 6.16 plotted over time. Green vertical lines indicate the last period of operation.

The adjoint variable $\lambda(t, t_{\text{end}})$ for transient ASA such as the Parareal ASA can be depicted as a time dependent graph as well. Considering the adjoint variable $\lambda(t, 300\,\mu\text{s})$ at the node OP_{out} results in the plot Fig. 6.19.

The adjoint variable contains high frequency oscillations as well as some periodically occuring spikes. The Parareal is not well suited to handle discontinuities or fast oscillations [28]. Following this, the Parareal simulation for $\lambda(t, t_{\text{end}})$ does not fall below the discontinuity threshold at all time instances represented by t_{end}. But, for other time instances, the Parareal cuts down the wall clock time nonetheless. Followingly, the solutions for non-convergent time instances is replaced by a conventional transient simulation. On average, 10 iterations are required for the adjoint simulation to converge, leading to a theoretic speedup of 2.4 using the Parareal approach with the given constraints compared to the purely transient simulation.

In contrast, the TFHA requires around 30 minutes for the assembly of the harmonic Jacobian matrix. The required assembly time for the harmonic Jacobian matrix can be severely cut down in future developments, as this

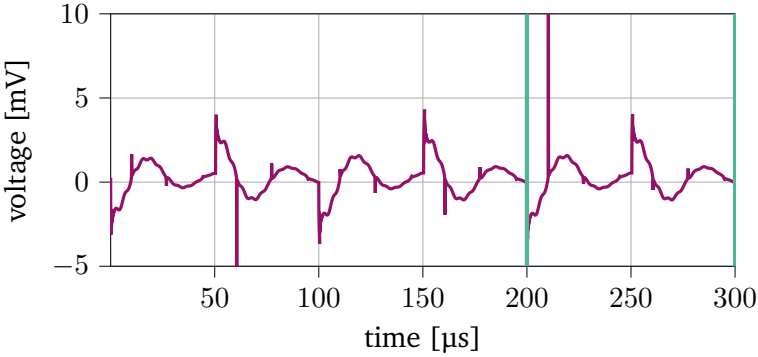

Figure 6.18.: The QoI at the negating filter input OP_{in} in circuit 6.16 plotted over time. Green vertical lines indicate the last period, which is considered as the steady state here.

procedure was not optimized in this work. Subsequent sensitivity analysis is then executed in around 10 seconds with 20 seconds post-processing in order to obtain the sensitivities w.r.t. all design parameters. This means, that the TFHA is particularly quick for the defined setting.

The accuracy of the TFHA simulation is limited by the considered number of harmonics k. The resulting error can be quantified using the approximation presented in section 3.3.4. If only one harmonic Jacobian matrix is assembled, the number of harmonics k is fixed. In this case, the error can be quantified by comparing the results with a reference solution.

The reference solution is obtained by executing a transient DSA using Xyce [43]. Both proposed QoIs are compared with the reference solution.

The results of the first sensitivity analysis with the voltage at the filter output stage OP_{out} serving as QoI, showing the comparison of the proposed methods with the Xyce DSA reference solution, is plotted in Fig. 6.20. Clearly, both analysis methods are well suited to deliver accurate results for this analysis. The Parareal ASA produces a small offset in some interval.

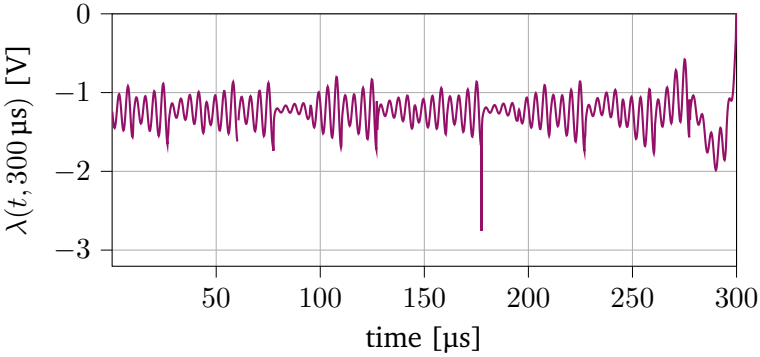

Figure 6.19.: Adjoint variable $\lambda(t, 300\,\mu s)$ at the QoI node OP_{out} plotted over time.

On the other hand, the TFHA can not account for sharp peaks. The second sensitivity analysis focuses on the voltage at the negating filter input node OP_{in} as QoI. This simulation is more challenging due to the faster oscillations of the signal. The comparison of the proposed methods with the Xyce DSA reference solution for this second simulaton is plotted in Fig. 6.21. The TFHA is not able to approximate the shape of this sensitivity in any kind with the given number of harmonics. This is explained with the larger oscillations, that would require more harmonics for simulation. Given that the system matrix is very large for the analysis with 50 harmonics already, increasing the number of harmonics further would significantly escalate the storage requirements.

Compared to the TFHA solution, the Parareal ASA solution is closer to the reference. Since the speedup is not large in comparison with the transient adjoint sensitivity analysis, the advantages to existing methods for this applications are not significant.

Conclusively, the TFHA is a superior approach for sensitivity analysis for this circuit example. However, the results must be evaluated cautiously.

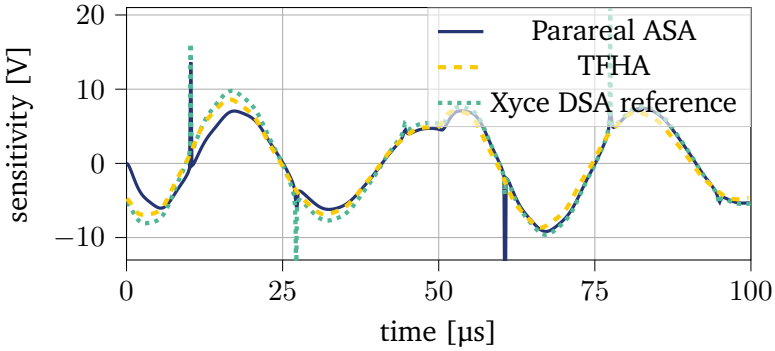

Figure 6.20.: Stepwise sensitivity in the last period of operation for the sensitivity of the filter output voltage at node OP_{out} (see Fig. 6.17) of the active filter circuit 6.16 w.r.t. the most influential design parameter C_1 plotted over time.

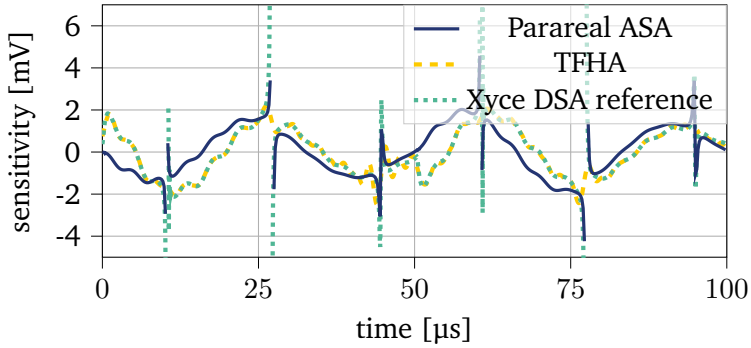

Figure 6.21.: Stepwise sensitivity in the last period of operation for the sensitivity of the filter input voltage at node OP_{in} (see Fig. 6.17) of the active filter circuit 6.16 w.r.t. the most influential design parameter C_1 plotted over time.

Fast oscillations in some QoIs cannot be represented accurately using the TFHA. Nonetheless, the approach is well suited indicate the most influential design parameters even for these QoIs.

6.5. B6 Bridge-Motor Supply Circuit

The most complex circuit with the most components that is used as an example is a B6 bridge-motor supply circuit. B6 circuits in general are described detailed in [87]. Fig. 6.22 shows the functional devices of the circuit. The complete circuit contains more than 4000 devices in total. As inputs, the circuit is supplied by six PWM sources, which are phase shifted in order to produce a three-phase current at the output. PWM controlled circuits are further described in section 2.2.3.

The switching cycle of the PWM is 1 ms, whereas the period length of the entire PWM is 10 ms. In contrast, the transition time between the on- and off-states of the voltage is several magnitudes smaller at 1 µs. Resultingly, in order to resolve the transitions accurately, a transient circuit simulation requires a very large number of timesteps.

Consequently, this circuit is a very challenging example. It contains a very large number of design parameters for one point, which would make the transient ASA a suitable choice. But, on the other hand, the circuit solution requires a very large number of timesteps, reducing the performance of the transient ASA. The Parareal ASA, published in [71] aims to tackle this problem by improving the transient ASA.

In this section, the Parareal ASA is utilized to speed up the analysis in comparison to the transient ASA and making an analysis possible for this numerically expensive circuit example. The other proposed methods are not well suited. The TFHA requires a sufficient number of harmonics to estimate the circuits behavior accurately. Due to the PWM excitation, the B6 bridge circuit has a broadband solution, which would require a very

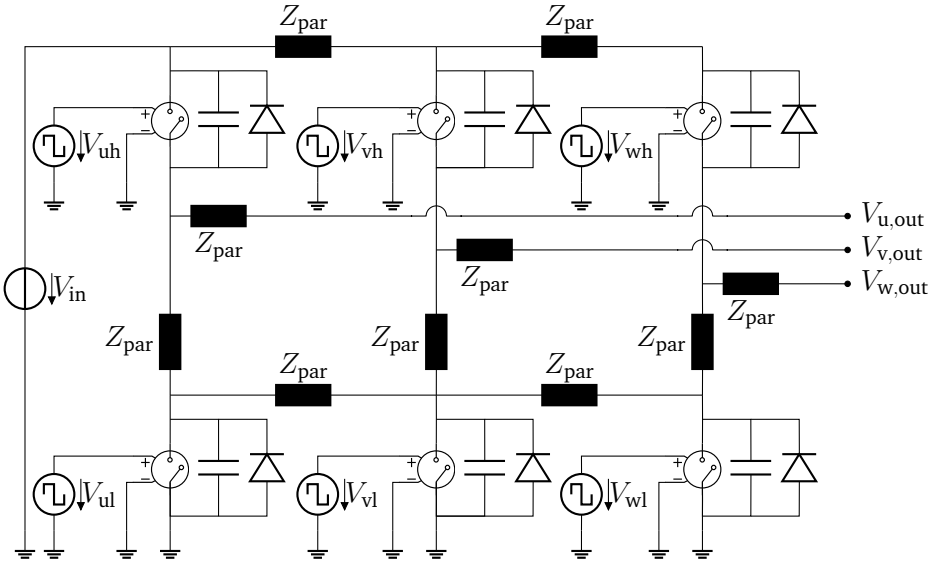

Figure 6.22.: Functional schematic of a B6 bridge-motor supply circuit with added parasitic EEC impedances Z_{par}. V_{uh}, V_{vh}, V_{wh}, V_{ul}, V_{vl}, V_{wl} are PWM gate voltages controlling the switches respectively.

large number of harmonics. Combined with the large scale of the circuit, the TFHA becomes unfeasible, as it would be impossible to store the system Jacobian matrix due to its extensive dimensionality.

The PP-PC ASA might look like a well suited approach on the first hand. However, the number of required timesteps per period is extremely large. Furthermore, the transient is only in the order of few periods, until the steady state has been reached, which spoils the advantages of the PP-PC if it does not converge in the first two iterations. Resultingly, the PP-PC ASA does not provide any advantages over the Parareal ASA for this example.

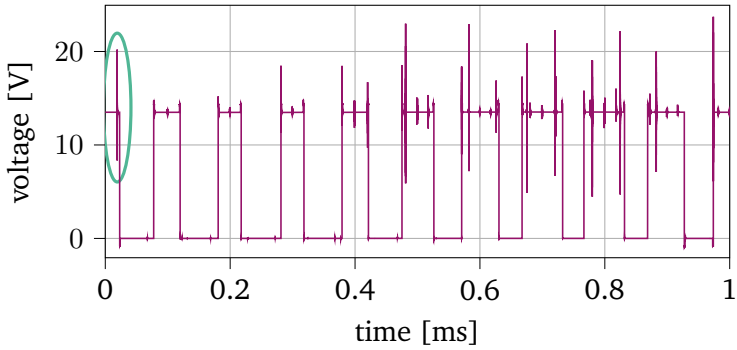

Figure 6.23.: The QoI plotted over time for the first PWM-cycle period of the switch voltage. The green circle highlights the first oscillation, which is shown enlarged in Fig. 6.25.

To define the QoI that must be observed, the sensitivity of the voltage at the upper u-phase switch is considered. The behavior of the other voltages in the circuit is analogous, as the voltages are largely controlled by the PWM switches. The QoI over one entire period of operation is shown in Fig. 6.23. The first oscillation is highlighted by the green circle. Because the behavior at each switching process is very similar, and the number of required timesteps for one period is very extensive even when using Parareal, the performance is demonstrated for only one oscillation. This first oscillation is shown in Fig. 6.24. This oscillation originates either from the switching of the u-phase switch itself, or, as in the observed case, by the switching of one of the neighboring phases. These oscillations are particularly interesting to analyze, since these can raise the voltage over the maximum operation limit of the switch for a short period of time. To avoid any damage to the electronic components, this must be avoided.

In practice, these overshoots can be limited by adding capacitors to the circuit, that can filter the high frequency oscillations. Consequently, the

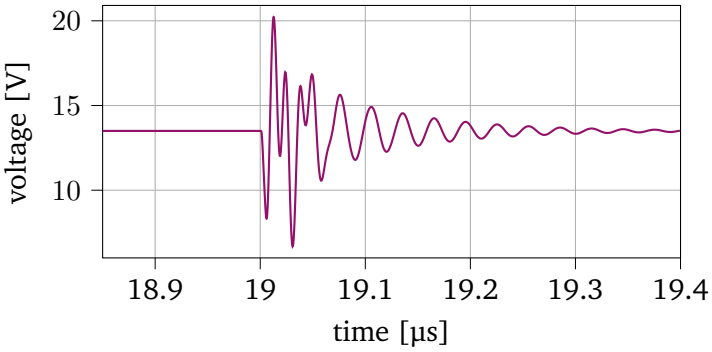

Figure 6.24.: The QoI plotted over time for the first switching oscillation.

sensitivity w.r.t. the most influential capacitor C_{DS_uh} is further observed. The sensitivity directly follows the shape of the QoI. The result of the ASA is shown in Fig. 6.25. The Parareal ASA has an average error distance of $0.418\,\%$ compared to the Xyce DSA reference. This error results from the Parareal solvers threshold as well as propagated errors from the solution of the integral equation (3.20).

To compare the influence of different design parameters, a stackplot representation poses a good representation. This type of plot is often used to depict Sobol indices as explained in section 1.1. The ten most influential design parameters are shown in stackplot form in Fig. 6.26. For that, the sensitivity w.r.t. each respective design parameter is normalized for the total sensitivity value of all sensitivities contained in the plot. Following this, the sensitivities can be presented analogously to Sobol indices as shown in section 1.1. The stackplot shows the sensitivities w.r.t. the ten most influential design parameters.

In many instances, the interpretation of the results is more straightforward in the frequency domain. Given the non-periodicity of the signal, the power spectra for the sensitivities are estimated using Welch's method, as

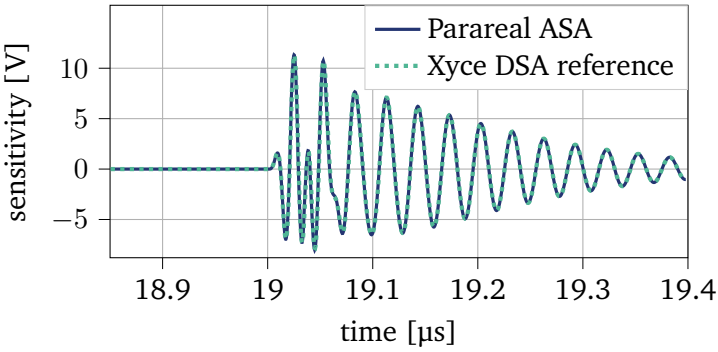

Figure 6.25.: Output voltage sensitivity w.r.t. the switch capacitance of the upper u-phase $\mathrm{d}V_{\mathrm{qoi}}/\mathrm{dC}_{\mathrm{DS\_uh}}$. Parareal ASA solution compared to the Xyce reference solution.

explained in appendix A.1.2. The frequency domain graph (Fig. 6.27) gives a clearer depiction of the mentioned properties.

Connecting the sensitivity results to their physical meaning aids the interpretation and therefore further development. Here, this interpretation is given for two design parameters: $\mathrm{L}_{\mathrm{uh-vh3}}$ and $\mathrm{C}_{\mathrm{DS\_uh}}$. The inductance $\mathrm{L}_{\mathrm{uh-vh3}}$ is associated with the connection between the high-side switch U_h in the u-phase and the high-side switch V_h in the v-phase. Consequently, $\mathrm{L}_{\mathrm{uh-vh3}}$ provides a bypass route for the switch voltage.

The influence of $\mathrm{L}_{\mathrm{uh-vh3}}$ on the oscillation originates from its interaction with switch capacitances in the u- and v-phases. Particularly the capacitance $\mathrm{C}_{\mathrm{DS_uh}}$ influences the QoI before the initial switching event. Afterwards, its relative influence diminishes, as the oscillation of the QoI is mainly influenced by the neighboring v-phase. This is explained by the fact that the oscillation is triggered by the switching event in the v-phase.

The inductor $\mathrm{L}_{\mathrm{uh-vh3}}$ exerts strong influence on the relaxation oscillations, which occur at lower frequencies of 2 MHz. This oscillation is also seen in

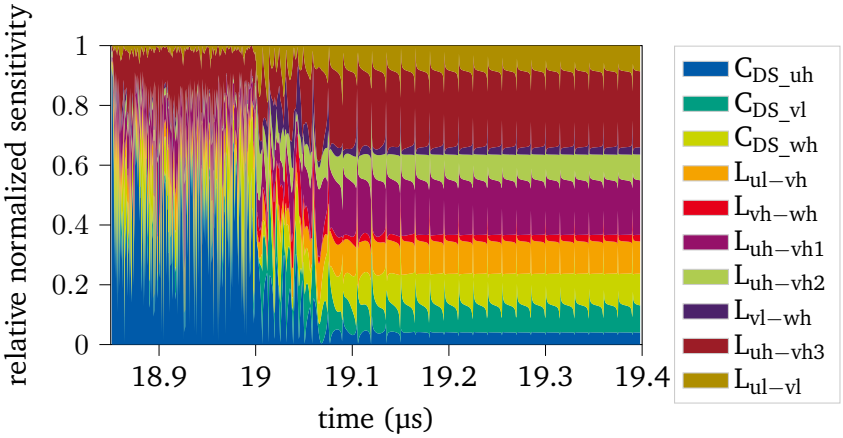

Figure 6.26.: Stackplot of the relative normalized sensitivity for the ten most influential design parameters plotted over time.

Fig. 6.25 after 19.1 s. The capacitance C_{DS_uh} weakly influences the lower frequency oscillations but significantly influences the high-frequency components of the signal. These findings are valuable during the optimization stage in order to make the operation of the B6 bridge more robust.

The efficiency of the Parareal ASA is quantified using the metrics introduced in section 5.1, namely the speedup (5.1) and the parallel efficiency (5.2). Both metrics are depicted in Fig. 6.28. The speedup (5.1) exhibits a linear growth, whereas the parallel efficiency (5.2) remains constant with an increasing number of subintervals. This is due to the negligible share of the coarse solver on the overall serial runtime and the absence of any noticeable communication overhead. As a result, the algorithm scales very well with additional computational units (threads, tasks, processors) as indicated by the linear speedup in Fig. 6.28. Conclusively, the Parareal ASA is significantly advantageous for the sensitivity analysis of the given

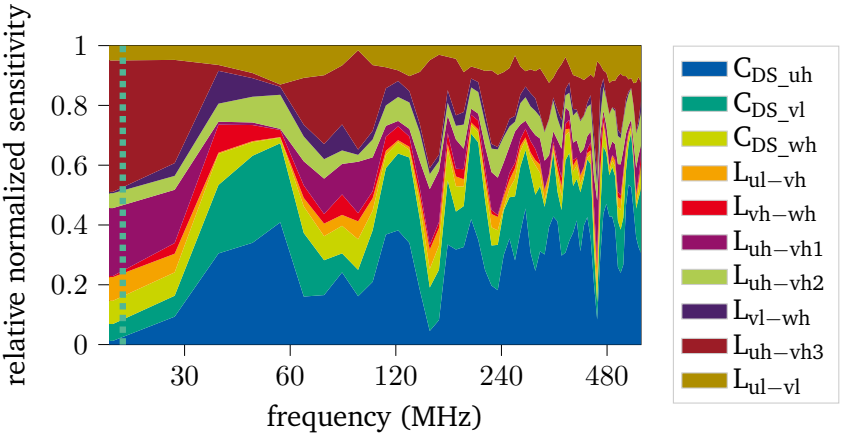

Figure 6.27.: Power spectrum of the relative normalized sensitivity for the ten most influential design parameters. The vertical dotted line (···) indicates the relaxation oscillation frequency.

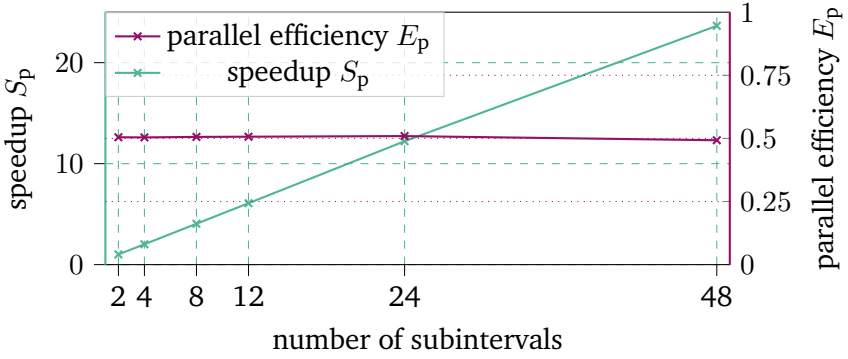

Figure 6.28.: Speedup S_p and parallel efficiency E_p for different numbers of subintervals.

circuit example. The accuracy compared with the reference is well below a 1 %. Additionally, the Parareal ASA results in a linear speedup for more computational units, substantially reducing the wall-clock time for simulation.

6.6. Additional Applications for Adjoint Sensitivity Analysis

In addition to the plain sensitivity analysis that is used in root cause analysis and optimization, the proposed ASA methods can help in the engineering process. These applications include the sensitivity based netlist reduction as a straight forward model order reduction (MOR) approach as well as utilization of ASA in EMC systems.

6.6.1. Sensitivity Based Netlist Reduction

Netlists describe electric circuits in a form that can be processed by simulation programs such as SPICE. Netlists may contain several thousand elements, especially when parasitic elements are contained. A reduction of the circuit can accelerate subsequent analysis steps.

One way to achieve a netlist reduction is sensitivity based reduction [41, 52]. The sensitivity based reduction approach utilizes the property that parameters with minimal influence on the Quantity of Interest (QoI) may be disregarded without strongly altering the simulation outcomes.

A sensor circuit is used as example for the algorithm. The unreduced circuit in figure 6.29 (a) contains more than 1400 elements total, while the reduction gives a reduced circuit 6.29 (b) with only 22 elements, while the deviation of the simulation results remain in a predefined error margin of less than 5 % for the frequency of 1 MHz.

To illustrate the effects of the circuit reduction. the potential at the line

impedance stabilization network (LISN) is considered. In this circuit example, the AC sensitivity analysis at specific frequencies is used. However, the method for sensitivity analysis can be chosen differently if necessary [41]. The reduction is then executed by eliminating elements based on the sensitivity values that are obtained from the AC sensitivity analysis. Depending on the frequency that is used to calculate the sensitivities, different reductions are obtained. To illustrate this, the sensitivity analysis is performed for different frequencies and the resulting reduced circuits are simulated. The frequencies for sensitivity analysis are $1\,\mathrm{MHz}$, which is a frequency in the middle of the spectrum, and $1.26\,\mathrm{kHz}$, $66\,\mathrm{kHz}$ as well as $35\,\mathrm{MHz}$, which are resonance frequencies.

Achieving a reduction while maintaining a $1\,\%$ error margin is most severe when the sensitivities are calculated for $1.26\,\mathrm{kHz}$. Consequently, this reduced circuit cannot provide correct results for high frequency components of the simulation. For the simulation at higher frequencies, a larger number of circuit elements is needed to match the results of the original circuit. Fig. 6.30 shows the simulation results for the respective reduced circuits. For a better overview, the relative size of the netlists is given as a percentage in the graph legends.

The lower frequency components of the solution can accurately be described with the circuit that contains only $3\,\%$ of the elements from the original circuit. Only above $8\,\mathrm{MHz}$ the solution deviates completely. Resultingly, the sensitivity based netlist reduction is a very strong tool to reduce the size of the netlist, particularly when only a small frequency range must be simulated.

6.6.2. Sensitivity Analysis for Harmonic Resonance Analysis

The sensitivity analysis for harmonic resonance analysis was originally published by Zhenyu Huang, Yu Cui, and Wilsun Xu for the optimization of power systems in [40]. In the process of harmonic resonance mode analysis,

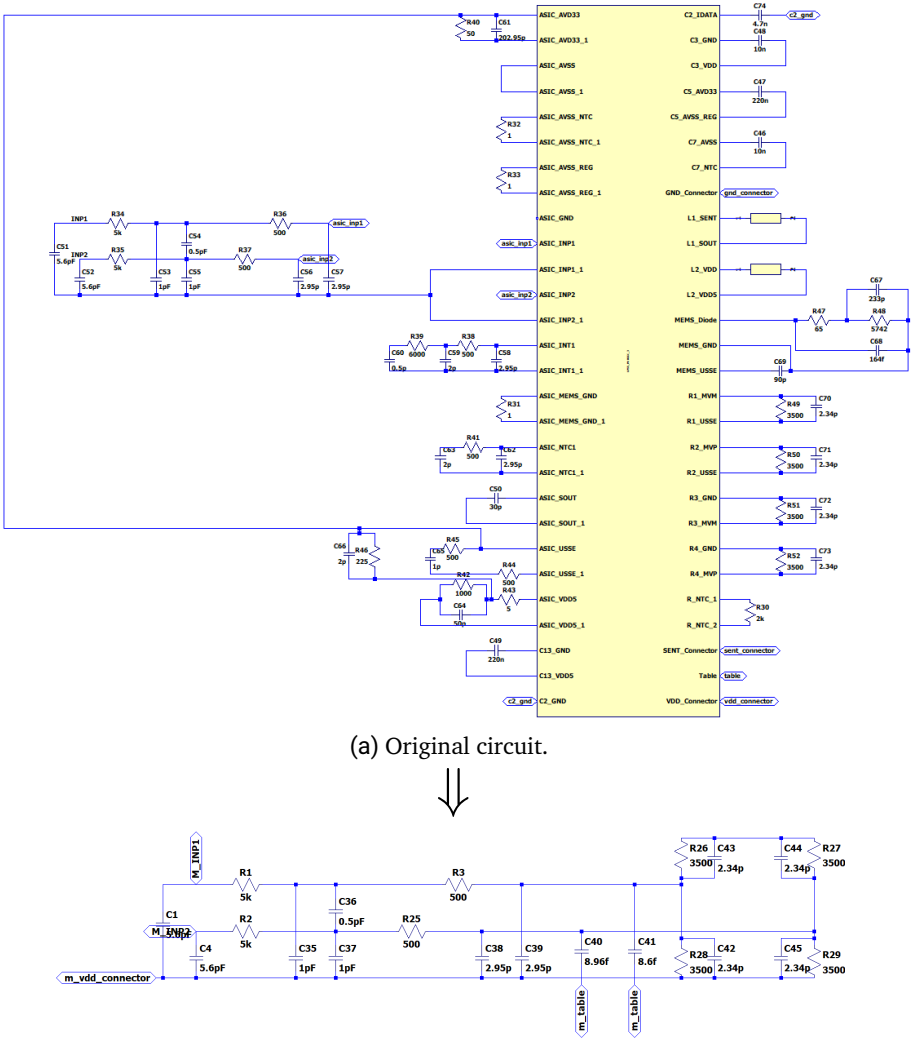

(a) Original circuit.

(b) Reduced circuit.

Figure 6.29.: Reduction of a circuit example. The original circuit, containing 1400 elements is reduced to only 22 elements.

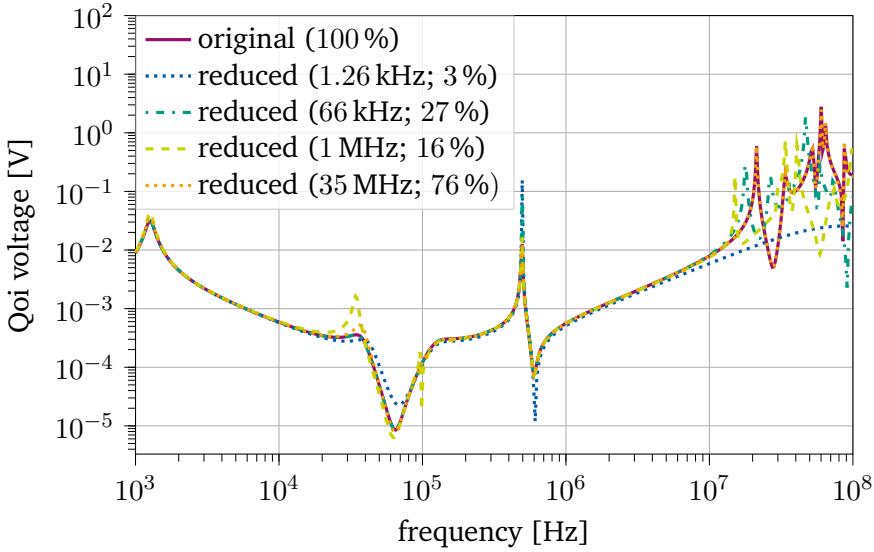

Figure 6.30.: Comparison for the QoI between the original circuit solution and several reductions according to different frequencies.

critical resonance modes are identified by calculating the sensitivities for all the resonance modes w.r.t. the circuit's design parameters. One important finding of this analysis is that a harmonic resonance is closely related to the singularity of a circuit admittance matrix. Thereby, the smallest eigenvalue of the admittance matrix defines the mode of the harmonic resonance. In contrast to earlier methods for sensitivity analysis, the combination of harmonic resonance analysis for power systems with the sensitivity analysis allow a specific quantification of the influence of design parameters on harmonic resonance phenomena [40]. This is particularly advantageous when the bandwidth of the resonances is very small, since existing methods for sensitivity analysis will overemphasize the influence of the design

parameters if the resonance is slightly shifted by their uncertainty.

A similar approach was developed based on the adjoint sensitivity analysis (ASA) presented in this thesis. This approach is mainly focused on the optimization of the EMC properties of electric sensors [5, 6]. For the analysis of these sensors, it is advantageous to relate the relative influence of the design parameters on a given resonance as a QoI. As in [40], this QoI is found by eigenmode decomposition of the electric circuit system.

6.7. Conclusion

The developed methods for ASA in this thesis were applied to a variety of circuit examples from different domains of electrical engineering. For each example, specific properties of the respective methods proved to be advantageous. While the TFHA is particularly efficient in weakly nonlinear circuits with a medium scale, such as the active filter example, it fails for very large scale and broadband circuits. The Parareal ASA and the related Parareal based methods require the circuit to be damped to be able to converge [28]. Strong oscillations can lead to convergence issues which will counteract the simulation speedup of the method. The PPPC ASA is well suited for the analysis of circuits where the transient is long compared to the period duration and only the steady state is the target.

Depending on the specific circuit problem, different approaches out of the proposed methods for sensitivity analysis must be chosen. If chosen accordingly, the methods hold significant advantages when compared to existing methods for sensitivity analysis. This holds a large value in future development and optimization steps, where strong performance of sensitivity analysis methods is required.

7. Conclusion and Outlook

7.1. Conclusion

Based on existing methods for sensitivity analysis, several novel approaches were developed in the course of this thesis. The transient forward harmonic adjoint (TFHA) method combines transient circuit simulation with harmonic adjoint simulation, which circumvents the necessity for a harmonic balance iteration that could possibly cause stability issues of the solver. The Parareal adjoint sensitivity analysis (ASA) combines the Parareal solver with the ASA to speed up both the transient circuit simulation and transient adjoint simulation. Particularly noteworthy is the periodic ASA, which, in addition to improving existing methods through combination with improved solvers, also modifies the transient ASA to incorporate the adjoint integral for periodic problems.

The developed methods in this thesis were derived mathematically and numerically applied to a variety of practical circuit examples. These examples most notably include a DC-DC converter, a B6 bridge-motor supply circuit and an active filter.

In all of these examples, the newly developed methods avoid performance issues that arise when using commonly used approaches for sensitivity analysis. The sensitivity analysis for the DC-DC converter particularly benefits from the periodic ASA, as the transient is much longer than the period length. In contrast, the B6 bridge-motor supply circuit has a very long period length and benefits from the Parareal ASA since the simulation requires

a very large number of timesteps. Lastly, the active filter benefits from the TFHA due to two reasons. Firstly, the circuit has a rather small bandwidth and can be efficiently approximated in frequency domain. Secondly, the interpretability of the results is much better in frequency domain when analyzing filter circuits in general. Consequently, the methods are very valuable tools when chosen accordingly for the problem setting.

7.2. Outlook

From the developed methods, some additional future developments would be particularly interesting. Based on the transient forward harmonic adjoint sensitivity analysis (TFHA), the additional implementation for multitone excitation can be interesting. For the harmonic balance (HB) analysis, multitone HB analysis means that the impact of multiple input tones and their harmonics on the circuit's response is considered. This can be particularly advantageous if the timescales of the excitation are largely scattered. One example for a circuit where this occurs is a power electronics circuit that also incorporates a logic circuit partition. The logic circuit partition contain much higher frequencies in these applications. To apply HB analysis in these examples, multitone analysis is highly advantageous. The same approximation can be utilized to calculate the Jacobian for the TFHA. The multitone Jacobian approximation can be performed by modification of the DFT operator defined in Eq. (2.32). Approaches for this modification are presented in literature [48].

Another interesting work revolves around the use of multirate methods as published in [9, 67] or [60]. These methods split the time integration, which can be more efficient if the timescales are largely scattered. For example, Pels et al. [60] use a Galerkin approach to simulate the fine time resolution, which reduces the actual time integration to a small number of steps. If this could be intelligently coupled with sensitivity analysis methods

such as the ASA, this could be utilized to severely reduce the number of necessary integral solver runs for the sensitivity.

And lastly, the developed methods can be applied to a larger variety of circuit examples. Ideally, this would be implemented in a tool that can be used by engineers without deep knowledge of the topic, such that the tool decides which method is most suited based on the presented advantages and disadvantages. Particularly the Parareal ASA and the periodic ASA, which involve parallelization, can also benefit from the simulation on resources with large parallelization availability.

A. Appendix

A.1. Spectrum Estimation

Spectrum estimation is a mathematical concept that has its roots in signal processing. It can be used to analyze the spectral components of a given time-dependent signal. This analysis is motivated by the fact that a time-domain representation of a signal can be hard to interpret in some cases. These cases include electromagnetic filters where specific frequency components must be filtered, or detection methods where different periodicities or frequency bands must be available. While infinite time-series or ideally periodic signals can be transformed to spectral domain by a simple DFT, this is not as easy for finite signals that are not ideally periodic. In the latter case, some considerations must be made to estimate the spectrum. One common method for spectrum estimation is the periodogram, which is briefly introduced here.

A.1.1. Periodogram

The periodogram is a widely used method for the estimation of the power spectral density (PSD) of a discrete-time signal [15]. The steps along the spectrum estimation using a periodogram are as follows [75]:

1. DFT: As in the ideal case, the first step for the spectrum estimation is the transformation of the time sequence into the frequency domain

using a DFT. The DFT is defined analogously to the definition in section 2.4 such that:

$$X_N\left(e^{\mathrm{j}\omega}\right) = \sum_{n=0}^{N-1} X(n)e^{-\mathrm{j}\omega n} \tag{A.1}$$

2. PSD: Based on the DFT of the signal, the periodogram is obtained as an estimate for the PSD. The PSD is the signal's power distribution across the spectrum. Mathematically, the periodogram is represented as:

$$I_{XX}^N\left(e^{\mathrm{j}\omega}\right) = \frac{1}{N}\left|X_N\left(e^{\mathrm{j}\omega}\right)\right|^2 \tag{A.2}$$

where N is the length of the signal. Following this definition, the expected value of the spectral estimate obtained by the periodogram converges to the real PSD $C_{XX}\left(e^{\mathrm{j}\omega}\right)$ as N approaches infinity:

$$C_{XX}\left(e^{\mathrm{j}\omega}\right) = \lim_{N\to\infty} \mathrm{E}\left[I_{XX}^N\left(e^{\mathrm{j}\omega}\right)\right]. \tag{A.3}$$

3. Plotting the periodogram: In order to identify the signal properties, the periodogram is usually plotted as a function of frequency.

The periodogram has a major disadvantage that is cured in modified methods. While the expected value converges towards the real spectrum, the variance of the periodogram does not converge to zero but rather as [15]:

$$\lim_{N\to\infty} \mathrm{Var}\left[I_{XX}^N\left(e^{\mathrm{j}\omega}\right)\right] = C_{XX}\left(e^{\mathrm{j}\omega}\right)^2. \tag{A.4}$$

As a result, the periodogram often converges to the correct solution, but is highly noisy due to the large variance. This is described in more detail in [15]. A method that tackles this issue is Welch's method.

A.1.2. Welch's Method

Welch's method modifies the periodogram in a way that reduces the variance of the spectral estimates. This is done by dividing the signal into overlapping segments and computing periodograms for each segment. The spectral estimate is then obtained by averaging the results of the periodogram of each of the segments respectively. The steps along Welch's method are as follows:

1. Segmenting the signal: For Welch's method, the signal is divided into overlapping segments. Overlapping signals can capture non-stationary signal properties. Additionally,spectral leakage effects are reduced. This makes spectral estimates smoother and reduces its variance.

2. Windowing: Before computing the periodogram for each of the overlapping segments, a window function is applied to smoothen the spectral estimate. Most commonly used window functions are Hamming, Hanning, or adaptive Kaiser windows.

3. Periodogram: For each of the segments, the PSD is computed using the. The resulting PSDs are then averaged over all segments, further reducing the estimates's variance.

4. Overlapping and averaging: After computing the periodograms, the resulting PSDs are averaged over all segments, further reducing the estimates's variance.

Spectrum estimation is crucial in spectral analysis where signals are not ideally periodic or include uncertainties. The periodogram is a very simple and straight forward method for the spectrum estimation. However, the estimate's variance does not converge to 0 as the number of samples increases, leaving a noisy estimate. Welch's method tackles this issue by

segmenting, windowing, and averaging, which reduces the variance and delivers a better estimate for the spectrum.

A.2. Adjoint Sensitivity Analysis using Tellegen's Theorem

Tellegen's theorem directly follows from Kirchhoff's laws and states that no power can leave or enter the lumped element circuit. In mathematical terms, this is written as:

$$\sum_{k=1}^{n} V_k I_k = 0. \tag{A.5}$$

In contrast to the general derivation for equation systems, no derivative of the system matrix is necessary for the implementation of the adjoint sensitivity analysis. Additionally, the sensitivity analysis based on Tellegen's theorem is graphically descriptive as the adjoint problem is represented by an adjoint circuit problem. Tellegen's theorem holds equally true not only for the same circuits, but also for circuits with an identical topology, i.e. circuits that are described by the same incidence matrix (see section 2.2.1). Since the adjoint circuit problem is a topologically identical circuit [94], this property can be utilized. For this, an adjoint circuit is introduced with the edge voltages $\hat{V}_k$ and the currents $\hat{I}_k$. A simple voltage divider serves as an illustration of a circuit with its corresponding adjoint circuit A.1. Following this, a modified Tellegen's theorem relating a given circuit with its adjoint can be defined such that:

$$\sum_{k=1}^{n} \left(\hat{I}_k V_k - I_k \hat{V}_k \right) = 0. \tag{A.6}$$

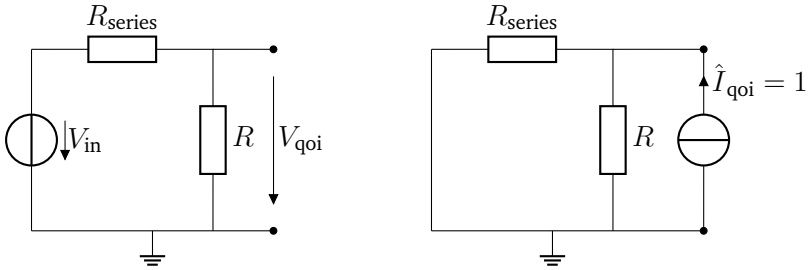

Figure A.1.: Voltage divider (left) with its adjoint circuit (right) as an illustration example.

If small variations of the quantities $V_k = V_{k,0} + \Delta V_k$ and $I_k = I_{k,0} + \Delta I_k$ are imposed in the original circuit, Tellegen's theorem reads [8]:

$$\sum_{k=1}^{n} \left(\hat{I}_k \left(V_{k,0} + \Delta V_k \right) - \left(I_{k,0} + \Delta I_k \right) \hat{V}_k \right) = 0. \tag{A.7}$$

Subtracting the relation (A.6) for the unvaried circuit containing the quantities $V_{k,0}$ and $I_{k,0}$ from (A.7) yields [94]:

$$\sum_{k=1}^{n} \left(\hat{I}_k \left(V_{k,0} + \Delta V_k \right) - \left(I_{k,0} + \Delta I_k \right) \hat{V}_k \right) - \sum_{k=1}^{n} \left(\hat{I}_k V_k - I_k \hat{V}_k \right) = \sum_{k=1}^{n} \left(\hat{I}_k \Delta V_k - \Delta I_k \hat{V}_k \right) = 0 \tag{A.8}$$

Using only fundamental theorems, a relation between the solutions of the topologically identical adjoint circuit and variations of the quantities of the original circuit is implied. To utilize this relation for sensitivity analysis, the varied terms ΔV_k or ΔI_k are rewritten using Ohm's law and the chain rule.

As an example, it is assumed that the edge k is connected by a resistor R:

$$\Delta V_k = I_k \Delta R + R \Delta I_k. \tag{A.9}$$

Plugging (A.9) into (A.8) results in:

$$\sum_{k=1}^{n} \left(\hat{I}_k \left(I_k \Delta R + R \Delta I_k \right) - \Delta I_k \hat{V}_k \right) = \sum_{k=1}^{n} \left(\Delta I_k \left(\hat{V}_k - \hat{I}_k R \right) - \hat{I}_k I_k \Delta R \right). \tag{A.10}$$

Applying sum formula (A.10) to the example circuit shown in Fig. A.1 gives the relation:

$$\sum_{k=1}^{n} \left(\Delta I_k \left(\hat{V}_k - \hat{I}_k R \right) - \hat{I}_k I_k R \right) = -\hat{I}_0 I_0 \Delta R - \hat{I}_1 I_1 \Delta R_{\text{series}} = 0. \tag{A.11}$$

Mapping the sensitivity to the QoI requires a consideration for the QoI edge $U = V_{\text{qoi}}$ in the adjoint circuit problem. Using relation:

$$\hat{I}_{\text{qoi}} \Delta U - \Delta I_{\text{qoi}} \hat{V}_{\text{qoi}} = 0. \tag{A.12}$$

Defining the QoI as an open loop in the original circuit, for example a voltage parallel to an element, the current I_{qoi} and therefore also the variation of the current ΔI_{qoi} is assumed to be zero. Since the adjoint circuit can be chosen freely as long as the topology remains the same, the adjoint current at the QoI is chosen as 1. Without further considerations, the voltage variation at the QoI is :

$$\Delta U = 0, \tag{A.13}$$

and therefore:

$$\Delta U - \hat{I}_0 I_0 \Delta R - \hat{I}_1 I_1 \Delta R_{\text{series}} = 0. \tag{A.14}$$

Deriving this equation exemplary by ΔR and building the limit for ΔU and ΔR gives the relation for the sensitivity at the QoI w.r.t. the resistance R as design parameter p:

$$\frac{\mathrm{d}U}{\mathrm{d}R} = \hat{I}_{\mathrm{R}} I_{\mathrm{R}}. \tag{A.15}$$

Implementation of the ASA using Tellegen's theorem is very straight forward as it is less intrusive because the system matrix is not required to be known. This is particularly advantageous if the analysis needs to be implemented using commercial tools, because commercial tools to not generally grant access to the system matrices and the underlying indexing of the solver itself. Furthermore, this approach for sensitivity analysis is limited to linear circuits since relation (A.10) cannot be simplified in the same way if nonlinear devices are present.

A.3. Analytical Solution for the Output Voltage of the RC-Filter

The homogeneous part of ODE (6.4) reads:

$$\frac{\mathrm{dV_{out,h}}}{\mathrm{d}t} + \frac{1}{RC} V_{\mathrm{out,h}} = 0, \tag{A.16}$$

with the model homogeneous solution such that:

$$V_{\mathrm{out,h}} = K e^{-\frac{1}{RC}t}. \tag{A.17}$$

Since V_{in} is a sinusoidal time-dependent variable, the particular solution is found by the Ansatz:

$$V_{\mathrm{out,p}} = A \sin \omega t + B \cos \omega t, \tag{A.18}$$

and resultingly:

$$\frac{\mathrm{dV_{out,p}}}{\mathrm{d}t} = A\omega \cos \omega t - B\omega \sin \omega t. \tag{A.19}$$

Substituting (A.19) and (A.18), as well as the definition for V_{in} into the original ODE reads:

$$A\omega \cos \omega t - B\omega \sin \omega t + \frac{A}{RC} \sin \omega t + \frac{A}{RC} \cos \omega t - \frac{1\,\text{V}}{RC} \sin(\omega t) = 0 \tag{A.20}$$

$$\Rightarrow \cos \omega t \left(A\omega + \frac{B}{RC} \right) + \sin(\omega t) \left(\frac{A}{RC} - B\omega - \frac{1\,\text{V}}{RC} \right) = 0. \tag{A.21}$$

Using comparison of coefficients, the constants A and B can be derived as:

$$A = \frac{1\,\text{V}}{1 + (\omega RC)^2} \tag{A.22}$$

$$B = -\frac{(1\,\text{V})\omega RC}{1 + (\omega RC)^2}. \tag{A.23}$$

The complete solution is the superposition of homogeneous and particular solution:

$$\begin{aligned} V_{\text{out}} &= V_{\text{out,p}} + V_{\text{out,h}} \\ &= \frac{1\,\text{V}}{1 + (\omega RC)^2} \left(\sin(\omega t) - \omega RC \cos(\omega t) \right) + K e^{-\frac{1}{RC} t}. \end{aligned} \tag{A.24}$$

Requiring $V_{\text{out}} = 0$ for $t = 0$ gives the constant K as:

$$K = -B = \frac{(1\,\text{V})\omega RC}{1 + (\omega RC)^2}. \tag{A.25}$$

Thus, the final solution for V_{out} reads:

$$V_{\text{out}} = \frac{1\,\text{V}}{1 + (\omega RC)^2} \left(\omega RC e^{-\frac{1}{RC} t} + \sin(\omega t) - \omega RC \cos(\omega t) \right). \tag{A.26}$$

Analytical Sensitivity Using Symbolic Derivation

Eq. (6.5) is derived w.r.t. the design parameter R symbolically using the quotient rule. The individual derivatives for each summation are as follows. First, the exponential term is derived:

$$\exp_{\text{diff}} = \frac{\mathrm{d}}{\mathrm{d}R}\left(\frac{1\,\mathrm{V}}{1+(\omega RC)^2}\omega RC e^{-\frac{1}{RC}t}\right) \tag{A.27}$$

$$= \frac{\omega C e^{-\frac{1}{RC}t}\left(\frac{t}{RC}+1\right)\left(1+(\omega RC)^2\right) - 2(\omega C)^2 R\left(e^{-\frac{1}{RC}t}\omega RC\right)}{\left(1+(\omega RC)^2\right)^2}\mathrm{V}\,\Omega^{-1} \tag{A.28}$$

$$= \frac{\omega C e^{-\frac{1}{RC}t}\left(\frac{t}{RC}+1\right)\left(1+(\omega RC)^2\right) - 2(\omega RC)^2}{\left(1+(\omega RC)^2\right)^2}\mathrm{V}\,\Omega^{-1}. \tag{A.29}$$

Here, the nominator is derived with the product-rule:

$$\frac{\mathrm{d}}{\mathrm{d}R}\left(e^{-\frac{1}{RC}t}\omega RC\right) = \frac{t\omega C}{RC}e^{-\frac{1}{RC}t} + \omega C e^{-\frac{1}{RC}t} \tag{A.30}$$

$$= \omega C e^{-\frac{1}{RC}t}\left(\frac{t}{RC}+1\right) \tag{A.31}$$

Secondly, the sine term is derived:

$$\sin_{\text{diff}} = \frac{\mathrm{d}}{\mathrm{d}R}\left(\frac{1\,\mathrm{V}}{1+(\omega RC)^2}\sin(\omega t)\right) = -\frac{2(\omega C)^2 R\sin(\omega t)}{\left(1+(\omega RC)^2\right)^2}\mathrm{V}\,\Omega^{-1}. \tag{A.32}$$

Finally, the cosine term is derived:

$$\cos_{\text{diff}} = \frac{\mathrm{d}}{\mathrm{d}R}\left(-\frac{1\,\mathrm{V}}{1+(\omega RC)^2}\omega RC\cos(\omega t)\right) \tag{A.33}$$

$$= -\frac{\omega C\cos(\omega t)\left(1+(\omega RC)^2\right) - 2(\omega C)^2 R\omega RC\cos(\omega t)}{\left(1+(\omega RC)^2\right)^2}\mathrm{V}\,\Omega^{-1} \tag{A.34}$$

$$= -\frac{\omega C\cos(\omega t)\left(\left(1+(\omega RC)^2\right) - 2(\omega RC)^2\right)}{\left(1+(\omega RC)^2\right)^2}\mathrm{V}\,\Omega^{-1} \tag{A.35}$$

$$\tag{A.36}$$

The total derivative follows as the superposition of the three terms:

$$\frac{\mathrm{d}V_{\text{out}}}{\mathrm{d}R} = \exp_{\text{diff}} + \sin_{\text{diff}} + \cos_{\text{diff}}\,. \tag{A.37}$$

Bibliography

[1] Technologies Agilent. *Advanced Design System - Sensitivity Analysis*. Tech. rep. 2011.01. Feb. 2011. URL: http://edadownload.software.keysight.com/eedl/ads/2011_01/pdf/sensana.pdf.

[2] A. Ales, F. Tahar Belkacem, and D. Moussaoui. "Laboratory Line Impedance Stabilisation Network: Experimental studies". In: *2011 10th International Conference on Environment and Electrical Engineering*. Rome, Italy: IEEE, May 2011, pp. 1–4. ISBN: 978-1-4244-8779-0. DOI: 10.1109/EEEIC.2011.5874774. URL: http://ieeexplore.ieee.org/document/5874774/.

[3] Howard Anton and Chris Rorres. *Elementary linear algebra: applications version*. 11th edition. Hoboken, NJ: John Wiley & Sons Inc, 2014. ISBN: 978-1-118-43441-3 978-1-118-47422-8.

[4] J.W. Bandler, Q.J. Zhang, and R.M. Biernacki. "A unified framework for harmonic balance simulation and sensitivity analysis". In: IEEE, 1988, pp. 1041–1044. DOI: 10.1109/MWSYM.1988.22209. URL: http://ieeexplore.ieee.org/document/22209/.

[5] Jan Benz, Jan Hansen, and Stephan Frei. "Eigenmode Based Optimization of Sensors". In: *2020 International Symposium on Electromagnetic Compatibility - EMC EUROPE*. Rome, Italy: IEEE, Sept. 2020, pp. 1–6. ISBN: 978-1-72815-579-1. DOI: 10.1109/EMCEUROPE48519.

2020.9245652. URL: https://ieeexplore.ieee.org/document/9245652/.

[6] Jan Benz et al. “Generation and EMC Optimization of Compact Equivalent Electrical Circuits of Industrial Electronics”. In: *IEEE Transactions on Electromagnetic Compatibility* (2023), pp. 1–9. ISSN: 0018-9375, 1558-187X. DOI: 10.1109/TEMC.2023.3321078. URL: https://ieeexplore.ieee.org/document/10280746/.

[7] Oszkár Bíró, Gergely Koczka, and Kurt Preis. “Finite element solution of nonlinear eddy current problems with periodic excitation and its industrial applications”. en. In: *Applied Numerical Mathematics* 79 (May 2014), pp. 3–17. ISSN: 01689274. DOI: 10.1016/j.apnum.2013.04.007. URL: https://linkinghub.elsevier.com/retrieve/pii/S0168927413000779.

[8] J. L. Bordewijk. “Inter-reciprocity applied to electrical networks”. en. In: *Applied Scientific Research* 6.1 (Jan. 1957), pp. 1–74. ISSN: 0003-6994, 1573-1987. DOI: 10.1007/BF02410413. URL: http://link.springer.com/10.1007/BF02410413.

[9] H. G. Brachtendorf et al. “Numerical steady state analysis of electronic circuits driven by multi-tone signals”. en. In: *Electrical Engineering* 79.2 (Apr. 1996), pp. 103–112. ISSN: 0003-9039, 1432-0487. DOI: 10.1007/BF01232919. URL: http://link.springer.com/10.1007/BF01232919.

[10] R.K. Brayton, F.G. Gustavson, and G.D. Hachtel. “A new efficient algorithm for solving differential-algebraic systems using implicit backward differentiation formulas”. In: *Proceedings of the IEEE* 60.1 (1972), pp. 98–108. ISSN: 0018-9219. DOI: 10.1109/PROC.1972.8562. URL: http://ieeexplore.ieee.org/document/1450492/.

[11] K. E. Brenan, S. L. Campbell, and L. R. Petzold. *Numerical Solution of Initial-Value Problems in Differential-Algebraic Equations*. en. Society for Industrial and Applied Mathematics, Jan. 1995. ISBN: 978-0-89871-353-4 978-1-61197-122-4. DOI: 10.1137/1.9781611971224. URL: http://epubs.siam.org/doi/book/10.1137/1.9781611971224.

[12] Julian Buschbaum. "Adjoint Sensitivity Analysis of Time Periodic Electrical Networks". MA thesis. Technische Universität Darmstadt, 2020.

[13] Yang Cao, Shengtai Li, and Linda Petzold. "Adjoint sensitivity analysis for differential-algebraic equations: algorithms and software". en. In: *Journal of Computational and Applied Mathematics* 149.1 (Dec. 2002), pp. 171–191. ISSN: 03770427. DOI: 10.1016/S0377-0427(02)00528-9.

[14] I. Charpentier. "Checkpointing Schemes for Adjoint Codes: Application to the Meteorological Model Meso-NH". en. In: *SIAM Journal on Scientific Computing* 22.6 (Jan. 2001), pp. 2135–2151. ISSN: 1064-8275, 1095-7197. DOI: 10.1137/S1064827598343735.

[15] Guanrong Chen. "Introduction to random signals and applied Kalman filtering, 2nd edn. Robert Grover Brown and Patrick Y. C. Hwang, Wiley, New York, 1992. ISBN 0-471-52573-1, 512 pp., $62.95." en. In: *International Journal of Adaptive Control and Signal Processing* 6.5 (Sept. 1992), pp. 516–518. ISSN: 0890-6327, 1099-1115. DOI: 10.1002/acs.4480060509. URL: https://onlinelibrary.wiley.com/doi/10.1002/acs.4480060509.

[16] Chung-Wen Ho, A. Ruehli, and P. Brennan. "The modified nodal approach to network analysis". en. In: *IEEE Transactions on Circuits and Systems* 22.6 (June 1975), pp. 504–509. ISSN: 0098-4094. DOI: 10.1109/TCS.1975.1084079.

[17] Michael E. Coltrin, Robert J. Kee, and James A. Miller. “A Mathematical Model of the Coupled Fluid Mechanics and Chemical Kinetics in a Chemical Vapor Deposition Reactor”. In: *Journal of The Electrochemical Society* 131.2 (Feb. 1984), pp. 425–434. ISSN: 0013-4651, 1945-7111. DOI: 10.1149/1.2115598. URL: https://iopscience.iop.org/article/10.1149/1.2115598.

[18] D. Coppersmith and S. Winograd. “On the Asymptotic Complexity of Matrix Multiplication”. en. In: *SIAM Journal on Computing* 11.3 (Aug. 1982), pp. 472–492. ISSN: 0097-5397, 1095-7111. DOI: 10.1137/0211038. URL: http://epubs.siam.org/doi/10.1137/0211038.

[19] S. Costanzo et al. “Parallel-in-time adjoint-based optimization – application to unsteady incompressible flows”. en. In: *Journal of Computational Physics* 471 (Dec. 2022), p. 111664. ISSN: 00219991. DOI: 10.1016/j.jcp.2022.111664. URL: https://linkinghub.elsevier.com/retrieve/pii/S0021999122007276.

[20] *DC Electrical Circuit Analysis A Practical Approach*. eng. OCLC: 1409437724. Place of publication not identified: dissidents, 2020. ISBN: 978-1-65451-547-8.

[21] S. Director and R. Rohrer. “The Generalized Adjoint Network and Network Sensitivities”. In: *IEEE Transactions on Circuit Theory* 16.3 (1969), pp. 318–323. ISSN: 0018-9324. DOI: 10.1109/TCT.1969.1082965.

[22] L. Donzel and J. Schuderer. “Nonlinear resistive electric field control for power electronic modules”. In: *IEEE Transactions on Dielectrics and Electrical Insulation* 19.3 (June 2012), pp. 955–959. ISSN: 1070-9878. DOI: 10.1109/TDEI.2012.6215099. URL: http://ieeexplore.ieee.org/document/6215099/.

[23] Matthew Emmett and Michael Minion. “Toward an efficient parallel in time method for partial differential equations”. en. In: *Communications in Applied Mathematics and Computational Science* 7.1 (Mar. 2012), pp. 105–132. ISSN: 2157-5452, 1559-3940. DOI: 10.2140/camcos.2012.7.105. URL: http://msp.org/camcos/2012/7-1/p04.xhtml.

[24] Robert W. Erickson and Dragan Maksimović. *Fundamentals of power electronics*. eng. Second edition, softcover reprint of the hardcover 2nd edition 2001. New York, NY: Springer Science+Business Media, LLC, 2001. ISBN: 978-0-306-48048-5 978-1-4757-0559-1.

[25] Harley Flanders. “Differentiation Under the Integral Sign”. In: *The American Mathematical Monthly* 80.6 (June 1973), p. 615. ISSN: 00029890. DOI: 10.2307/2319163. URL: https://www.jstor.org/stable/2319163?origin=crossref.

[26] Martin J. Gander and Stefan Güttel. “PARAEXP: A Parallel Integrator for Linear Initial-Value Problems”. en. In: *SIAM Journal on Scientific Computing* 35.2 (Jan. 2013), pp. C123–C142. ISSN: 1064-8275, 1095-7197. DOI: 10.1137/110856137. URL: http://epubs.siam.org/doi/10.1137/110856137.

[27] Martin J. Gander, Iryna Kulchytska-Ruchka, and Sebastian Schöps. “A New Parareal Algorithm for Time-Periodic Problems with Discontinuous Inputs”. en. In: *Domain Decomposition Methods in Science and Engineering XXV*. Ed. by Ronald Haynes et al. Vol. 138. Cham: Springer International Publishing, 2020, pp. 243–250. ISBN: 978-3-030-56749-1 978-3-030-56750-7. DOI: 10.1007/978-3-030-56750-7_27. URL: http://link.springer.com/10.1007/978-3-030-56750-7_27.

[28] Martin J. Gander and Stefan Vandewalle. “Analysis of the Parareal Time-Parallel Time-Integration Method”. en. In: *SIAM Journal on Scientific Computing* 29.2 (Jan. 2007), pp. 556–578. ISSN: 1064-

8275, 1095-7197. DOI: 10.1137/05064607X. URL: http://epubs.siam.org/doi/10.1137/05064607X.

[29] Martin J. Gander et al. "Analysis of Two Parareal Algorithms for Time-Periodic Problems". en. In: *SIAM Journal on Scientific Computing* 35.5 (Jan. 2013), A2393–A2415. ISSN: 1064-8275, 1095-7197. DOI: 10.1137/130909172. URL: http://epubs.siam.org/doi/10.1137/130909172.

[30] C. Gear. "Simultaneous Numerical Solution of Differential-Algebraic Equations". In: *IEEE Transactions on Circuit Theory* 18.1 (1971), pp. 89–95. ISSN: 0018-9324. DOI: 10.1109/TCT.1971.1083221.

[31] Boole George. *A treatise on the calculus of finite differences*. Stechert, 1946.

[32] Michael B. Giles and Niles A. Pierce. "An Introduction to the Adjoint Approach to Design. Flow, Turbulence and Combustion". In: *Flow, Turbulence and Combustion* 65.3/4 (2000), pp. 393–415. ISSN: 13866184. DOI: 10.1023/A:1011430410075. URL: http://link.springer.com/10.1023/A:1011430410075.

[33] Sebastian Götschel and Michael L. Minion. "An Efficient Parallel-in-Time Method for Optimization with Parabolic PDEs". en. In: *SIAM Journal on Scientific Computing* 41.6 (Jan. 2019), pp. C603–C626. ISSN: 1064-8275, 1095-7197. DOI: 10.1137/19M1239313. URL: https://epubs.siam.org/doi/10.1137/19M1239313.

[34] "A DICTIONARY OF MUSIC AND MUSICIANS". In: *A Dictionary of Music and Musicians (A.D. 1450–1880)*. Ed. by George Grove. 1st ed. Cambridge University Press, July 1883, pp. 1–26. ISBN: 978-1-108-00421-3 978-0-511-70331-7. DOI: 10.1017/CBO9780511703317.001. URL: https://www.cambridge.org/core/product/identifier/CBO9780511703317A005/type/book_part.

[35] John L. Gustafson. “Reevaluating Amdahl’s law”. en. In: *Communications of the ACM* 31.5 (May 1988), pp. 532–533. ISSN: 0001-0782, 1557-7317. DOI: 10.1145/42411.42415.

[36] Johan Gyselinck, Claudia Martis, and Ruth Sabariego. “Using dedicated time-domain basis functions for the simulation of pulse-width-modulation controlled devices–application to the steady-state regime of a buck converter”. In: Cluj-Napoca, Romania, Oct. 2013.

[37] J. M. Hammersley and D. C. Handscomb. *Monte Carlo Methods*. en. Dordrecht: Springer Netherlands, 1964. ISBN: 978-94-009-5821-0 978-94-009-5819-7. DOI: 10.1007/978-94-009-5819-7. URL: http://link.springer.com/10.1007/978-94-009-5819-7.

[38] Henry Helson. *Harmonic Analysis*. en. Boston, MA: Springer US, 1991. ISBN: 978-0-534-15570-4 978-1-4615-7181-0. DOI: 10.1007/978-1-4615-7181-0. URL: http://link.springer.com/10.1007/978-1-4615-7181-0.

[39] D. Grahame Holmes and T. A. Lipo. *Pulse width modulation for power converters: principles and practice*. Hoboken, NJ: John Wiley, 2003. ISBN: 978-0-471-20814-3.

[40] Zhenyu Huang, Yu Cui, and Wilsun Xu. “Application of Modal Sensitivity for Power System Harmonic Resonance Analysis”. In: *IEEE Transactions on Power Systems* 22.1 (Feb. 2007), pp. 222–231. ISSN: 0885-8950. DOI: 10.1109/TPWRS.2006.883678. URL: http://ieeexplore.ieee.org/document/4077113/.

[41] Z. (Zoran) Ilievski. “Model order reduction and sensitivity analysis”. en. In: (2010). Publisher: Technische Universiteit Eindhoven. DOI: 10.6100/IR685256.

[42] Richard C. Jaeger and Travis N. Blalock. *Microelectronic circuit design*. Fifth edition. New York, NY: McGraw-Hill, a business unit of The McGraw-Hill Companies, Inc, 2015. ISBN: 978-0-07-352960-8 978-0-07-338045-2.

[43] Eric R. Keiter et al. *Sensitivity Analysis in Xyce.* en. Tech. rep. SAND2016-9437, 1562422. Sept. 2016, SAND2016–9437, 1562422. DOI: 10.2172/1562422. URL: http://www.osti.gov/servlets/purl/1562422/.

[44] Marinko Kovacic et al. "Analytical Wideband Model of a Common-Mode Choke". In: *IEEE Transactions on Power Electronics* 27.7 (July 2012), pp. 3173–3185. ISSN: 0885-8993, 1941-0107. DOI: 10.1109/TPEL.2011.2182060. URL: http://ieeexplore.ieee.org/document/6117090/.

[45] Iryna Kulchytska-Ruchka and Sebastian Schöps. "Efficient Parallel-in-Time Solution of Time-Periodic Problems Using a MultiHarmonic Coarse Grid Correction". en. In: *SIAM Journal on Scientific Computing* 43.1 (Jan. 2021), pp. C61–C88. ISSN: 1064-8275, 1095-7197. DOI: 10.1137/20M1314756. URL: https://epubs.siam.org/doi/10.1137/20M1314756.

[46] J. M. Lambert and W. T. Williams. "Multivariate Methods in Plant Ecology: IV. Nodal Analysis". In: *The Journal of Ecology* 50.3 (Nov. 1962), p. 775. ISSN: 00220477. DOI: 10.2307/2257482. URL: https://www.jstor.org/stable/2257482?origin=crossref.

[47] Jacques-Louis Lions, Yvon Maday, and Gabriel Turinici. "Résolution d'EDP par un schéma en temps «pararéel »". fr. In: *Comptes Rendus de l'Académie des Sciences - Series I - Mathematics* 332.7 (Apr. 2001), pp. 661–668. ISSN: 07644442. DOI: 10.1016/S0764-4442(00)01793-6.

[48] Stephen A. Maas. *Nonlinear microwave and RF circuits*. 2nd ed. Boston, MA: Artech House, 2003. ISBN: 978-1-58053-484-0.

[49] R.C. Melville et al. “Artificial parameter homotopy methods for the DC operating point problem”. In: *IEEE Transactions on Computer-Aided Design of Integrated Circuits and Systems* 12.6 (June 1993), pp. 861–877. ISSN: 02780070. DOI: 10.1109/43.229761. URL: http://ieeexplore.ieee.org/document/229761/.

[50] N. Mohan, T.M. Undeland, and W.P. Robbins. *Power Electronics: Converters, Applications, and Design*. Power Electronics: Converters, Applications, and Design Bd. 1. John Wiley & Sons, 2003. ISBN: 978-0-471-42908-1. URL: https://books.google.de/books?id=wmTTnQEACAAJ.

[51] M. Nakhla and J. Vlach. “A piecewise harmonic balance technique for determination of periodic response of nonlinear systems”. en. In: *IEEE Transactions on Circuits and Systems* 23.2 (Feb. 1976), pp. 85–91. ISSN: 0098-4094. DOI: 10.1109/TCS.1976.1084181. URL: http://ieeexplore.ieee.org/document/1084181/.

[52] Bibhu Prasad Nayak et al. “Sensitivity Based Reduction of Equivalent Electrical Circuits in Power Electronics Application”. In: IEEE, May 2023, pp. 1–5. ISBN: 9798350338348. DOI: 10.1109/APEMC57782.2023.10217554. URL: https://ieeexplore.ieee.org/document/10217554/.

[53] J. Nievergelt. “Parallel methods for integrating ordinary differential equations”. en. In: *Communications of the ACM* 7.12 (Dec. 1964), pp. 731–733. ISSN: 0001-0782, 1557-7317. DOI: 10.1145/355588.365137. URL: https://dl.acm.org/doi/10.1145/355588.365137.

[54] N.K. Nikolova, J.W. Bandler, and M.H. Bakr. “Adjoint Techniques for Sensitivity Analysis in High-Frequency Structure CAD”. en. In:

IEEE Transactions on Microwave Theory and Techniques 52.1 (Jan. 2004), pp. 403–419. ISSN: 0018-9480. DOI: 10.1109/TMTT.2003.820905.

[55] Per Öberg. "A dae formulation for multi-zone thermodynamic models and its application to cvcp engines". PhD thesis. Linköping University Electronic Press, 2009.

[56] Yoshifumi Okamoto. "Topology optimization of DC-biased pot-type reactor using design sensitivity in steady state of electromagnetic field with magnetic nonlinearity". In: *International Journal of Applied Electromagnetics and Mechanics* 69.3 (July 2022). Ed. by Marcin Ziółkowski and Marek Ziółkowski, pp. 347–357. ISSN: 13835416, 18758800. DOI: 10.3233/JAE-210162. URL: https://www.medra.org/servlet/aliasResolver?alias=iospress&doi=10.3233/JAE-210162.

[57] A.V. Oppenheim et al. "Single-sensor active noise cancellation". In: *IEEE Transactions on Speech and Audio Processing* 2.2 (Apr. 1994), pp. 285–290. ISSN: 10636676. DOI: 10.1109/89.279277. URL: http://ieeexplore.ieee.org/document/279277/.

[58] Athanasios Papoulis and A. A. Maradudin. "The Fourier Integral and Its Applications". en. In: *Physics Today* 16.3 (Mar. 1963), pp. 70–72. ISSN: 0031-9228, 1945-0699. DOI: 10.1063/1.3050815. URL: https://pubs.aip.org/physicstoday/article/16/3/70/423392/The-Fourier-Integral-and-Its-Applications.

[59] *Parallel-in-Time References*. URL: http://parallel-in-time.org/references/index.html.

[60] Andreas Pels et al. "Solving Nonlinear Circuits With Pulsed Excitation by Multirate Partial Differential Equations". In: *IEEE Transactions on Magnetics* 54.3 (Mar. 2018), pp. 1–4. ISSN: 0018-9464, 1941-

0069. DOI: 10.1109/TMAG.2017.2759701. URL: http://ieeexplore.ieee.org/document/8071149/.

[61] Linda Petzold. “Differential/Algebraic Equations are not ODE”. en. In: *SIAM Journal on Scientific and Statistical Computing* 3.3 (Sept. 1982), pp. 367–384. ISSN: 0196-5204, 2168-3417. DOI: 10.1137/0903023.

[62] Lawrence Pillage. *Electronic Circuit & System Simulation Methods (SRE)*. 1st ed. USA: McGraw-Hill, Inc., 1998. ISBN: 0-07-134770-4.

[63] Vishwas Rao and Adrian Sandu. “An Adjoint Based Implementation of the Parareal Algorithm”. en. In: *Procedia Computer Science* 9 (2012), pp. 1021–1029. ISSN: 18770509. DOI: 10.1016/j.procs.2012.04.110. URL: https://linkinghub.elsevier.com/retrieve/pii/S1877050912002311.

[64] Robert D. Richtmyer and E. H. Dill. “Difference Methods for Initial-Value Problems”. en. In: *Physics Today* 12.4 (Apr. 1959), pp. 50–50. ISSN: 0031-9228, 1945-0699. DOI: 10.1063/1.3060778. URL: https://pubs.aip.org/physicstoday/article/12/4/50/895477/Difference-Methods-for-Initial-Value-Problems.

[65] V. Rizzoli et al. “General-purpose harmonic balance analysis of nonlinear microwave circuits under multitone excitation”. In: *IEEE Transactions on Microwave Theory and Techniques* 36.12 (Dec. 1988), pp. 1650–1660. ISSN: 0018-9480, 1557-9670. DOI: 10.1109/22.17396. URL: http://ieeexplore.ieee.org/document/17396/.

[66] V. Rizzoli et al. “State-of-the-art harmonic-balance simulation of forced nonlinear microwave circuits by the piecewise technique”. In: *IEEE Transactions on Microwave Theory and Techniques* 40.1 (Jan. 1992), pp. 12–28. ISSN: 00189480. DOI: 10.1109/22.108318. URL: http://ieeexplore.ieee.org/document/108318/.

[67] J. Roychowdhury. “Analyzing circuits with widely separated time scales using numerical PDE methods”. In: *IEEE Transactions on Circuits and Systems I: Fundamental Theory and Applications* 48.5 (May 2001), pp. 578–594. ISSN: 10577122. DOI: 10.1109/81.922460. URL: http://ieeexplore.ieee.org/document/922460/.

[68] A.E. Ruehli. “Equivalent Circuit Models for Three-Dimensional Multiconductor Systems”. en. In: *IEEE Transactions on Microwave Theory and Techniques* 22.3 (Mar. 1974), pp. 216–221. ISSN: 0018-9480. DOI: 10.1109/TMTT.1974.1128204. URL: http://ieeexplore.ieee.org/document/1128204/.

[69] Yousef Saad. *Iterative Methods for Sparse Linear Systems*. en. Second. Society for Industrial and Applied Mathematics, Jan. 2003. ISBN: 978-0-89871-534-7 978-0-89871-800-3. DOI: 10.1137/1.9780898718003. URL: http://epubs.siam.org/doi/book/10.1137/1.9780898718003.

[70] A. Saltelli, ed. *Global sensitivity analysis: the primer*. OCLC: ocn180852094. Chichester, England ; Hoboken, NJ: John Wiley, 2008. ISBN: 978-0-470-05997-5.

[71] Julian Sarpe, Andreas Klaedtke, and Herbert De Gersem. “A Parallel-In-Time Adjoint Sensitivity Analysis for a B6 Bridge-Motor Supply Circuit”. In: *IEEE Transactions on Magnetics* (2023), pp. 1–1. ISSN: 0018-9464, 1941-0069. DOI: 10.1109/TMAG.2023.3334727. URL: https://ieeexplore.ieee.org/document/10330636/.

[72] Julian Sarpe, Andreas Klaedtke, and Herbert De Gersem. “Transient forward harmonic adjoint sensitivity analysis”. en. In: *Electrical Engineering* (May 2024). ISSN: 0948-7921, 1432-0487. DOI: 10.1007/s00202-024-02463-z. URL: https://link.springer.com/10.1007/s00202-024-02463-z.

[73] Sebastian Schuhmacher et al. “Adjoint Technique for Sensitivity Analysis of Coupling Factors According to Geometric Variations”. In: *IEEE Transactions on Magnetics* 54.3 (Mar. 2018), pp. 1–4. ISSN: 0018-9464, 1941-0069. DOI: 10.1109/TMAG.2017.2774107. URL: http://ieeexplore.ieee.org/document/8259011/.

[74] Sebastian Alfred Schuhmacher. “Sensitivitätsanalyse mittels adjungierter Verfahren für äquivalente Ersatzschaltbilder extrahiert aus 3D Feldmodellen”. de. PhD thesis. Darmstadt: Technische Universität, Apr. 2018. URL: http://tuprints.ulb.tu-darmstadt.de/7386/.

[75] Arthur Schuster. “On the investigation of hidden periodicities with application to a supposed 26 day period of meteorological phenomena”. en. In: *Terrestrial Magnetism* 3.1 (Mar. 1898), pp. 13–41. ISSN: 0272-7528, 0272-7528. DOI: 10.1029/TM003i001p00013. URL: https://agupubs.onlinelibrary.wiley.com/doi/10.1029/TM003i001p00013.

[76] W. Shockley. “The Theory of *p-n* Junctions in Semiconductors and *p-n* Junction Transistors”. en. In: *Bell System Technical Journal* 28.3 (July 1949), pp. 435–489. ISSN: 00058580. DOI: 10.1002/j.1538-7305.1949.tb03645.x. URL: https://ieeexplore.ieee.org/document/6773080.

[77] RF Sincovec et al. *Solvability of large-scale descriptor systems*. Tech. rep. Seattle, Washington: Boeing Computer Services Company, 1979.

[78] C.S. Skene, M.F. Eggl, and P.J. Schmid. “A parallel-in-time approach for accelerating direct-adjoint studies”. en. In: *Journal of Computational Physics* 429 (Mar. 2021), p. 110033. ISSN: 00219991. DOI: 10.1016/j.jcp.2020.110033. URL: https://linkinghub.elsevier.com/retrieve/pii/S002199912030807X.

[79] Ilya M Sobol. “Sensitivity estimates for nonlinear mathematical models”. In: *Mathematical modelling and computational experiments* 1.4 (1993), pp. 407–414.

[80] Y. Spack-Leigsnering et al. “Electroquasistatic-Thermal Modeling and Simulation of Station Class Surge Arresters”. In: *IEEE Transactions on Magnetics* 52.3 (Mar. 2016), pp. 1–4. ISSN: 0018-9464, 1941-0069. DOI: 10.1109/TMAG.2015.2490547. URL: http://ieeexplore.ieee.org/document/7297858/.

[81] Jonathan Stysch. “Stable Broadband Finite Element Parasitic Extraction and Sensitivity Analysis”. In: (2022). Publisher: UNSPECIFIED. DOI: 10.26083/TUPRINTS-00021561. URL: https://tuprints.ulb.tu-darmstadt.de/id/eprint/21561.

[82] Bruno Sudret. “Global sensitivity analysis using polynomial chaos expansions”. en. In: *Reliability Engineering & System Safety* 93.7 (July 2008), pp. 964–979. ISSN: 09518320. DOI: 10.1016/j.ress.2007.04.002. URL: https://linkinghub.elsevier.com/retrieve/pii/S0951832007001329.

[83] Inc. Synopsis. *SaberRD Training Video Series - Video 11*. URL: https://www.synopsys.com/verification/resources/videos/robust-design-sensitivity-analysis.html.

[84] Bernard DH Tellegen. “A general network theorem, with applications”. In: *Philips Res Rep* 7 (1952), pp. 256–269.

[85] Riccardo Torchio. “A Volume PEEC Formulation Based on the Cell Method for Electromagnetic Problems From Low to High Frequency”. In: *IEEE Transactions on Antennas and Propagation* 67.12 (Dec. 2019), pp. 7452–7465. ISSN: 0018-926X, 1558-2221. DOI: 10.1109/TAP.2019.2927789. URL: https://ieeexplore.ieee.org/document/8764572/.

[86] Felix Maximilian Traub. “Automated Construction of Equivalent Electrical Circuit Models for Electromagnetic Components and Systems”. en. PhD thesis. Darmstadt: Technische Universität, Mar. 2014. URL: http://tuprints.ulb.tu-darmstadt.de/3805/.

[87] Heinz W. Van Der Broeck and Jacobus D. Van Wyk. “A Comparative Investigation of a Three-Phase Induction Machine Drive with a Component Minimized Voltage-Fed Inverter under Different Control Options”. In: *IEEE Transactions on Industry Applications* IA-20.2 (Mar. 1984), pp. 309–320. ISSN: 0093-9994. DOI: 10.1109/TIA.1984.4504413. URL: http://ieeexplore.ieee.org/document/4504413/.

[88] E. Van Dijk et al. “PWM-switch modeling of DC-DC converters”. In: *IEEE Transactions on Power Electronics* 10.6 (Nov. 1995), pp. 659–665. ISSN: 0885-8993, 1941-0107. DOI: 10.1109/63.471285. URL: https://ieeexplore.ieee.org/document/471285/.

[89] Jiří Vlach and Kishore Singhal. *Computer methods for circuit analysis and design*. 2nd ed. New York: Van Nostrand Reinhold, 1994. ISBN: 978-0-442-01194-9.

[90] Ralph A. Willoughby, ed. *Stiff Differential Systems*. en. Boston, MA: Springer US, 1974. ISBN: 978-1-4684-2102-6 978-1-4684-2100-2. DOI: 10.1007/978-1-4684-2100-2. URL: http://link.springer.com/10.1007/978-1-4684-2100-2.

[91] Ketian Ye et al. “Global Sensitivity Analysis of Large Distribution System With PVs Using Deep Gaussian Process”. In: *IEEE Transactions on Power Systems* 36.5 (Sept. 2021), pp. 4888–4891. ISSN: 0885-8950, 1558-0679. DOI: 10.1109/TPWRS.2021.3084455. URL: https://ieeexplore.ieee.org/document/9442807/.

[92] Jeng Yen, Linda Petzold, and Soumyendu Raha. “A time integration algorithm for flexible mechanism dynamics: The DAE α-method”. en.

In: *Computer Methods in Applied Mechanics and Engineering* 158.3-4 (June 1998), pp. 341–355. ISSN: 00457825. DOI: 10.1016/S0045-7825(97)00261-2. URL: https://linkinghub.elsevier.com/retrieve/pii/S0045782597002612.

[93] Omer F. Yildiz et al. "Sensitivity analysis and empirical optimization of cross-domain coupling on RFICs using polynomial chaos expansion". In: *2017 IEEE International Symposium on Electromagnetic Compatibility & Signal/Power Integrity (EMCSI)*. Washington, DC, USA: IEEE, Aug. 2017, pp. 102–107. ISBN: 978-1-5386-2229-2 978-1-5386-2231-5. DOI: 10.1109/ISEMC.2017.8077849. URL: http://ieeexplore.ieee.org/document/8077849/.

[94] F. Yuan and A. Opal. "Sensitivity analysis of periodically switched linear circuits using an adjoint network technique". In: vol. 5. IEEE, 1999, pp. 331–334. ISBN: 978-0-7803-5471-5. DOI: 10.1109/ISCAS.1999.777576. URL: http://ieeexplore.ieee.org/document/777576/.

[95] O. C. Zienkiewicz and J. Z. Zhu. "The superconvergent patch recovery anda posteriori error estimates. Part 2: Error estimates and adaptivity". en. In: *International Journal for Numerical Methods in Engineering* 33.7 (May 1992), pp. 1365–1382. ISSN: 0029-5981, 1097-0207. DOI: 10.1002/nme.1620330703. URL: https://onlinelibrary.wiley.com/doi/10.1002/nme.1620330703.

Acronyms

2D	two-dimensional
3D	three-dimensional
AC	alternating current
ASA	adjoint sensitivity analysis
BDF	backward differential formula
CM	common mode
DAE	differential-algebraic equation
DC	direct current
DCOP	DC operation point
DFT	discrete Fourier transform
DoFs	degrees of freedom
DSA	direct sensitivity analysis
EEC	equivalent electric circuit
EMC	electromagnetic compatibility
FDF	forward differential formula
FEM	finite element method
FFT	fast Fourier transform
HASA	harmonic adjoint sensitivity analysis
HB	harmonic balance
IC	initial condition
ICs	integrated circuits
IDFT	inverse discrete Fourier transform
IGBT	insulated-gate bipolar transistor

IVP	initial value problem
KCL	Kirchhoff's current law
KVL	Kirchhoff's voltage law
LISN	line impedance stabilization network
MNA	modified nodal analysis
NFC	near field control
ODE	ordinary differential equation
OPAMP	operational amplifier
PCB	printed circuit board
PCE	polynomial chaos expansion
PDE	partial differential equation
PEEC	partial element equivalent circuit
PFASST	parallel full approximation scheme in space and time
PinT	parallel-in-time
PP-IC	periodic Parareal with initial-value coarse problem
PP-PC	periodic Parareal with periodic coarse problem
PWM	pulse-width modulated
QoI	quantity of interest
RHS	right-hand side
TFHA	transient forward harmonic adjoint sensitivity analysis
VSCI	voltage sensing current injection
w.r.t.	with respect to

Publications

J. Sarpe, A. Klaedtke, and H. De Gersem, “Periodic Adjoint Sensitivity Analysis”, arXiv e-prints, 2024.
doi:10.48550/arXiv.2405.19048. (only preprint available at time of publication of thesis)

J. Sarpe, A. Klaedtke, and H. De Gersem. “Transient Forward Harmonic Adjoint Sensitivity Analysis”. en. In: Electrical Engineering (May 2024). issn: 0948-7921, 1432-0487. doi: 10.1007/ s00202-024-02463-z.

J. Sarpe, A. Klaedtke and H. De Gersem, “A Parallel-In-Time Adjoint Sensitivity Analysis for a B6 Bridge-Motor Supply Circuit,” in IEEE Transactions on Magnetics, doi: 10.1109/TMAG.2023.3334727.

M.G. Ruppert, Y. Späck-Leigsnering, J. Buschbaum, and H. De Gersem, "Adjoint variable method for transient nonlinear electroquasistatic problems." Electr Eng 105, 2319-2325 (2023). https://doi.org/10.1007/s00202-023-01797-4

B. P. Nayak, S. Dhar, A. Klaedtke and J. Buschbaum, "Sensitivity Based Reduction of Equivalent Electrical Circuits in Power Electronics Application," 2023 Joint Asia-Pacific International Symposium on Electromagnetic Compatibility and International Conference on ElectroMagnetic Interference & Compatibility (APEMC/INCEMIC), Bengaluru, India, 2023, pp. 1-5, doi: 10.1109/APEMC57782.2023.10217554.